UNIVERSITÀ
DEGLI STUDI
FIRENZE

PhD School in Gas Engineering and Innovative Industrial and Environmental Technology

XXX CYCLE

Innovative design process for industrial gas turbine combustors

ING-IND/08 Fluid Machinery

Graduate Student	Academic Relator	Tutor
Dott. Pucci Egidio	Ph.D. Antonio Andreini	Prof. Bruno Facchini

Coordinator

Prof. Maurizio De Lucia

Years 2014/2017

Acknowledgments

This Ph.D. thesis was prepared synergistically with the employment in the Gas Turbine Combustion Design department of the Nuovo Pignone Tecnologie s.r.l. company. However, any opinions, findings, conclusions, or recommendations expressed herein are those of the author and do not necessarily reflect the views of the company.
The author gratefully acknowledges the Nuovo Pignone Tecnologie s.r.l. Combustion Design department, Test laboratory and Project Management for their support in NovaLT16 and NovaLT12 design, tests campaign data acquisition and processing, as well as for the permission for the publication of results herein.

I met many people who I would like to thank: first and foremost, prof. Bruno Facchini and Antonio Andreini from the Industrial Engineering Department of the University of Florence for their patience in driving me in the right direction and motivate me.
Among all managers, product and project leadership, technical chiefs and colleagues, I should express a special thanks to Guido Peano and Eugenio Del Puglia for their unfounded faith on the positive conclusion of this journey and to Matteo Cerutti for its wasting support... in the end, I appreciated his assistance.
Finally, I cannot forget the support of my wonderful wife Caterina and my son Edoardo, deprived too much time of its best friend game: he teaches me that it's not needed going fast to fly high.

Abstract

There is not a single way of design a combustor.
Best configuration selection depends on the objectives which would be satisfied by the design activity: a robust declaration of the design intent is the first mandatory step to reach a successful product configuration. Also, the design process is, in some respects, function of the specific product to be developed, therefor the contextualization of the design purpose, as well as the relevant requirements, can play a fundamental role in setting the right process for the right product.
Market demand for the gas turbine OEM is rapidly evolving as the human knowledge and needs: it is fundamental to be connected every day with the market evolutions to provide solutions that can be successful in a longer time frame perspective.
System engineers, design engineers need to answer quickly to sophisticate problems, searching the best solution from the architectural level down to the detailed solutions.
The even more larger availability of analysis systems leaves on open scenario of choices and, at the same time, poses the question about which should be the criteria for the selection of the most suitable models. To designer is asked not just performing the design, but also the selection of the system of models required to execute the design and demonstrate its reliability with the minimum industrial risk.
Especially in the early phase of design, designers need fast execution tools, able to capture strength and weakness of each configuration, helping the selection of alternative solutions, while meeting the peculiar project requirements.
This thesis is tracking the design process footprints, from the wide initial scenario of a new combustor design for industrial gas turbines, down to detailed design aspects,

passing through sealing system design with turbine nozzle, up to a specific liner cooling architecture and its optimization.

Main effort of this job has been focused on the creation of a numerical tool, able, since the early phase of development, to analyze the liner cooling with a one-dimensional conjugate aero-thermal-strain approach: liner cold side heat transfer coefficients in a turbulated forced convection region are iteratively computed updating metal and air temperatures and the deformed geometry of coolant passages from results of a heat balance. Coolant passages, in between the deformed surfaces of liner and baffle, influence the air velocity, changing in turn heat transfer coefficients and coolant pressure losses. The computation of liner and baffle strain has been validated comparing the code results with the ones obtained by a detailed finite element model.

Correlations embedded in the code have been calibrated thanks to a comparison with temperatures and pressures experimental measurements, which have been acquired in a full annular rig test campaign.

The code has been provided with two additional optimization routines, developed to automatically improve the baffle design for an enhancement of the liners durability, without penalizing engine performance. Maintaining the same coolant pressure losses and minimizing the axial gradients of metal temperature by means of a variable gap baffle geometry, a reduction of thermal induced stresses can be achieved.

The reader will follow problems and solutions, sizing criteria and uncertainties estimation of the combustor architecture adopted in the BHGE NovaLT™ industrial gas turbine class, up to reach the testing phase of the manufactured components and finally the baffle design solution optimization.

Reliability of the liner cooling system depends also by the reliability of the leakage prediction across the interface between liners and turbine first stage nozzles. In parallel to the baffle design optimization, studies have been performed on this sealing systems, aimed to increase the reliability of the combustor flow split prediction and to identify areas of improvement of the sealing. The criteria for selection and design of the most suitable sealing system and related durability analyses will be presented, completing the picture of the combustor flow split and synergistically improving the reliability of the liners cooling design presented.

Contents

List of Figures

List of Tables

List of Equations

Nomenclature

A	area	[m2]
AM	additive manufacturing	[-]
AWJ	abrasive water jet	[-]
BHGE	Baker Hughes, a Ge company	[-]
c	thermal capacity	[J kg^{-1} K^{-1}]
CAD	computer aided drafting	[-]
c_D	discharge coefficient	[-]
CDC	compressor discharge chamber	[-]
CDM	combustion dynamic monitoring	[-]
CHT	conjugate heat transfer	[-]
CO	carbonite oxides	[-]
CTE	thermal expansion coefficient	[K^{-1}]
d	diameter	[-]
D	equivalent hydraulic diameter	[m]
DMLM	direct metal laser melting	[-]
E	Young's modulus	[Nmm^{-2}]
EBW	electron beam welding	[-]
EDM	electro discharge machining	[-]
f	friction coefficient	[-]
FEM	finite element model	[-]
FEA	finite element model analysis	[-]
F_{obj}	objective function	[-]
FMEA	failure mode and effect analysis	[-]

FSFL	full speed full load	[-]
FSI	fluid structure interaction	[-]
FSNL	full speed not load	[-]
GT	gas turbine	[-]
HPT	high pressure turbine	[-]
HTC	heat transfer coefficient	[W m^{-2} K^{-1}]
k	thermal conductivity	[W m^{-1} K^{-1}]
LHV	lower heating value	[-]
m	mass flow	[kg s^{-1}]
MTBM	mean time between maintenance	[-]
NGV	nozzle guide vanes	[-]
NOx	nitrogen oxides	[-]
Nu	Nusselt number	[-]
OEM	original equipment manufacturer	[-]
PCD	compressor discharge pressure	[-]
PF	pattern Factor	[-]
Q	heat flux	[W]
r	radius	[m]
Re	Reynolds number	[-]
RQL	rich quick lean	[-]
s	length step	[m]
S1N	turbine first stage nozzle	[-]
Sr	Strouhal number	[-]
t	metal thickness	[m]
T	temperature	[°C]
TBC	thermal barrier coating	[-]
Thot	hot bulk temperature	[°C]
Tcold	cold bulk temperature	[°C]
u	velocity	[m s-1]
UHC	unburned hydro carbons	[-]
VF	view factor	[-]

w	weight	[-]

Greeks

α	angle	
Δx	axial variation	[m]
Δr	radial variation	[m]
ε	emissivity	[-]
π	pi constant	[-]
ρ	density	[kg m^{-3}]
σ	Stefan-Boltzmann constant	[W m^{-2} K^{-4}]

Subscripts

a	average
amb	ambient condition
b	baffle
c	coolant
corr	correction term
conv	convective
end	final axial step
i	axial step index
id	ideal
in	initial condition
j	optimization step index
l	liner
min	minimum
rad	radiative

1 Scope of the Work

The work developed in the frame of the present doctorate are based on the design process and optimization of the combustor cooling system of the BHGE NovaLT™ class of industrial gas turbine. The two most relevant parts of the presented work, contributing to improve the whole combustor cooling design, are the baffles design process and optimization and the detailed analysis and design of the sealing system between liners and turbine first stage nozzle.

Before to describe the baffle design process, in chapter 2 a contextualization of the work in the current state of art in the field of industrial gas turbine combustor design is reported, providing the design perspective by a systemic point of view.

Chapter 3 provide a specific focus on the combustor cooling architecture of the BHGE NovaLT™ class of industrial gas turbine and on the state of art in the numerical modelling for the conjugate analysis approach. A preliminary assessment of the combustor flow split architecture for the design case is also presented.

The baffles design process and optimization is in details presented in chapter 4, while the description of one-dimensional conjugate aero-thermal-strain code developed on purpose is presented in chapter 5. The work of validation and calibration of the code is then described in chapter 6. In the frame of a new combustor development for the NovaLT12 industrial turbine, the presented methodology for baffle design, as well as the numerical tool developed, have been adopted for the first attempt configuration and the sequent optimization, as reported in chapter 7.

A second relevant part of the work performed has been aimed to increase the reliability of the combustor flow split prediction and to identify areas of improvement of the sealing between liners and turbine first stage nozzle. In chapter 8, criteria for selection and design of the most suitable sealing system have been presented and specifically for the leaf seal sealing system durability analyses and risk assessment have been reported. A research on publications and patents on the sealing systems between liners and turbine first stage nozzle has been performed, helping the conceivement of a new alternative sealing design for the NovaLT gas turbine class: in the frame of this thesis, there is not

reported any detail about, since such new seal design is currently under a duty of confidentiality, as trade secret.

1.1 Advancement with respect to the State of the Art

As examined in depth in chapter 3.4, the strong coupling between cooling process and actual geometry of the system as determined by the components thermal expansion, suggest the development of a full conjugate aero-thermal-strain approach in the design of the baffle.

In feasibility studies first and then in conceptual and preliminary design phases, the most useful tools are the ones able to capture the main physical problems which shall be solved, with the minimum time required in modelling. Role of preliminary studies, supported by these tools, is to guide the system level trade-off to define main components size, interfaces and constraints among the different turbine modules and verify the design agreement with the product specification requirements.

The adoption of a one-dimensional conjugate tool for the quick design, since the early phases of combustor development, represents an element of novelty, moving a step forward the technology in the field of baffles design. A similar concept can be conveniently adopted also in other components of the hot gas path which can experience significant thermal induced deformations.

A second contribution to knowledge in the field of annular combustor cooling system design, has been reached in the area of sealing systems between liners and turbine first stage nozzle. By one side, a detailed methodology of durability analysis for the leaf seal sealing system has been developed. The proposed analysis and design process represents an improvement of the commonly adopted try and error design methodology, impacting significantly on the development time and costs for this kind of seals. By the other side, the design of a new seal specifically devoted to the industrial application has been obtained: testing phase in a full annular rig has been successfully completed and the alternative concept proposed has been introduced in the new engine configuration.

2 Industrial Gas Turbine Combustors design

There is not a single way of design a combustor.

We can also say that there is not a best configuration to be obtained, depending on the set of objectives which would be satisfied by the design activity.

Discussing about the design processes there is a consistent risk of describing something that could be judged banal, obsolete or too specific, not worldwide applicable, if not even incorrect. The discriminating factor, which can break this relativism about the design processes, is a robust declaration of the design intent.

The purpose of the design, like others human activities, is to satisfy commercial and technical needs: it's worth to discuss of which requirements shall be satisfied, before starting to debate about the best approach shall be used to comply with. A vision from above, inclusive of all the designed component life, from the manufacturing processes, through maintenance and repair, up to the final rejection and destruction, can take the difference between a successful product and just a good design result.

In the last decades different processes of design as design for reliability, design for cost, design for quality, just to mention some ones, have been established, each one emphasizing the weight of specific requirements over the all, which could be critical in specific products or industrial sectors.

The design process itself is, in some respects, function of the specific sector or products to be developed, therefor the contextualization of the design purpose as well as the relevant requirements can play a fundamental role in setting the right process for the right product.

Knowledge of combustion physical process, as well as technology involved in the combustor manufacturing, are key skills for the designer to enable a deep understanding of the combustor design requirements and assessment of the related effects: the definition of the design intent.

Effort dedicated to enhancing the own knowledge of the combustion physical process and, even more, of the manufacturing technology and the commercial strategy is a best practice to reach a consolidated expertise and, at the same time, it is a designer brain

exercise which should be continuously performed, to adequate the requirements satisfaction to the technological and commercial evolutions.
In the following chapters, the foundation of the combustor designer will be analyzed, to provide an overview of the design process and finally to contextualize the work performed in the specific industrial sector.

2.1 Industrial gas turbine combustors

In a gas turbine, the combustor is physically composed by the functional assembly of burners and combustion chamber, interfacing by one side the compressor diffuser and by the other side the first stage nozzle of the high pressure turbine.
Figure 2-1 shows a cross-section view of an example of industrial gas turbine annular combustor architecture, where labels of the main components are reported.

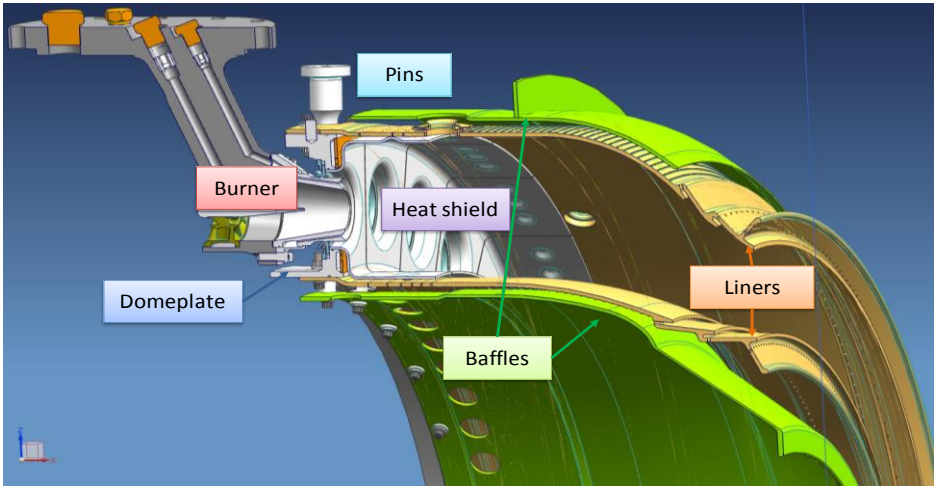

Figure 2-1, Heavy duty gas turbine annular combustor cross-section

The burner is the component which shall mix the fuels and air coming from the compressor to generate a stable flame in all the working conditions, while the combustion chamber defines the volume where the flame and the hot gas produce by the

oxidation process shall be contained, shielding the surrounding structures and guiding it toward the first stage nozzle of the high pressure turbine.

Baffles are the structures deputed to generate a compressor air high velocity region on the liners cold side, improving the heat transfer coefficient to obtain a cooling enhancement.

In the Brayton-Joule cycle the combustor is represented by an ideal isobar transformation (2-3) of the evolving fluid, while the real process can be closely approximated by an isothermal transformation (2'-3'), as schematically shown in the temperature-entropy diagram.

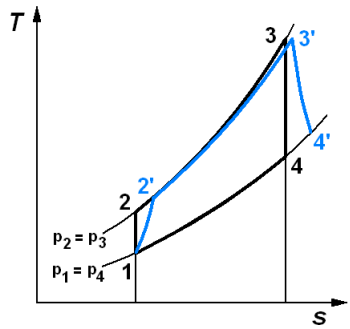

Figure 2-2, Brayton-Joule cycle in Temperature-Entropy diagram

The design of an industrial gas turbine combustor shall satisfy requirements deriving from the combustion chemical reaction process, the heat exchange process and the acoustic and mechanical vibrations interaction over the combustor structural components, as well as others system requirements deriving from the engine peculiar architecture.

2.2 Combustion process

2.2.1 Pollutant emissions

To meet the stringent legislation requirements on emissions it's fundamental the knowledge of the mechanisms leading the pollutant emission formation and abatement. Figure 2-3 shows the dependency of emissions concentrations in function of the air fuel ratio (AFR): AFR values higher than the stoichiometric one (lean combustion) can generate lower NOx with a progressively increase of CO and UHC [Ref. 3].

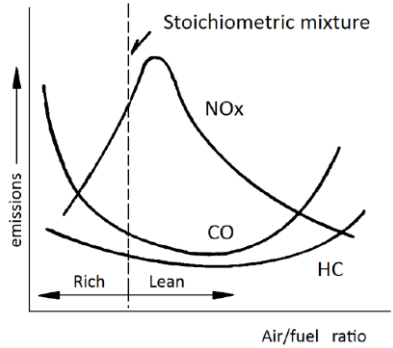

Figure 2-3, Dependence of NOx, CO and UHC emissions upon the AFR

Since 1992, investigations performed by Zeldovich et al. [Ref. 4] showed that in combustion processes the thermal NOx contribution is predominant comparing to other mechanisms (see Correa [Ref. 5] for a complete review of nitrous oxide formation mechanisms) and in fact, as shown in Figure 2-3, the maximum concentration occurs with a nearly stoichiometric mixture. Higher CO and UHC concentrations are generated with rich or lean mixtures due to low flame temperatures and incomplete combustion, as shown in Figure 2-4: from an operational point of view, the aim is to operate the engine in a temperature range where a trade-off of aforementioned species is achieved.

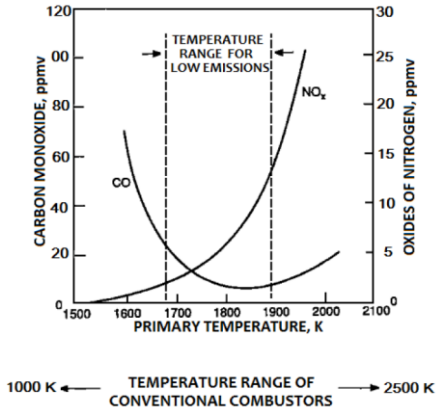

Figure 2-4, Temperature range where CO, NOx and UHC concentrations are lower

Low burning temperatures can lead to a CO concentration increase, due to high conversion times which can be of the same order of flow residence times in the flame tube: the result is an inefficient oxidation to CO_2 determining a limitation to mixture leanness (Correa [Ref. 6]). The turbulence structures produced in the combustion chamber play a key role as well: they can alter the residence time and improve the mixing between the burnt mixture and dilution flow.

The dilution flow, used to cool the liners and control the exit gas temperature profile, inhibits CO oxidation and, at the same time, NOx production.

Conventional combustors are of diffusion type: the fuel is injected in the primary zone where burns with a local stoichiometric AFR at very high temperatures thus generating a large quantity of NOx.

One of the most effective technologies in reducing pollutant emissions is the lean premixed combustor with the ultimate target of providing a homogeneous mixture of fuel and air to the primary zone at an AFR close to the lean blow-out, thus avoiding local fuel rich pockets.

2.2.2 Pressure fluctuations

Compared with the diffusive flames, premixed flames are less stable, due their stronger capability to excite the combustor acoustic tones: blow-off, flashback, as well as mechanical integrity of the combustor, are posing more stringent limitations for premixed flames to the range of regulations required at different engine operating conditions, see Figure 2-5.

Flashback can cause the flame to move towards premixing regions and auto-ignition can occur in the premixing ducts.

Lean premixed combustors are prone to combustion instabilities characterized by large amplitude pressure oscillations sustained by fluctuating heat release which could cause a significant reduction of durability of combustor components.

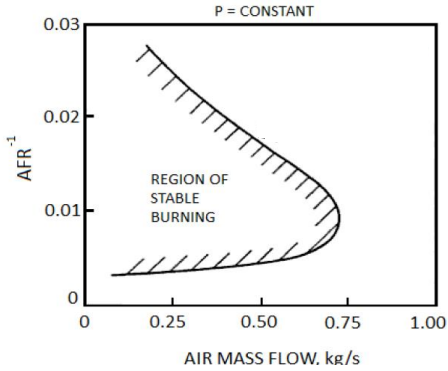

Figure 2-5, Typical combustor chamber stability range

As shown in Figure 2-6, at extremely low equivalence ratios, even small changes of AFR, or equivalence ratio in turn, affect the heat release rate: the fluctuation of heat release is low near the stoichiometric condition, while it rapidly increases near the lean blow-out.

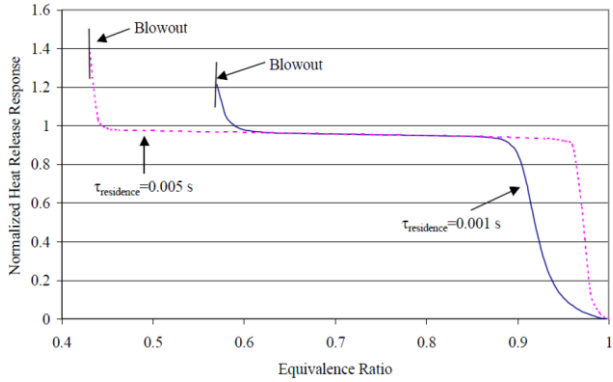

Figure 2-6, Fluctuating heat release vs equivalence ratio for a lean mixture

Combustion instabilities, which in technical literature are generally referred to as thermoacoustic instabilities as well, are large amplitude oscillations of pressure and velocity within the combustor, with the flame acting as an instability source due to the unsteady heat release [Ref. 7 and Ref. 8].

Gas turbine combustor manufacturer develops its own strategy for preventing and reducing the coupling between acoustic waves and unsteady heat release [Ref. 9].

To reduce the development risks associated with the combustion instabilities in new burner and combustor design, typically a testing phase in real dimension of the combustor with its instrumentation is performed. During the testing phase, many actions can be introduced to limit or prevent the coupling of the unsteady heat release with the combustor acoustic frequencies, as not exhaustive example: change in the fuel ratio between burner pilot and premix line or change of fuel mass flow feeding different sectors of burners.

When all the simpler fuel line tuning actions and burner design changes are still marginal in controlling the pressure oscillation in the combustor, over the range of expected operating conditions, additional system of control can be introduced in the design.

Active control strategies consist in a broadband and continuous control of the amplitude of pressure oscillations in the combustor chamber by means of sensors and actuators:

sensors continuously control the pressure amplitude within the combustor and, in case of an excessive pressure, a controller acts with a feedback mechanisms on actuators.
Traditional approach to suppress combustion instabilities consists in passive devices; active controls are still restricted to demonstration levels and truly successful application are still to be found.
Two of the most used passive control devices are the Helmholtz resonators [Ref. 10] and the quarter wave tubes [Ref. 11]. Both these devices act as a notch filter to reduce the excitation of a predetermined instability frequency, removing energy from the sound waves, in a narrow frequency range [Ref. 12]. These devices are heavy and their installment is difficult in a compact combustor. One promising front of development are the perforated liners, since they are very attractive in mitigating combustion instabilities, as well as metal cooling device: perforated liners, in combination with a bias flow, are very effective sound absorbers and applied to gas turbine combustors they can suppress thermoacoustic instabilities.

2.3 Design Requirements

In this chapter, a synthesis of the typical requirements affecting the design of a modern industrial combustor is reported: the presented list is intercepting the requirement flow-down process, from the customer needs to the engine components design, at the combustion system level.

Combustion requirements:

- High combustion efficiency at base load and partial load: the fuel shall be completely burned so that all its chemical energy is liberated as heat;
- Reliable and smooth ignition in all the engine operative conditions;
- Wide stability limits: the flame should stay alight over wide ranges of pressure and air/fuel ratio;
- Low emission of smoke and gaseous pollutant species NOx, CO and UHC;
- Minimizing pressure pulsations and other manifestation of combustion induced instabilities;

- Minimizing pressure losses;
- Fuel flexibility: capability to burn different kinds of fuels, in gaseous or liquid physical state;

System and Mechanical requirements:

- Flow split congruence with the engine secondary flow architecture: compressor air distribution shall be divided by the part required for chemical reaction and the part for components cooling;
- An outlet temperature distribution (PF) that is tailored to maximize the durability of turbine blades and nozzle guide vanes;
- Available room: mechanical design and sizing of combustor components with a size and shape compatible with engine architecture;
- Combustor mechanical interfaces: capability to accommodate relative thermal strain of the surrounding engine components over all the engine operative conditions;
- Components high durability: capability of combustor components to withstand high pressure and temperature for the MTBM interval;
- Sealing system: compliant design with the sealing needs between combustor and first stage nozzle;

Commercial requirements:

- Design for minimum cost and easy of manufacturing;
- Minimum time to market: in the industrial competitive market, the time required for design, manufacturing and testing the HW shall be minimized;
- Parts maintainability (condition based maintenance);
- Parts reparability.

A help to understand the interconnections among all these requirements, could be provided by reviewing the combustor evolution history from the Worldwide War II to the recent aero and industrial engine architectures [Ref. 3]: the development of more

complex and reliable combustors received a significant trust from the even more stringent legislation requirements on NOx emissions, since the last three decades.
Ultra-lean premixed technology combustors, developed to limit emissions generation, are subjected to stronger combustion instabilities and require higher percentage of compressor air, limiting the amount of air appointed to the cooling systems.
New combustors research and development strategies are strongly investing on emissions targets achievement, managing the partial satisfaction of the other performance requirements, since outstanding results of combustion system on the emissions level, can leads to un invincible commercial advantage of the produced gas turbine.
In general, the mentioned requirements are intimately interconnected by many factors not only limited to the physical processes involved in the combustion process: engine operability strategy, manufacturing capabilities as well as marketing needs and maintenance strategy are all players that can move the barycenter of the best fitting among the possible design solutions.
This aspect opens a wide scenario of possible configurations, where many engine architectures can be an optimal solution: based on the weights selection for the competitor requirements, the designer Pareto front can change.

2.3.1 Evolving markets

One example, over all, can help to understand the importance to be connected every day with the market evolutions to provide solutions that can be successful in a longer time frame perspective.
The variability over a day in the electrical energy production is in the last years significantly increasing as effect of the pervasive introduction of renewable energies, like the ones based on wind and solar, which cannot be predicted with a high level of accuracy [Ref. 2].
Such change in the demand is pushing, among other effects, the electrical energy producers to increase the frequency of gas turbines adoption as peak demand players, thanks to the higher responsiveness of these systems compared to nuclear or steam turbine plants.

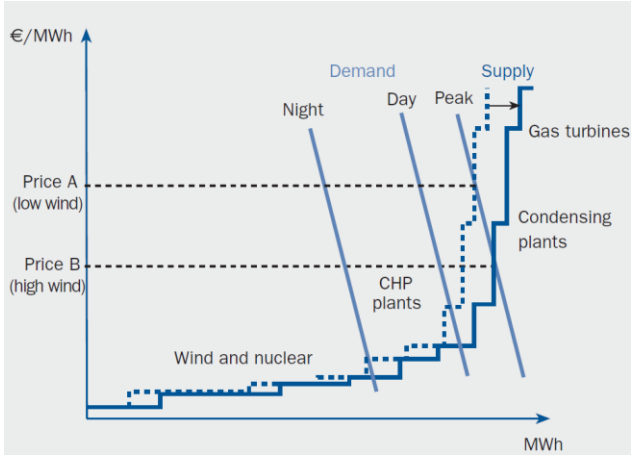

Figure 2-7, Electrical energy demand/offer curve

Among the all, requirements as fast start capability, high partial load efficiency and high durability in terms of start-stop cycles will be in the next future more demanding and potential discriminating factors for the most attractive gas turbines on the market.

Performing a flow-down process up to combustor design level of these system requirements having an estimated relevance increase, the impact can be individuated in:

- Higher start-stop cycles: required better liners cooling to target a higher number of LCF cycles in the same MTBM;
- High number of transients: reduced life of liners / first nozzle sealing system;
- Extended partial load operations: required a more accurate design against acoustic pressure pulsation over all the operating conditions.

2.4 Designer responsibility

Not less important of the process, is the role of the process owner.

Who is taking responsibility of the intelligent and correct execution of the design process?

Each industry is leveraging in its employees expertise and in the consolidated practices to guarantee a high quality, homogenous, repeatable and low risk execution of the development projects. This aspect is fundamental but a not exhaustive answer to the need of developing new products, condition where different skills or different use of existing skills could be required.

The designer role is the neuralgic node, from which a network of relations can be radiated toward all the actors involved in the design development: he is the who shall perform a summary of all requirements, typically not just synergic between them, but antagonist.

System and design engineers need to answer quickly to sophisticate problems, searching the best solution from the architectural down to the detail level.

What is the best schematization, models, analytical approach shall be used to solve the problem and demonstrate with the minimum risk the goodness of the desired results?

The designer shall answer to this need following the practices, the tested and validate models and the expertise costly acquired in the time, but also, he shall be the one able to expand or modify this background, if not fitting properly the new development needs.

The designer shall individuate for each specific problem to be solved what is the best model to be used: the even more easy availability of analysis systems leaves on open scenario of choices and, at the same time, poses the question about which should be the criteria for the selection of the most suitable models.

To designer is asked not just performing the design, but also the selection of the system of models required to execute the design and demonstrate its reliability with the minimum industrial risk.

2.5 Preliminary design process

Each OEM structures the own design process, to minimize the development risk, all along the different phases of the project, starting from simple evaluation up to the most sophisticated predictions. The fundamental concept behind all the design processes is the iterative engagement of all the designer to verify a progressively increasing accomplishment of all the requirements defined for the new design development: successful design requires numerous trade-offs.

Each combustor mechanical design process defines specific considerations related to structural integrity and structural deformation of combustion mechanical systems to ensure that the part life, reliability and functional performance requirements are met. Fundamental design goals are safety, function, maintainability, producibility, life, reliability, and minimum cost.

Typically, at the start of a design project, a literature search for relevant information is made to ensure use of best practice and lessons learned, including patents search as well. Sources include drawings and documentation of previous designs, field data and reports, patents and competitor machine information. Of particular interest, are materials, connection details, seals and manufacturing methods.

The internal flow geometry is designed to satisfy the combustion aerothermal requirements, as:

- Meet required exhaust emissions;
- Provide controllable enthalpy increase between the compressor and turbine using a wide range of fuels at all transient and steady state operating modes;
- Limit combustion system pressure drop to a value consistent with target machine heat rate and output;
- Provide reliable ignition, cross firing, and no flame loss at prescribed operating conditions;
- Prevent flame back flow and flashback that can cause hardware damage;
- Limit acoustic pressure pulsation to levels consistent with acceptable life by means of burning zone geometry selection and, if any, fuel scheduling;
- Provide exit gas temperature profiles consistent with acceptable turbine life.

Components cooling is designed to reduce metal temperatures and thermal stresses to acceptable limits. The component structure is designed to achieve life, manufacturability, maintainability and cost objectives. All the above design objectives are interrelated; a change to accomplish one goal affects others, causing additional iterations. Throughout the design iterations, durability estimations and component specific considerations, progressively more accurate, must be used to verify that design requirements are satisfied.

When the initial aerothermal design is complete, metal temperature measurements from laboratory tests can be made to support detailed stress and life calculations.

Low cycle fatigue (LCF) and high cycle fatigue (HCF) have been historical failure modes for combustor components. LCF typically results from cycling of metal temperatures, which cause stresses higher than material yield strength for combustor designs. LCF is usually considered to be cracking in less than 10^4 cycles. High cycle fatigue is caused by high frequency mechanical vibration in the elastic range. Interaction of the two mechanisms has also occurred where cracks are initiated by LCF and propagated by HCF.

HCF crack propagation due to combustion dynamics can be very rapid, therefore, it is important that this failure mechanism be considered if the part cannot be designed to prevent initiation of LCF cracking during its service life.

Giving a reference, to contextualize the frame of the present job, here after the preliminary phase of the combustor design process is listed in the following main steps:

1. Combustor system requirements
    - Thermodynamic cycle definition
    - Component repair and replacement interval
2. Development of conceptual architecture
    - Burner selection
    - Number of burners
    - Combustion gasses residence time: liners length and diameters
    - Interfaces with engine parts
    - Sealing methods

- Assembly sequence

3. Estimation of average metal temperatures
    - Estimation of combustor steady state and transient deflections
4. Selection of component cooling architecture
    - Estimation of maximum metal temperatures and thermal gradients
5. Selection of material and manufacturing processes
    - Start of experimental test for unknown material characteristics
6. Reliability risk assessment

In this preliminary phase of design, all the main functional and geometrical parameters have been estimated by previous design and testing experiences, correlations and design best practices. All the areas of new development are conceptually individuated and base criteria for the relevant trade-off has been established.

All the cooling techniques involve increased aerodynamic losses, due to coolant air friction with air passages surfaces (distributed losses) and velocity dissipation in vortices fluid structure localized in passage section changes (concentrated losses).
In vane nozzle and blade design, such aerodynamics losses lead to a decreased of global engine efficiency, so the design shall select the best compromise between increasing fire temperature and cooling effectiveness against the increased aerodynamics losses, to target the maximum engine efficiency.
In a combustor cooling system design such aerodynamics losses could not lead to decreased engine efficiency if the coolant air is injected into mainstream before to reach the turbine first nozzle section: the high-pressure coolant flow participates to the turbine expansion. In this case the only reduction of global engine efficiency is related to the pressure drop associated with coolant flow injected in the mainstream: a contributor generally negligible, due to the low quantity of mass flow involved.
In the combustor design an upper limit to the aerodynamics losses is defined by the burners pressure drop: generally, such pressure drop is consistent (ranging between 2.5 - 7% of the compressor flow pressure) to allow a proper flame holding in all the combustor operating conditions and for a good control of flow splitting among the

combustion chamber. In addition, coolant features shall never overcome the burner pressure drop, typically increased with a consisted design margin, to avoid hot gas ingestion, in particular at engine partial loads.

All the potentially critical locations, typically where welding, brazing, bolted joints are present and where strong temperature gradients or peak temperatures are predicted, are analyzed to confirm the suitability of the produced materials to withstand the related level of stress. Understanding of the liner and baffle mechanical behavior by static and dynamic point of view, mandatory for the durability estimation of the components, requires knowledge of material characteristics under the expected temperature range, as:

- Static modulus of elasticity;
- Mean coefficient of thermal expansion;
- Thermal conductivity;
- Specific heat;
- Ultimate tensile strength;
- 0.2% yield strength;
- Percentual elongation;
- Percentual area reduction;
- Total oxidation;
- Isothermal rupture;
- Creep stress rupture (Larson-Miller equation parameters);
- Isothermal creep;
- Cycles to crack initiation (LCF);
- Goodman diagram (HCF);
- Fatigue crack growth rate.

Some of the previous listed tests, require a significant amount of time to be experimentally investigated. It's evident the effort required in case of new material selection to analyze the peculiar mechanical characteristics: such eventual need is a critical aspect for the project management, to be evaluated since the earlier phases of the design.

A typical final verification of critical points can be conducted for components subjected mainly to static and thermal loads by means of a low cycle fatigue assessment: the resulting number of cycles to crack nucleation is typically compared with the MTBM requirement of engine cycles. Where dynamic loads are not negligible, adding alternating stress to the static and thermal induced ones, the durability assessment is performed by means of the Goodman diagram, comparing high cycle fatigue material characteristics at the expected temperature with the predicted combinations of mean and alternating stress, as in Figure 2-8. For each critical location, many different points can be verified against HCF failure, due to temperature, mean and alternating stresses variability over the expected engine mission.

Combination of the different failure modes, sometime can lead to a request of additional design margins: oxidation and creep as well as wear out, can reduced size of components, increasing the level of stresses under same loads over the time and engine starts cycles. As general case, all the combinations shall be assumed between the different failure modes, reducing then assessment effort where some of the mentioned failure mechanisms are negligible or not involved at all.

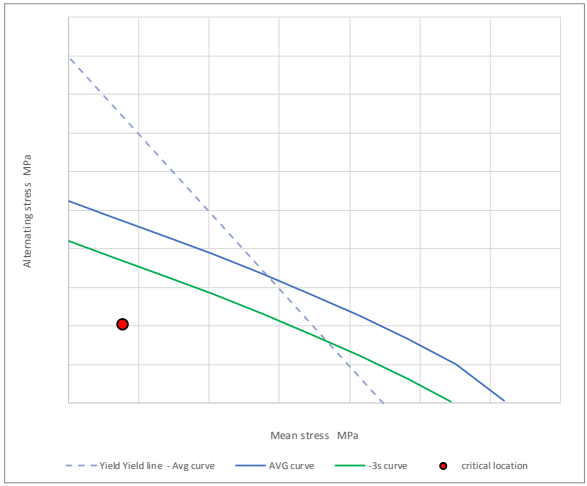

Figure 2-8, Critical points - Goodman diagram assessment

2.6 Manufacturability assessment

Manufacturability assessment is a fundamental part of the design process, which, starting from a concept, ends with the verifications of related manufacturing processes. Cost and time effective projects require a deep co-design between the designers conceiving the ideas to the ones investigating the best manufacturing solution for the desired components, respecting all the design and quality requirements.

The manufacturing process selection is an iterative process, based on the research of the best solution fitting all the product requirements coming from the manufacturing, sourcing, quality and design intent points of view.

The designer starts the design loop providing for the component the first attempt geometry, material, technological process supposed and linear and shape tolerances. Then the co-design phase with manufacturing, souring and quality experts help to select the most promising technological processes and for each of the proposed ones, to understand where specific modifications are strictly needed or suggested. Required changes on the design parameters could lead to a redesign of the component, based on the predicted deformation, stress, oxidation, creep and, in general, all the conditions could affect the component function and durability.

These definitions, correctly representing the technological process worldwide adopted in the engineering could be partially superseded by recent evolutions in the manufacturing technologies. What is the technological revolution which are changing the traditional boundary between the concept development and the manufacturability assessment?

2.6.1 The tridimensional printing of the ideas

Concept development and manufacturability assessment can be conceived at the same time adopting the addictive manufacturing technology.

Then the first question a concept designer should ask to himself when he starts conceiving a new product or component is if it can be realized by AM.

Addictive manufacturing is the process of producing parts through the successive layering of material rather than the removal of material, which is the case with conventional machining. Additive manufacturing can create complex geometries without the use of any sort of tools, molds or fixtures, and without producing waste material: instead of machining components from solid billets of metal, much of which is cut away and discarded, the only material used in AM is what's required to shape the part.

The geometrical freedom of AM technologies allows a part to be engineered as the designer envisions it, without traditional manufacturing constraints. This can translate to extremely lightweight designs and extremely complex tridimensional geometry.

Once the geometry is defined, the manufacturing time is comparable with the fast prototyping schedule: this aspect provides an important advantage in the product managing in general, and especially for new design introduction, which typically requires some different kind of validation tests.

On already existing products, a general criterion to understand if the AM could be successfully introduced as alternative manufacturing process for a component is to consider the current manufacturing complexity: more is complex, more could be the advantage to realize it by AM. In addition, shall considered also if the current AM technology limitations could represent a blocking point: two of the constrains are the envelope of total dimensions and the level of LCF cycles expected [Ref. 16].

The cost trade-off between AM and the other technologies is difficult to be realized: components to be realized by the addictive manufacturing are designed for additive manufacturing. Choices assumed at the basis of the design, indeed, can make this technology the only cheap process to build components not feasible by traditional technologies, or not convenient in the conceived configuration.

One example how the addictive manufacturing is used to reduce manufacturing costs, is the printing of separated components in a single piece, removing the need of joint components, like bolts, nuts or similar, and the flange for joint itself. Already in 2015, a Royal Air Force Eurofighter Typhoon fighter jet flew with printed parts and the Israeli Air Force has also begun to work with 3D printers to print spare parts [Ref. 20]. In 2017, GE Aviation revealed that it had used design for additive manufacturing to create a

helicopter engine with 16 parts instead of 900, with great potential impact on reducing the complexity of supply chains [Ref. 21].
A not negligible aspect, finally, is also the possibility to use AM for the repair of existing components after their maintenance interval: adding material on worn surfaces or repair local defects can be affordable to refurbish components, which are expensive to be manufactured completely new [Ref. 17 and Ref. 19].
Being one of the most recent and attractive technological process it is reasonable to expect further performances increase both from manufacturing and design point of view.

2.6.2 Combustor cooling and technologies

One interesting example of the technological revolution, before mentioned, is contained in the trade-off activities involved by the combustor cooling development and the related technologies adopted.
Combustor cooling is a battle between the desire for longer hot gas path components life and the techno-economic demands of the marketplace. The evolution of cooling system is starting from highly simplistic forms and progressing to increasingly more complex designs having greater capabilities. Yet even with the several generations of design advances, limitations are becoming apparent as complexity sometimes leads to less robust outcomes in operation.
Furthermore, the changing environment for operation and servicing of cooled components, both the natural and the imposed environments, are resulting in new failure modes, higher sensitivities, and more variability in components life.
Over the last approximately 50 years, advances have led to an overall increase in component cooling effectiveness from 0.1 to 0.7. Innovation and invention aside, the performance of the engine has always dictated which technologies advance and which do not. Cooling technologies have been aided by complimentary and substantial advancements in materials and manufacturing. The state-of-the-art now contains dozens of components cooling methods with their many variations, yet still relies mainly on only a handful of basic film cooling forms that have been known for 40 years. Even so, large decreases in coolant usage, up to 50%, have been realized over time in the face of increasing turbine firing temperatures.

Primary areas of greatest impact for the cooling systems are the evolving engine operating environments and the components and systems integration effects, while, from the manufacturing side, the revolutionary manufacturing processes like addictive manufacturing family of technologies.

The selection and detailed design of combustor cooling systems is significantly influenced by the technology adopted to realize the cooling holes. In the wide spectrum of available technology for perforate, an assessment of the most suitable ones for the cooling holes realization in the combustor components has been realized, considering the requirements which identify the peculiar characteristics of geometry and material to be perforated and holes functionalities.
Typical requirements for heavy duty combustor cooling holes are:

- High number of holes;
- Small and very small holes diameter;
- Long length to diameter ratio;
- Tilted perforation angle;
- Typical metal thickness to be perforated less than 10 mm;
- Not high precision required;
- Low cost.

The most diffuse perforation technologies are:

- Punching
- Chip removal machining (drilling)
- Laser
- EBW - Electron Beam Welding
- AWJ - Abrasive Water Jet
- EDM - Electro Discharge Machining

Figure 2-9 is presenting a comparison among the mentioned cooling holes technologies based on the two fundamental geometrical parameters in the design selection: minimum hole dimension and maximum length/diameter ratio.

About the minimum diameter achievable of the hole is not the technological process the real limiting factor: size of the hole by laser, EBW or EDM process small up to 0.2 mm can be obtained, but are not requested for the risk of blocking by dust and other dirty particles. In the practice, the minimum diameter typically required is about 0.5 mm.

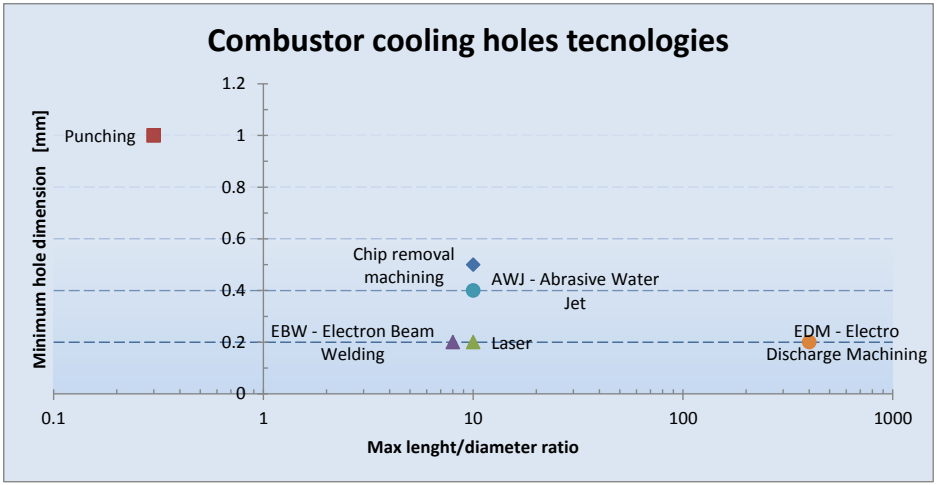

Figure 2-9, Combustor cooling holes technologies

In the following chapters, a description of the mentioned technologies is reported, with the aim to provide useful information for the selection of the most suitable technology for the desired cooling holes application.

2.6.2.1 Punching

In the old-technology heavy duty combustor the cooling air passages was obtained punching the thin metal sheet of liners: a chip process to obtain a high number of slotted holes with a rough geometry. Such simple process was adopted, considering the large amount of coolant air available and the short mean time between maintenance required. The metal plastic deformation caused by the punching process generates peculiar geometries with corners where high stress concentration occurs, caused by temperature gradients and vibration loads, affecting at the end the combustor liner durability.

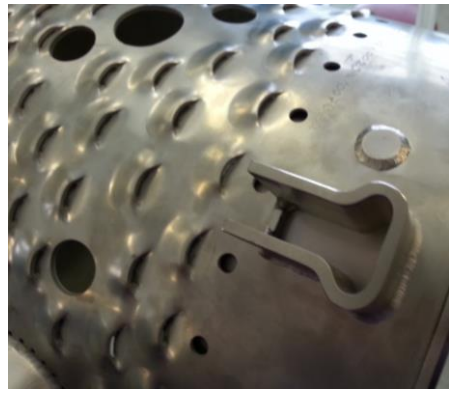

Figure 2-10, Typical punched holes of a liner

A reliable estimation by thermal and structural models of the corners zones is quite difficult for the uncertainties affecting the thermal boundary conditions, as well as the geometrical discontinuity. Finally, the infield experience is showing these potential critical areas as real limiting factors for parts life extension.

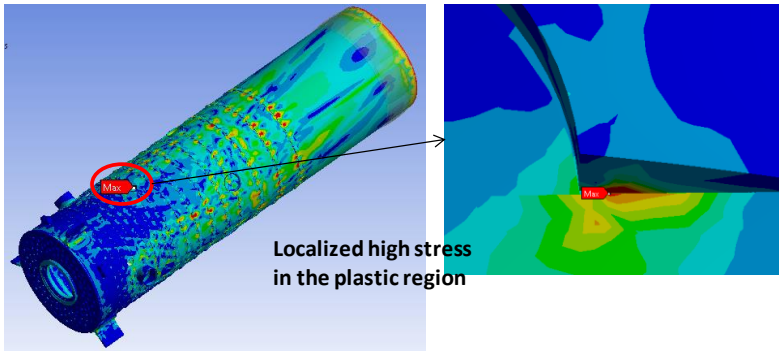

Figure 2-11, FEM detail in the punched region

As the market request of increasing MTBM raises the durability standard for the industrial combustors, punching process has been supported by additional and, in some

cases, alternative cooling holes perforation technologies, as drilling and others chip removal machining processes.

2.6.2.2 Chip removal machining (drilling)

Among the chip removal machining, the most common used is the drilling technology: a rotating drill bit remove material with a high precision, realizing a cylindrical hole.
The small tolerance on the hole shape achievable, quite good in general, are in any case affected by the length to diameter ratio of the required hole: the flexural vibration of the tool during the drilling phase can produce worse shape tolerances in long holes.
Main drawback of this well-known and wide diffused technology is the long-time of execution, wear of the drill bit and risk of its rupture.
All these aspects contribute to classify this technology as expensive.

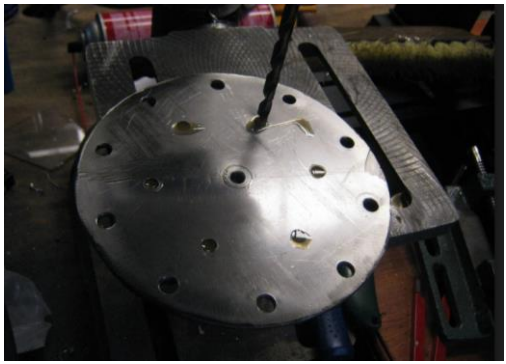

Figure 2-12, Drilling of a combustor end plate

2.6.2.3 Laser

The laser technology key drivers are the fast drilling execution and the capability to drill also coated surfaces with thermal barrier coatings. These two aspects make laser application one of the most adopted technology for cooling holes realization.

However, it's worth to know that there are two main drawbacks, common with all the laser cutting technological processes: the achievable accuracy of the final shape of the hole and the presence of superficial recast metal layer.
The hole shape is influenced by the vapor of the melt material expulsion from the zone of perforation, leading to a typical geometry as shown in Figure 2-14.

Figure 2-13, Laser drilling of a liner

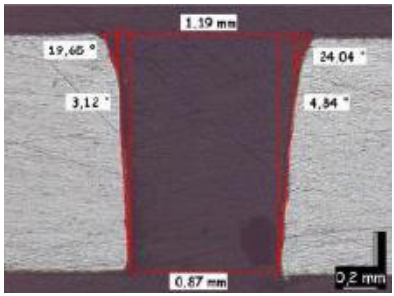

Figure 2-14, Microsection of a laser hole

In complex component geometry, where the hole shall be realized between parallel surfaces, one close to another one, as common required in impingement holes cooling architectures, also a required long sequence of actions shall be considered, aimed to protect the back side surface, which shall not be perforated.
An example of the required sequence of actions is:

- Application of an anti-debris spray;
- Insert sheet of PTFE to avoid back wall strike;

- Melting the PTFE protection sheet in an oven;
- Inspection with mills of each hole to remove internal debris.

However, the limited cost and the fast execution of the holing phase make this process one of the first selection in the cooling hole technology selection, where a lot of holes shall be realized, as common in liner components.

2.6.2.4 EDM - Electro Discharge Machining

In the EDM technology, holes are generated by a series of rapidly recurring current discharges between two electrodes, separated by a dielectric liquid and subject to an electric voltage; the process depends upon the tool and the workpiece are not in contact. Fast execution and capability to drill hard metal alloy, as the commonly adopted super nickel alloys for liners, as well as ceramics coatings, are two characteristics which are making the EDM one of the adopted process for making holes in the combustor components.

Figure 2-15, EDM drilling process

In addition, EDM can cut intricate contours or cavities in pre-hardened steel without the need for heat treatment to soften and re-harden them.
Small hole EDM is also used to create microscopic orifices for fuel system components.

Some small-hole drilling EDM tools can drill through 100 mm of hardened steel in less than 10 seconds: holes of 0.3 mm to 6.1 mm can be achieved in this drilling operation.
In application where the highest length to diameter ration is required, EDM process is the best technological process selection, while, despite of the velocity of execution, cannot be considered a cheap process.

2.6.2.5 Addictive manufacturing

An alternative manufacturing process to obtain cooling holes is the additive manufacturing, already presented in chapter 2.6.1.
The AM technologies leave to the designer the freedom to conceives extremely lightweight designs and extremely complex tridimensional cooling holes geometry.

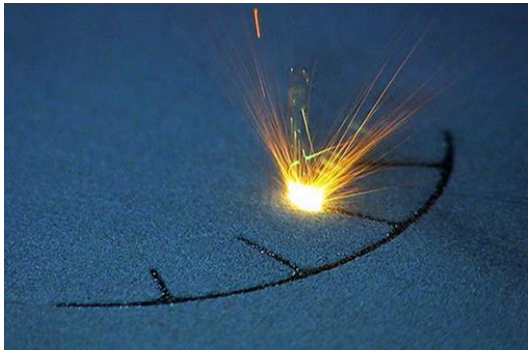

Figure 2-16, Direct metal laser melting machine in action

AM technology uses different raw materials in the form of fine-grain powder, liquid, sheet. A thin layer of raw material is spread out as the blank canvas from which each successive slice of the final part will be created. The DMLM machine uses a high-powered 200-1000 Watt Yb-fiber optic laser to fuse fine metallic powders together to form functional 3D parts from successive layers ranging in thickness from 20 to 100 microns. Specialized equipment reads data from the CAD file, dividing the whole design into a series of thin slices that it assembles in successive layers of liquid, powder, sheet

or other material. Each layer is melted to the geometry defined by the CAD model and fused to the preceding layer.

The build chamber includes a material dispensing platform and a build platform, along with a recoater blade that distributes each new powder layer over the build platform to be fused in a tightly controlled inert atmosphere. The complete part is removed from the powder bed for heat treatment and finishing depending on the application.

A peculiar aspect to be considered about the holes realization is their shape: the only way to obtain perfect circular hole is printing components with the growth direction parallel to the hole axis. Of course, components having holes axes not all parallel, cannot be printed with perfect circular shapes. But it is really needed? Practice demonstrate that if properly considered in the design, such condition does not represent a design significant limitation.

3 Industrial Combustor Cooling Architecture

The activities developed in the frame of the present doctorate include a preliminary assessment of the combustor flow split architecture and the studies on the sealing system between combustor liners and the high pressure turbine first stage nozzle, presented in chapter 8. Then the most relevant part of improvement and innovative development, introduced by the present work, is in the design process analyses and optimization of combustor cooling system, shown in Figure 3-1, of the BHGE NovaLT^{TM} class of industrial gas turbine; see for references from [Ref. 22] to [Ref. 25]. This class is conceived as a family of scalable modules (axial compressor, combustion chamber, high pressure turbine and low pressure turbine) that can be matched to obtain a specific power size in the 5- 20 MW space. The NovaLT16 is a two-shaft gas turbine with a pressure ratio of 19.3: its nominal rating at ISO no losses condition is a shaft power of 16.8 MW and a shaft efficiency of 37.3% [Ref. 22]. Its peculiarity is the adoption of variable NGV at power turbine inlet, a distinctive feature of BHGE products.

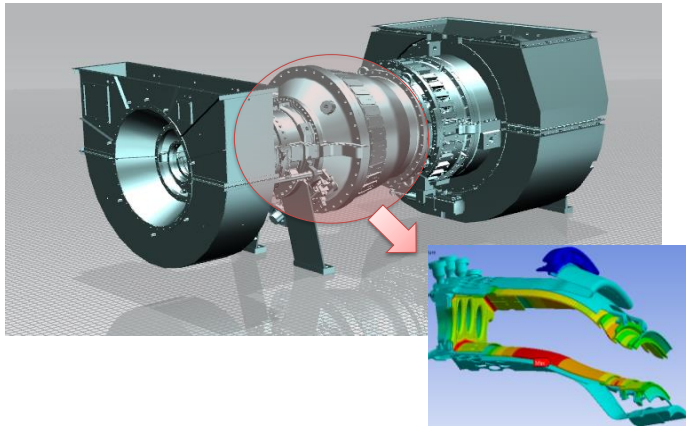

Figure 3-1, NovaLT16 combustor architecture

3.1 Combustor flow split analysis

Considering the NovaLT16 combustor architecture, depicted in the following meridian section view, and the percentage flow split reported in Table 3-1, it's possible to highlight the main requirements can affect the selection of best flow split configuration:

- Flow available for combustion chamber:
  - Reactive air mass flow;
  - Pressure drop;
  - Output temperature;
  - Pattern factor and profile factor.
- Flow available only for cooling purpose of outer and inner parts:
  - Mass flow;
  - Max pressure drop;
  - Max temperature increase.

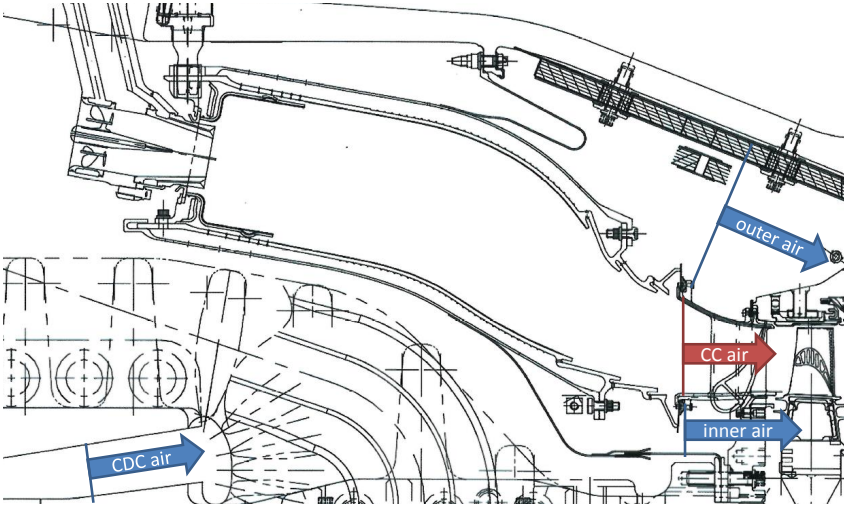

Figure 3-2, Industrial annular combustor cross-section

In the Table 3-1 a typical flow split allocation of an annular industrial combustor is reported, with a cooling schema architecture depicted in Figure 3-2.

To have the most air flow available for liners cooling, assuming the same flow request for the combustion process, the sealing parts design shall meet the following internal requirements:

- Inner baffle leakage should be the minimum possible;
- Outer baffle leakage should be just the minimum required for purging the cavity between casing and outer baffle.

Air split		*%W25*
Compressor Inlet Flow	W2	
Air extraction before Combustor		
Total air flow available before combustor	W*	
outer baffle leakage inner baffle leakage		
Total air flow available before combustor without baffles leakage		
Air flow for nozzles cooling, outer Air flow for nozzles cooling, inner		
		OMIT
Total air available for CC		
available air <u>only</u> for cooling outer **available air <u>only</u> for cooling inner**		
Compressor air nor available for combustion, nor for liners cooling		

Table 3-1, Gas turbine flow split before combustor

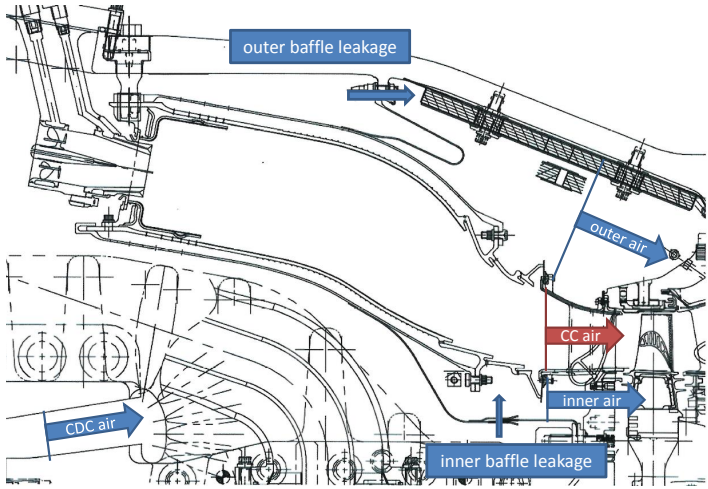

Figure 3-3, Industrial annular combustor cross-section – baffles leakage

A first attempt internal flow split allocation within the combustor design is reported in Table 3-2: analysing these data it can be concluded that, to maximize the air available for combustion process and cooling of heat shields and liners, the leakage of the seals between liners aft-end and first stage nozzle should be the minimum possible.

Combustor air split		*%W25*
fuel mass flow		OMIT
air flow burners (primary zone)		
Outer domeplate air flow (primary zone) Inner domeplate air flow (primary zone)		
HS outer air flow (primary zone) HS inner air flow (primary zone)		
air flow instrumentation ferrules outer (primary zone)		
air flow nuggets outer (secondary zone) air flow nuggets inner (secondary zone)		
gas flow combustor exit	**WA39**	
leaf seals leakage - outer leaf seals leakage -inner	W leaf outer W leaf inner	
gas flow entry S1N	**W395**	

Table 3-2, Combustor flow split

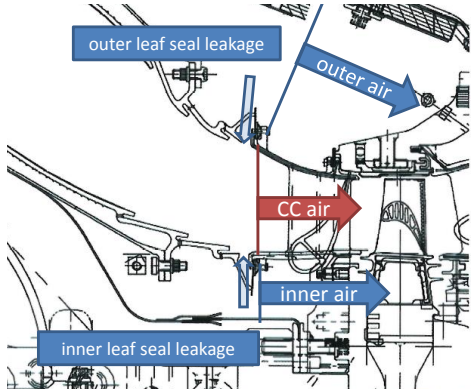

Figure 3-4, Combustor cross-section – liners aft-end / first nozzle seals leakages

The NovaLT16 nozzles cooling flow is in series with respect to combustor cooling one, with exception only for the small amount of leakage across baffles sealing system (0.5% of compressor outlet mass flow).

The main drawbacks of such cooling architecture are:

- Reduced available pressure drop for the nozzle cooling holes: the first stage nozzle is the most critical in the inner side, where start the ducts which food the holes located in the vane stagnation point;
- Higher coolant temperature: the cooling flow for the nozzle is heated during the passage into liner / baffle gaps;
- Reduced reliability of the cooling system: a failure mode of the combustor cooling system (as example the gap closure between baffles and liners) is directly affecting the nozzles durability.

In the following sketched cross-section, an example of a nozzle cooling system in parallel with respect to the combustor is reported.

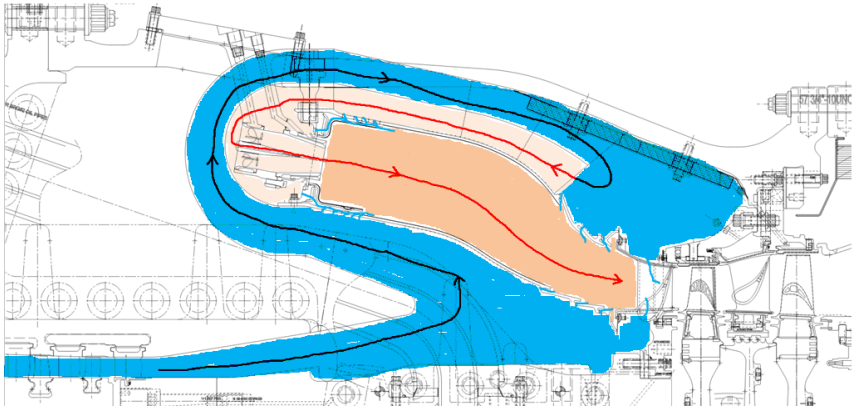

Figure 3-5, Sketched cross-section of a in parallel nozzles cooling system

Such flow split schema has been obtained maintaining the same flow speed in the baffles / liner gaps, avoiding the introduction of higher pressure losses with respect to the current architecture and maintaining the same domeplate and liners dimensions.
The main drawbacks of in parallel nozzles cooling system are:

- Coolant air coming from the CDC to nozzles is not used for any additional cooling purpose of combustor liners cold side;

- Increased radial envelope pf the high pressure turbine vessel of about 50 mm;
- Elongation of the pins supporting the combustor and subsequently increase also of dimension, for their structural resistance;
- Complex arrangement of the domeplate and burner interface, requiring two separate sealing systems:
    - Seal between burner and a hypothetic cowl structure guiding the compressor air flow toward the outer path;
    - Seal between burner and domeplate, by means of analogous ferrule system already implemented in the current architecture.

3.2 Combustor cooling

Although the mechanical stresses experienced by combustor chambers are small in comparison with those affecting many other engine components, liner and flame holding segments are called to withstand high temperature and steep thermal gradients that threaten the structural integrity of the whole module. To meet liner and dome durability requirements, it is important to keep temperature down to an acceptable level. Definitions of "acceptable" are almost arbitrary, but according to Lefebvre [Ref. 3] for nickel-based alloys in common use the maximum operating temperature should not exceed 1300 K against flame temperature that can reach and usually exceed 2000 K. Therefore, the design of a combustion chamber cannot exclude a correct layout of an effective cooling system for the two main critical components of the combustor chamber, which are the dome and the liners. If the impingement cooling has been long recognized as the most performing arrangement for the dome cooling, as far as the liner is concerned the research is still on going, especially with the strong reduction of coolant availability in ultra-lean burn combustors.

The dome is aimed at holding the fuel injectors and above all at protecting them from the severe radiative and convective heat loads from the burning gas. Therefore, this component can be subjected to high thermal gradients and it requires a very effective cooling. Jet impingement is the cooling method that has the most significant potential to increase the local heat-transfer coefficient among all heat transfer enhancement techniques. However, as it will be explained below, the construction of this flow arrangement weakens the structural strength of the component and moreover it requires higher pressure with respect to other cooling architectures [Ref. 33]. These considerations support its use for dome cooling, where pressure level and structural issues are less important than in other components. With respect to other impingement applications in gas turbine cooling, like blade leading edge and endwalls, dome impingement cooling is often applied to quite large surfaces.

Regular arrays of impingement jets are quite commonly used within combustors dome to provide relatively uniform and controlled cooling of the back surface of the heat shield, which is the metal sheet of the dome exposed to the flame: part of the compressor air does not take part to the combustion process and it is used to feed the impingement

array (Figure 3-6). Such regular array is generally directed against the back surface of the heat shield by means of a sheet metal baffle plate, or jet plate, that is fixed in position relative to the dome surface.

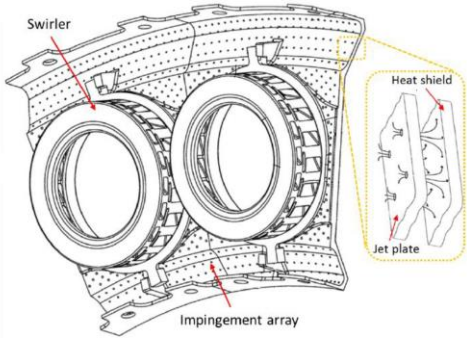

Figure 3-6, Impingement schema for dome cooling

One of the milestone available in open literature focused on impingement cooling was done by Florschuetz et al. [Ref. 34]; besides a comprehensive analysis of the phenomenon, the authors present a correlation that is still commonly employed in technical community as a term of comparison to validate new results. However, it is important to remark that the work of Florschuetz et al. was mainly dedicated to blade and vane cooling arrangements, which typical present higher values of pressure drop across the jet plate with respect to combustor domes. More recently, a deep investigation on impingement cooling from regular and sparse arrays for combustor cooling applications was carried out by Surace [Ref. 35].

For a more effective protection, in some application a TBC is employed to the external surface of the dome to provide a very low conductive layer and thus increase the thermal insulation of the heat shield. Except for this further device, impingement is still the main cooling technique adopted for the dome. With the exception of a geometrical optimization of the array aimed at reducing the air consumption and increase the cooling effectiveness, this method almost remained unchanged switching from RQL to Lean and Ultra-Lean Burn combustors.

Forced convection inside the annulus is the basic method to cool the liners. However, the high temperatures and thermal gradients acting on these components make the forced convection alone not suitable for combustion chamber cooling. Consequently, efforts were spent to integrate systems able of increasing heat transfer surfaces and coefficients that were historically developed for blade cooling. Among them, the most practical to use for liner cooling purposes should be the ribs: indeed, they allow both an augmentation of the heat transfer surface and an increase in heat transfer coefficient due to the high turbulent and unsteady flow field they promote. Ribs have been widely investigated in literature, mainly for blade cooling, and, as a rule of thumb, their use typically permit an increase in the heat transfer coefficient of 2-3 times with respect to smooth surface. Studies on the application of further combustor cooling methods are available in literature, such as impingement cooling or alternative arrangements obtained combining different techniques. Nevertheless, due to their additional manufacturing costs and the increase of the complexity of the system, these techniques have found difficulties to be integrated in the combustor.

The most widely used technique to control the liner temperature is film cooling. It is implemented by injecting relatively cold air bled from the annulus on liner inner side through holes or slot, thus creating a protective film that shields the liner from a direct contact with hot gases.

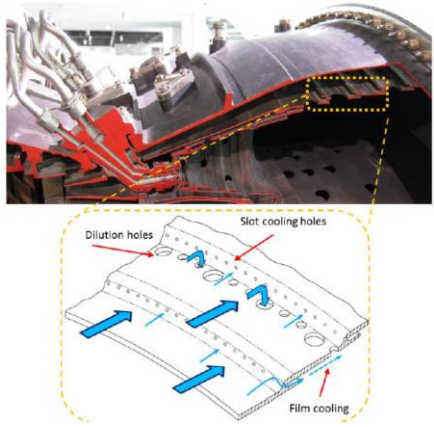

Figure 3-7, Example of liner cooling arrangement

In its basic design, film cooling makes use of a number of annular 2D slots injecting the coolant axially along liner hot surface; the film cooling is gradually destroyed downstream the injection point by the turbulent mixing with hot gas flow, so the normal practice is to repeat a succession of slot along the liner length.
Mechanical robustness and low weight are the mayor advantages of such a technique which has found widespread application in both industrial and aircraft gas turbines. An example of slot cooling configuration is displayed in Figure 3-7; the picture shows also the dilution holes located in some sections of the liner: these holes are necessary to complete the combustion process in a RQL combustor, but they do not contribute to film cooling.
Due to the intensive use of film cooled solutions in the years of combustors development, a great number of theoretical and experimental studies are available in literature. A full description of the flow field behaviour downstream from a slot injection was given by Stollery and El-Ewany; according the authors, three separated regions can be identified: the first comprising a potential core in which wall temperature is very close to that of the coolant, followed by a region where the velocity profile is similar to that of a wall jet, which finally evolves into a third zone where flow conditions become similar to a turbulent boundary layer. The main parameter governing the extension of these zones is the coolant-to mainstream velocity ratio; however, for combustor applications, which are characterized by highly swirled and turbulent gas flow fields, a high dependency on region extension from the swirl number and the turbulence level of free-stream and coolant was found respectively by Yang et al. and Simon.
Effusion cooling is realized drilling a dense array of closely spaced cylindrical holes with a small diameter in the order of few tenths of millimeters (see Figure 3-8).

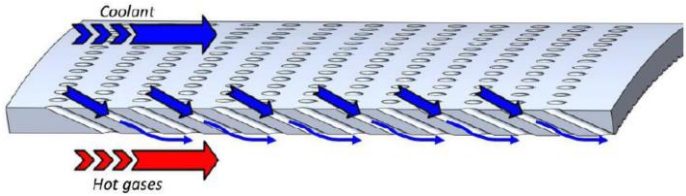

Figure 3-8, Scheme of an effusion cooled liner

The holes have small injection angles, usually 30°, even though it is possible to achieve angles up to 10° to obtain a better coolant protection in the proximity of the wall, in spite of increased manufacturing costs.
The intrinsic features of this cooling technique determine several favorable characteristics:

- the dense array of holes provides a uniform protecting layer, ensured by the continuous coolant injection that gradually increases due to the film superposition;
- holes are characterized by a high length-to-diameter ratio that involves a significant heat sink effect, as a consequence of the force convection with high heat transfer surface [Ref. 36, Ref. 37and Ref. 38];
- the mass bleeding on the coolant side provides a significant increase in HTC, which can contribute up to 30% to total cooling effectiveness [Ref. 39].

Despite the higher manufacturing costs and the lower film protection if compared to 2D slots, at least in the first part of the liner, where superposition is not fully developed, this technique allows to overcome some technological issues given by classical cooling arrangements, making it very attractive for lean burn combustors. First of all, it ensures a very efficient cooling performance with a reduced coolant consumption with respect to 2D slots, as shown in Figure 3-9.
Moreover, effusion systems permit to avoid the protection degradation downstream of the injection point: in typical 2D slot cooling a large amount of air is injected through each slot to ensure a sufficient survival of coolant without using an excessive number of injection points. This leads to an over-cooling in the regions immediately downstream to the slot, involving dangerous thermal gradients that could generate cracks formation, whereas effusion cooling provides a uniform protection and heat removal within the liner.

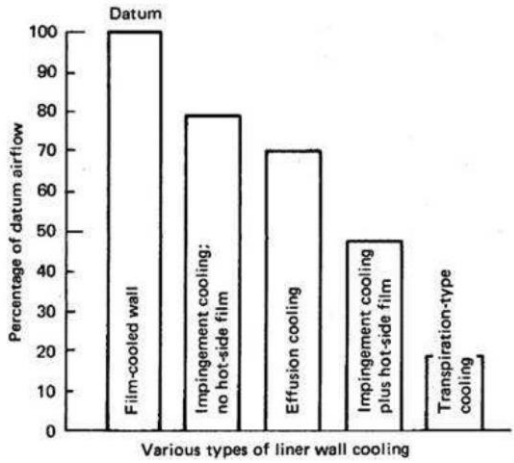

Figure 3-9, Airflow percentage of various type of liner wall cooling

The engineering problem of applying effusion to combustor liner cooling, together with all related physical aspects, has been widely analyzed over the last 40 years, with several contributions available in the open literature. In particular, most part of the studies has usually been aimed at investigating the role of the various flow and geometric parameters on the film cooling effectiveness, generally with simplified configurations (flat plates with uniform mainstream flow). One of the first contribution is due to Kasagi et al. [Ref. 40], where the overall cooling effectiveness of full coverage film cooling plates was measured at different blowing ratios with liquid crystals technique. The focus was put on the role of thermal properties of the plate material. Among the pioneering studies it is worth to cite the contributions by Andrews and co-workers [Ref. 41 and Ref. 42] where the effects on film effectiveness of several parameters, as the number of holes, length and arrangement, were investigated. In their study, [Ref. 43] evaluated row by row adiabatic film effectiveness via Infra-Red thermography and performed flow visualizations by means of Schlieren photography on a full coverage film cooling plate with highly inclined holes (17 degrees) at different blowing ratios, from 0.5 to 4.0, it was observed that, even with high blowing ratio and therefore with full penetration of jets, an appreciable cooling benefit can be measured in terms of adiabatic film effectiveness. This is due to a reduction of gas temperature in the mixing region

contributing to keep near wall temperature low, even without the presence of a coherent film: this is expected to be the process in actual combustor where high blowing ratios are commonly observed.

More recently Martin and Thorpe [Ref. 45] observed an increase of adiabatic effectiveness with realistic high free stream turbulence when using inclined holes at blowing ratio above 1.0: this is due to an increased mixing rate of the jet with the mainstream, which enhance the amount of coolant close to wall region. The investigation carried out by Scrittore et al. [Ref. 46] was focused on the measurement of adiabatic film effectiveness and flow field from inclined effusion cooling jets in a range of blowing ratios (3.2 to 5.0) that can be observed in actual combustors. A large number of effusion rows was considered (20) permitting to observe the achievement of fully developed film after the 15th row. In their recent study, Ligrani et al. [Ref. 47] showed adiabatic film effectiveness and heat transfer for full coverage film cooling configurations in the presence of a streamwise pressure gradient; the effect of the blowing ratio and the influence of dense/sparse hole arrays on the thermal effectiveness are discussed.

One of the most important parameter affecting the final adiabatic film effectiveness of multi row effusion cooling is certainly the inclination angle of the holes.

Among the first systematic studies concerning this aspect is worth to be mentioned Foster and Lampard [Ref. 48] who analyzed the effects of the injection angle investigating a set of geometries with α=35°, 55°, 90°. Great dependence from this parameter was observed, with small injection angle that showed the highest cooling effectiveness at low blowing ratios, while large injection angles were advantageous at high blowing ratios.

First attempts to take into account actual combustor flow field features (not uniform velocity) are due for instance to Ceccherini et al. [Ref. 54], where the interactions of effusion cooling flow with dilution jets or starter film cooling were investigated on single flat plate configurations. The use of high swirling flows for flame stabilization purposes may result in a great interaction between swirl jet and combustor liner, which can deeply affect both convective heat transfer and film cooling protection.

3.3 State of art of numerical modelling

An analysis of the state of art of the approach used in the combustors development by means of numerical modelling has been performed, to contextualize the relevance of the work performed and the level of innovation proposed in the industrial sector.
The design of modern combustors is largely based on the use of numerical tools.

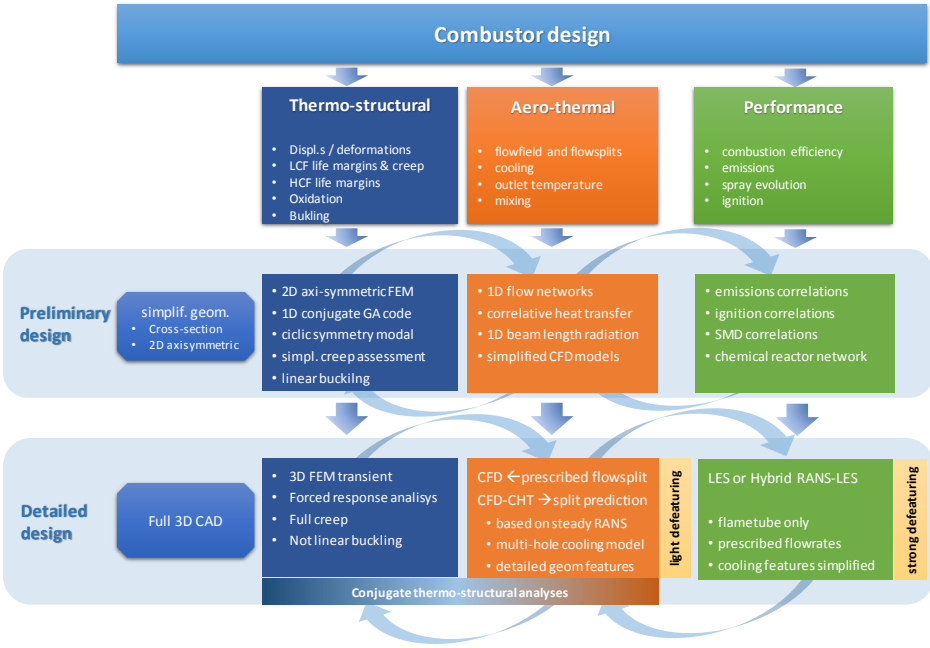

Table 3-3, Diagram of numerical combustor design flow

According to the flow diagram represented in Table 3-3, we may divide combustor design into three streams: the thermo-structural design, the definition of aero-thermal behavior of combustor and the evaluation of the performance related to the combustion process. The three streams are obviously closely linked to each other, but the necessity to introduce assumptions and simplifications in the numerical models brings to adopt different tools for the prediction of the specific targets. Thanks to the improvement in physical models and computational resources, in the last years the use of CFD is getting

more and more important in the overall process, moving to the earliest design phases and allowing the use of more accurate approaches.

In particular, it can be stated that, in each line, the state of the art in the most accurate numerical tool is represented by different CFD modelling strategies. It is widely accepted and recognized that LES or hybrid RANS-LES calculations could be an accurate method to analyze turbulent spray flames thanks to a more physical predictions of turbulence effects on flow-field, mixing, spray evolution and combustion process. However, high computational costs related to such type of models force to often limit the investigation to flame-tube only, with strong geometry de-featuring and simplification of geometrical details especially in the cooling system. On the other side, the requirement to have a full prediction of combustor flow-split and metal temperature brings to the adoption of CHT calculations, which are usually carried out with steady RANS methods because of the necessity to have a more precise discretization of detailed geometrical features.

A separate tool conjugate heat transfer calculation (ST-CHT), as proposed by Andreini and Mazzei [Ref. 60], can be used for the prediction of aero-thermal behavior of the combustor, mainly focusing on liner metal temperature, flow splits and outlet temperature distribution. The ST-CHT calculation is realized by a runtime coupling of different numerical tools modelling the different physics involved the process. Basically, three different 3D numerical models are coupled (see Figure 3-10):

- Steady reactive RANS CFD model of the fluid domain;
- Radiative heat transfer model of the flame domain;
- Heat conduction in the solid parts.

The advantage of this approach, with respect to fully coupled CHT strategies, commonly provided also by commercial codes, can be summarized in the possibility to use specific and dedicated tools for each physics. Despite the use of separate solvers to handle the various physics aspects involved may affect computational costs, the use of dedicated optimized tools for each physics may help to recover this gap and permit to adopt optimal models for each step. This approach provides also the possibility to play on heat loads exchange among domains to introduce specific corrections coming from design

best practices. The produced results can be post-processed in a design-oriented fashion, making possible to easily understand the single contributions concurring at final aero-thermal state. Separate domains allow to more easily introduce simplifications to handle complex geometric features in a cost effective way.

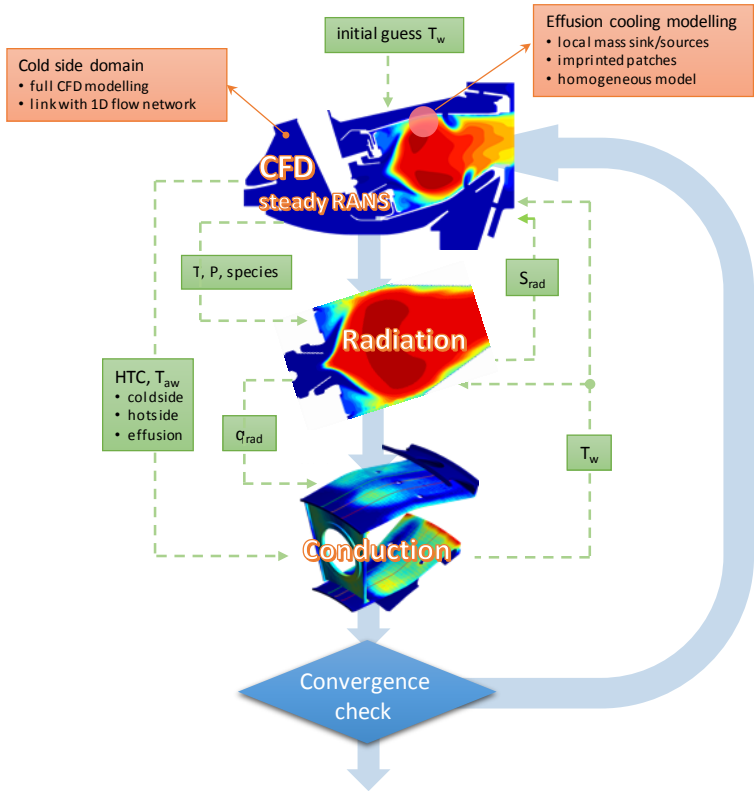

Figure 3-10, Schematic description of ST-CHT methodology

An example in this sense is the modelling strategy required to consider multi-hole cooling without having to explicitly mesh each hole. A proper discretization of a single cooling hole would require over than 500 thousand cells. Thousands of perforations that can be encountered in a real combustor makes this direct approach not feasible in terms of computational costs.

An available option, proposed by Andreini et al. [Ref. 58], consists in replacing full explicit meshing of each hole with local source / sink points for mass and heat. Such elements are applied on cold-side (sinks), hot-side (sources) and metal (only heat sinks): delivered mass flow and heat exchanged by each hole is computed at runtime starting from the pressure drop probed in the CFD domain and according to a set of inputs provided by the user (see Figure 3-11).

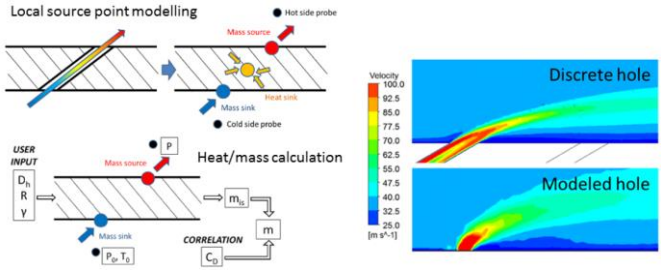

Figure 3-11, Description of the local source point modelling for multi-hole cooling

In an early phase of the design, the ST-CHT model can be setup by replacing the CFD modelling of the fluid domain on the cold-side by a runtime coupling with a 1D flow network solver, depicted in Figure 3-12. This option can be very useful during design phase permitting to rapidly test different cooling perforation geometries without having the necessity to modify the CFD domain and simply working on the 1D flow network.
The drawback of the decoupling behind ST-CHT methodology is the impact on computational costs due to the segregation of the single executions and the necessity to introduce specific tools to manage data transfer and mapping among the different domains.

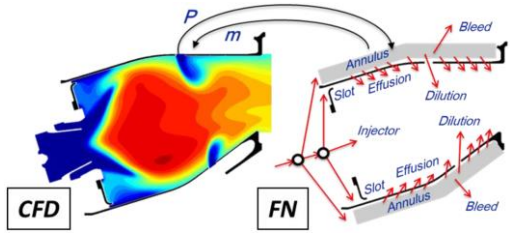

Figure 3-12, Description of the runtime coupling CFD-Flow network

Hereafter, restricting the scenario, a state of art assessment of combustor CFD predictions by Scale Resolving methods and most recent advancements regarding unsteady Conjugate Heat Transfer is reported.

Multi-scale physics phenomena contributing to spray flames, have always represented a very challenging task for CFD modelling, especially in presence of high turbulence levels usually required in real scale devices to obtain stable compact flames with high heat release rates per unit volume. Limitations connected with RANS approaches in predicting the mixing process and the role of fluctuating scalar fields on the chemical reactions, have represented a great penalty in the prediction capabilities of CFD methods for this type of flows. LES methods for the investigation of turbulent spray flames have therefore become a more and more common tool in last 15 years, thanks to the continuous developments in numerical schemes and turbulent combustion models prompted by a constant increase of computational power.

The analysis of laboratory scale configurations (simplified burner geometries with operating conditions close to atmospheric) has represented the most common application of LES, aiming at validating new models or at improving the basic understanding of involved physics. In the last 20 years, several fundamental studies have contributed to define and validate reliable and accurate models for LES codes, especially regarding turbulent combustion and basic numerical discretization schemes.

The application of LES to the study of real scale combustors at realistic operating conditions has started in the last 10 years with pioneering studies dated around 2006. According to the recent review of Gicquel et al. [Ref. 61], when LES is used to investigate annular aero-engine combustors two distinct families of applications can be differentiated for single sector or full annular combustors.

Single sector combustors represent the most common approach. As discussed in previous sections, domain is often limited to the so-called flame-tube with prescribed flows at air and fuel inlets coming from measurements or other CFD simulations. Relevant early applications are the contributions due to [Ref. 62] and [Ref. 63] where aero-engine RQL combustors are investigated.

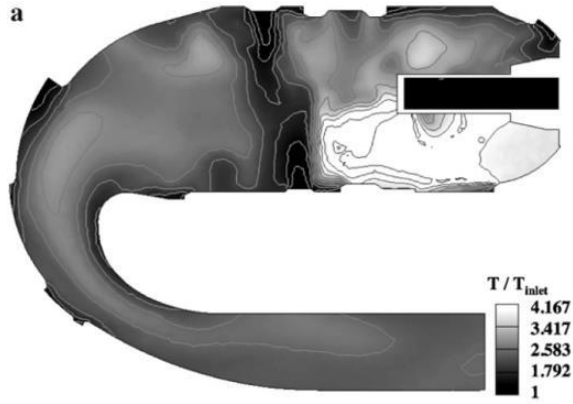

Figure 3-13, Instantaneous temperature field obtained by LES

The introduction of hybrid RANS-LES formulations, mainly DES, DDES and SAS have progressively allowed to carry out investigations including additional geometrical details up to the full chamber casing. Particularly interesting are the recent contributions due to Pratt&Whitney [Ref. 64] and Honeywell [Ref. 65 and Ref. 66]. Particularly relevant is the contribution of Rida and coworkers regarding the assessment of SAS on Honeywell combustors: even with larger time steps with respect to full LES, SAS draw out comparable results confirming its potentiality as a cost effective Scale Resolving approach.

Figure 3-14, SAS (left) and LES (right) time averaged temperature prediction

Thanks to the regular increase of the computing power and of the scalability efficiency of parallel numerical codes, the application of LES to the analysis of full annular combustors has become a possible approach in the last years. This type of huge effort is however justified only where the presence of azimuthal modes in the dynamic behavior of the investigated case become a key aspect. The most relevant application is certainly the prediction of thermoacoustic modes which is becoming a key design issue also in aero-engine applications with the introduction of lean burn combustion: the study reported in [Ref. 67] represents one the first applications.

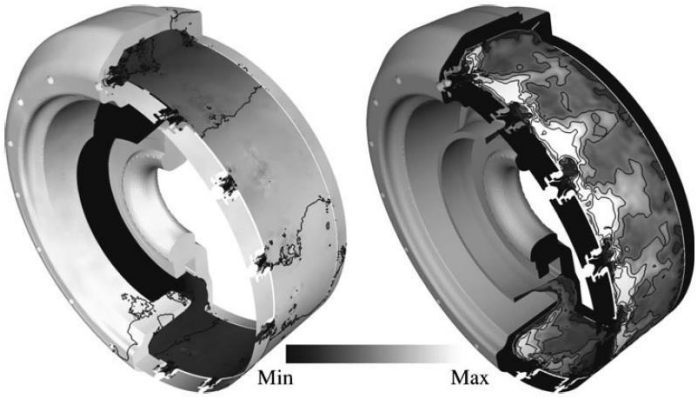

Figure 3-15, Full annular LES calculation predicting azimuthal pressure oscillations

Another ground-breaking application for LES in full annular domain is the simulation of ignition process and in particular of the light-around sequence. In the work of Boileau et al. [Ref. 68] a complete ignition sequence of an aero-engine combustor started from two opposite ignitors is studied, pointing out modes and velocity of the light-around process. Particularly relevant is the work of Fedina et al. [Ref. 69]: objective of the calculation, carried out with Open-FOAM, was to verify the impact of considering a single periodic sector or a full annular domain in the analysis of a reverse flow RQL combustor. Authors concluded that basic features of the flow, mixing and combustion are equally predicted by the two models but some detailed aspects of combustion dynamics can be captured only with full annular approach.

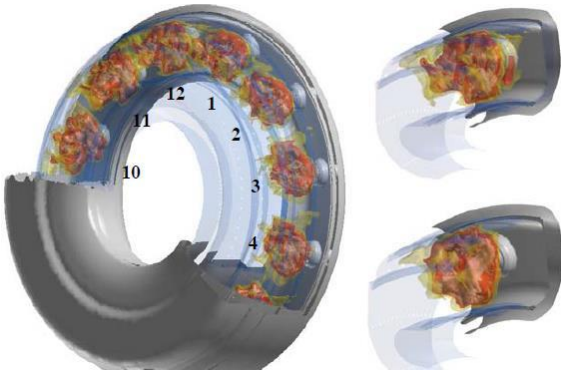

Figure 3-16, Comparison full annular to periodic single sector

It is worth to be mentioned some research activities of the DREAMCODE program performed in the SAGE6 demonstrator [Ref. 70]. A set of submodels to improve the prediction of pollutant emissions in LES calculations have been developed or further assessed: FGM turbulent combustion approach, the Smoothed Particle Hydrodynamics for the prediction of spray evolution and a detailed reaction mechanism for jet fuel surrogate. A larger set of design disciplines are on the contrary faced by DYNAMO project [Ref. 71], ranging from combustor cooling up to thermoacoustic prediction.

Conjugate Heat Transfer modelling is a typical multi-physics problem where interaction between different phenomena occurs. In a combustion chamber these phenomena are mainly fluid convection, combustion, solid conduction and radiation but, in aero-engine, the use of liquid fuels adds the requirement of two-phase flow characterization. Different physics require the choice of different domains, equations and nonetheless time and space scales, which often lead to prefer independent codes for each solver. Several works deal with CHT problems, mainly using steady solver for fluid computation. Gimenez et al. [Ref. 72] developed a coupling methodology for weakly transient CHT problems, where a transient calculation for solid was coupled with a steady solution for fluid updated every coupling loop. However, in combustion chamber the high turbulence generated by the swirler can cause considerable temperature fluctuations. When swirling jet impinges to the liner or the flame stabilized near the walls these

fluctuations result in strong variation of wall heat fluxes. Schmidt and Starke [Ref. 73] applied to gas turbine blade a thermal procedure in which the fluid flow is simulated in a time-resolved way, while the heat conduction in the solid is assumed to be in steady state. This methodology can be suitable for blade cooling problems, characterized mainly by coherent low frequencies – high energy fluctuations.

On the other hand, when unsteady heat fluxes with considerable energy are spanning a wide range of frequencies and solid walls thickness are very small, solid responds quickly to fluid temperature fluctuations. When this condition occurs, as in combustor liner cooling, both fluid and solid solvers need to work in an unsteady manner. He and Oldfield in [Ref. 74] concluded that taking into account the unsteady solid behavior is required to get accurate heat flux amplitudes. In this case, other different problems, such as the selection of boundary conditions at interface and of time steps, the synchronization of solvers and the interpolation schemes shall be addressed.

In the state of art regarding the application of unsteady conjugate heat transfer to gas turbine combustors, particularly relevant are the works of Jaure et al. [Ref. 75] and Duchaine et al [Ref. 76], where all the basic aspects related to a full unsteady CHT calculations are clearly addressed. An Unsteady-CHT simulation is definitely time consuming mainly because of the discretization and time scale requirements of the Scale-Resolving solution of the CFD domain. A so-called Parallel Coupling Strategy (PCS), where both solver run together, should be preferred with respect to a sequential approach (SCS) where long waiting times are needed on both solvers. In the former approach, therefore, the synchronization of the two solvers in CPU time becomes a key point to reduce wasting waits. Coupled simulations must attain the good physical events coupling time in the simulation at the same computational time in the computer. Usually, when the final steady state is the only objective of the analysis, a synchronization in the physical time is not required while it is important to allow the different solvers to run until steady state with the same convergence rate. Communication of the data at the interface of the solvers is usually performed by exploiting dedicated tools (see for instance OpenPALM [Ref. 77]), which could be able to directly access to memory. In this regard, proper interpolation schemes are required to avoid aliasing effects.

3.4 Liners cooling architecture

The combustor liners cooling architecture adopted in the BHGE NovaLT class of industrial gas turbine is based on improved cold side forced convection, to limit the use of film cooling, minimizing the impact on lean burning flame. Improvement is obtained by means of turbulators, applied on the liner cold side, and shaped flow sleeves, or commonly called baffles, able to control cooling air velocity within gaps, as shown in Figure 3-17. This type of cooling concept is common in heavy duty gas turbines, as it allows to control convective heat transfer on the cold side of the liner even in presence of large annulus volumes. A study of such cooling scheme can be found in Bailey et al. [Ref. 79], where CFD computations and measurements were carried out to support the design of GE F class heavy duty gas turbine.

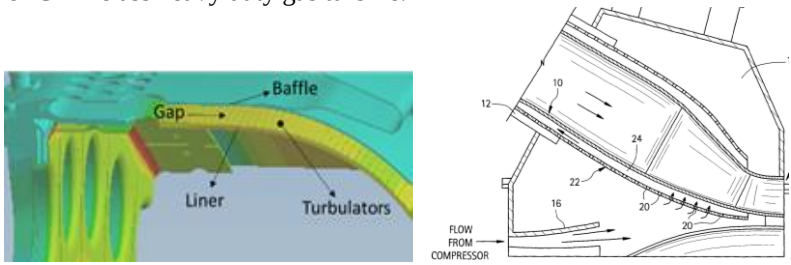

Figure 3-17, NovaLT class Baffle concept

One peculiar aspect of this cooling scheme is the strict dependence of the overall cooling effectiveness on the coolant passage areas into the gap obtained by the baffles. An increase in coolant passage area would result in a reduction of flow velocity and therefore heat transfer, while a reduction of the gap would increase pressure losses or become critical for undesired contact of liner and baffle surfaces.

Besides the strict requirements in terms of manufacturing and assembly to respect the desired radial envelopes of liner and baffles surfaces, the evaluation of overall cooling effectiveness should consider the thermal expansion of the solid parts, which may heavily affect the actual cooling passage area. Due to the strong coupling between cooling process and actual geometry of the system as determined by thermal expansion, a full conjugate aero-thermal-strain is in this case highly recommended.

A similar approach, which is sometimes also referred to as Fluid Structure Interaction (FSI), is up to now rarely applied to the prediction of liner metal temperature and very few published works can be found in literature.

3.4.1 Fluid-Structure Interaction state of art

First adoption of the FSI approach in literature can be found in the pioneering work of Bailey et al. [Ref. 79], where the suggested methodology is applied in the study of a can annular combustor configuration, provided with flow sleeves. In this work experiments and numerical simulations were conducted to understand the heat transfer characteristics of a stationary gas turbine combustor liner cooled by impingement jets and cross flow between the liner and sleeve. Heat transfer was also aided by trip-strip turbulators on the outside of the liner and in the flow sleeve downstream of the jets. The study was aimed at enhancing heat transfer and prolonging the life of the combustor liner components. Using a CFD model, the flow distribution within the flow sleeve and the heat transfer coefficients on the liner were both predicted and the results obtained were compared to the experimental data collected in a flat plate rig test setup.

Another reference work at the basis of multidisciplinary analysis tools development is the one of Kiewel et al. [Ref. 80], published since the 2002 and summarizing the experience of the comprehensive research activities sponsored by the Deutsche Forschungsgemeinschaft from the 1984 to 1998 at the University of Karlsruhe (TH) on the high intensity combustors – steady isobaric combustion. Such studies were applied both to aeronautic and industrial gas turbine combustors.

In a more recent paper, Kim et al. [Ref. 81] adopt the FSI approach on a combustor architecture with flow sleeves of a competitor engine, to obtain an accurate and reliable prediction of metal temperature, to be used in analysing liners deformation, thermal stresses and lifetime. Similarly, in the work documented by Matarazzo and Laget [Ref. 82] on a combustor architecture with flow sleeves of a competitor engine, despite of the not conclusive results in the combustor life prediction, several useful information in the model setup with FSI approach are provided.

Shahi et al. [Ref. 83] presents a simulation of two-way fluid structure interaction in a tridimensional model combustor for a coupled acoustic-elastic system composed of the

liner and the flue gas domain in the combustor. Computational fluid dynamics analysis is performed to obtain the thermal loading of the combustor liner and finite element analysis renders the temperature, stress distribution and deformation in the liner. The software used is ANSYS workbench 13.0 software, in which the pressure and displacement information is exchanged between fluid and structural domain transiently. In the recent study of Tinga and co-workers [Ref. 84 and Ref. 85], a more comprehensive approach is presented: a detailed description of the boundary conditions transition from the CFD model, analysed using the ANSYS CFX 5.7 solver, to the FE model, analysed with the commercial code MSC.Marc 2001, is provided. Of relevance, also the criteria provided for a simplified evaluation of the creep strain and for the number of cycles to cracks nucleation, to be used in the early stages of design, while detailed models cannot represent the best compromise between accuracy and computational effort.

3.4.2 FSI one-dimensional codes

In the development of new industrial gas turbines, short time to market is a requirement increasing every year its level of importance. Furthermore, testing phase is a mandatory step in the development process of ultra-lean premixed technology combustors for the full assessment of the flame ignition and stability as well as emission and acoustic pressure pulsations in a wide range of operability conditions. Most of times annular combustors require a full annular rig to be developed, manufactured and instrumented. Moreover, test results should be available since the earliest engine design phases, as reliable combustor design should be released well in advance with respect to other gas turbine modules, to execute the required engine manufacturing and testing phases.

Therefore, in the feasibility studies first and then in conceptual and preliminary design phases, the most useful tools are the ones able to capture the main physical problems which shall be solved with the minimum time required in modelling. Role of preliminary studies, supported by these tools, is to guide the system level trade-off to define main components size, interfaces and constraints among the different modules and verify the design agreement with the product specification requirements.

A compromise between accuracy and computational effort must be found for each application. Although the use of three dimensional CFD codes within conjugate multi-

disciplinary approaches [from Ref. 86 to Ref. 94] is getting more and more common approach since the early step of design, robust one-dimensional codes are still fundamental tools for the design of complex systems, such as cooling schemes for combustor chambers or gas turbine vanes and blades. They are usually based on the use of lumped parameters models, arranged in networks, to represent the whole combustor cooling circuit. Such type of codes should be characterized by a wide library of elements used to describe the different parts of the system, from simple models representing orifices or straight pipes, up to more complex ones, used to describe not trivial cooling arrangement, such as impingement or effusion cooling. Each model solves the one-dimensional form of the Navier-Stokes equation and it includes dedicated correlations to describe pressure losses and heat transfer of a specific part of the combustor [Ref. 90]. According to the methodology early proposed by Lefebvre [Ref. 3], to provide a complete analysis of the cooling system, the solution of the cooling network must be coupled with additional tools to predict heat loads on the critical parts of the chamber. The purpose is to set the boundary conditions to solve the thermal conduction across the solid volume: for instance, the output of this calculation can be the temperature distributions along the liner walls, which can be used to assess performances of the combustor cooling arrangement under investigation. An example of such type of methodology can be found in the work of Andreini et al. [Ref. 90].

The main strength of such 1D methodologies lies in the short time needed to model the system and to run the simulation, making them powerful tools in the conceptual and preliminary design phases. In addition, thanks to their ability of easily manage boundary conditions with complex geometries, they may also be used performing Design of Experiments calculations to indicate useful data correlations or trends and the relative importance of the operating parameters, as done by Bonini et al. [Ref. 94], Cerutti et al. [Ref. 95] and [Ref. 96].

Thanks to the above characteristics, meeting the typical industrial needs of new combustors development, a FSI code has been developed to be used in the baffle design and optimization: a detailed description of the code is in chapter 5, while in chapter 4 a comprehensive explanation of the design process is reported.

4 Baffles Design Process and Optimization

The design process of the baffles starts after the definition of the combustor liners geometry, as described in chapter 2.5.

Given the liner hot side thermal boundary, the maximum available pressure drop and the maximum acceptable liner temperature, a guess baffle geometry is typically introduced for the enhancement of the cold side forced convection.

In Figure 4-1 a schema of the baffles design process is reported.

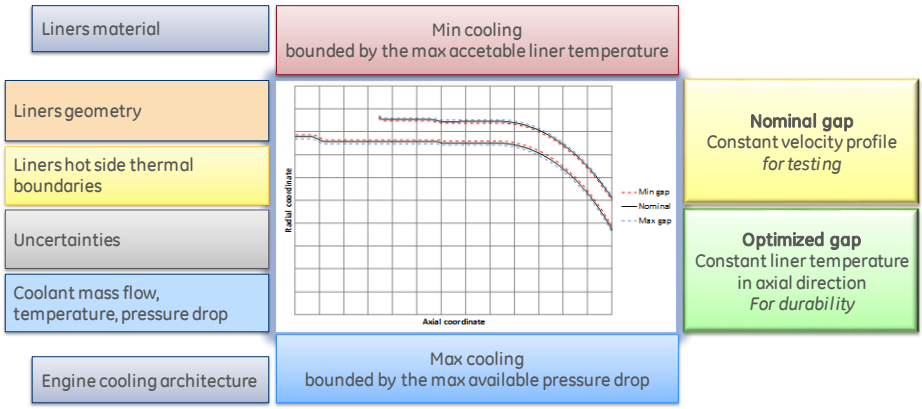

Figure 4-1, Baffles design process

Liner hot side thermal boundary is obtained during the early stages of the design by means of ad hoc correlations for the different liner cooling systems adopted and by means of CFD analyses.

Then, typically in the development plan of a new combustor, an experimental test is performed: one of the first and most important design variables shall be validated during combustor tests is the liners hot side thermal boundary, in the worst expected operating conditions. Liners hot thermal boundary, mainly function of the selected burner configuration and its operability, is typically validated by means of liners cold side metal temperature measurements.

The available pressure drop for the baffle design is defined considering the required pressure drop needed by all the cooling systems which can be positioned downstream to the liner / baffle gap, like coolant flow injections of the liner itself and of first stages nozzles. The computation of such value is performed typically my means of a hydraulic network model, linking the available coolant mass flow with its local pressure drop across the liner / baffle gaps.
Recalling the one of the conclusions reached from the flow split analysis described in chapter 3.1, to maximize the air available for combustion process and cooling of heat shields and liners, the leakage of the seals between liners aft-end and first stage nozzle should be the minimum possible. Therefore, in parallel to the design process and optimization of the baffle, plays an important role in the liners cooling enhancement the execution of studies aimed to increase the reliability of the combustor flow split prediction and to identify areas of improvement of the sealing; chapter 8 describes the investigations performed on the liners / S1N sealing systems.

A maximum acceptable liner metal temperature is defined based on the selected material characteristics against the LCF (number of cycles to crack initiation), oxidation and creep. Nickel super alloys, typically used as material for liners, have good resistance to LCF, oxidation and creep, reason for their wide application is this technical field, while in general limited to a limit operative temperature: overcoming this temperature the mentioned characteristic start decreasing rapidly with the temperature, as in Figure 4-2. During the preliminary design, such limit temperature is assumed as the maximum acceptable, while in the consecutive development phases can be increased, based on more accurate aerothermal and structural analysis results.
The selection of the maximum acceptable liner temperature can have a significant impact on the liner costs, since it impacts directly on the material selection.

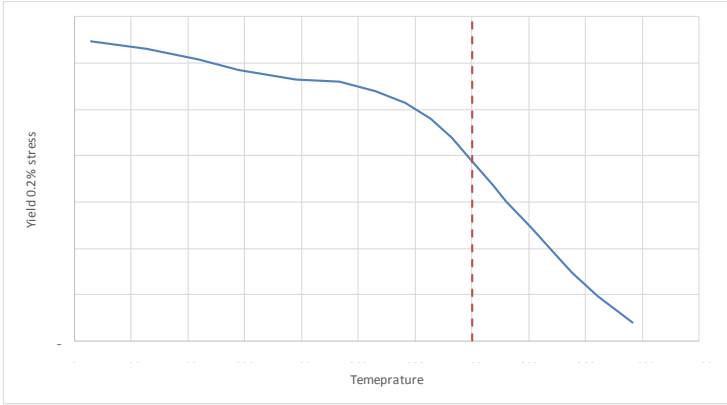

Figure 4-2, Nickel alloy yield stress as function of temperature

First attempt baffles geometry in hot condition is typically defined to generate an axial constant velocity gap, computing the desired cross-sectional area on the base of the available coolant mass flow and its density.
Selection of the axial constant velocity criteria for the gap sizing, which means an axial heat transfer coefficient substantially constant, is based on the validation strategy of the combustor design.
Considering that typically uncertainties in the thermal boundary estimation are higher for the liners hot side respect to the cold side, the more robust procedure to obtain the liners hot thermal boundary is to compute it, starting from the measured metal temperatures, having ideally an axial constant cold side heat transfer coefficient.

In hot conditions, the gap between the liner and baffle surfaces is affected by the thermal expansion of both the parts: baffle is substantially isothermal with a temperature close to the coolant one, while the liner reaches the highest temperatures with a not uniform distribution, function of the local heat balance. The considerable axial temperature gradients of liners, as well as manufacturing tolerances, can locally generate two possible undesired conditions: a gap larger than the expected, leading to less effective cooling, or a closer one, leading to higher pressure losses and risk of contact between liner and baffle during operation.

The combination of relative liner and baffle positions for the inner gap has an opposite sign with respect to the outer gap: outer gap is decreasing from cold to hot condition, while inner gap is increasing. This behavior results by the fact that liners are hotter then baffles.

Analysing the architecture of annular combustors, the outer baffle is a structure surrounding the outer liner, while the inner baffle is a structure surrounded by the inner liner. Radial deformation of both liners and baffles cannot be constrained, being thermal induced: as consequence, the only constrain can be applied shall work along the engine axis direction.

Baffle can be axially constrained to the liner body or to surrounding engine components, like the vessel. In case liner and baffle are not mutually constrained, axial relative displacements can occur between the liner and the baffle, due to the different thermal expansion of the chain of components which are providing the axial support of both liner and baffle. Such relative displacement, once the thermal behaviour of the relevant engine components is known, can be opportunely considered in the definition of the axial assembly position, to meet the desired relative position in hot operating conditions. This aspect can be relevant for baffle and liner geometries comprising conical sections, introducing also a radial variation of the gap with liner, once is not affecting cylindrical parts.

During the engine transients, and, in particular, at flame ignition and blow down, the different thermal inertia of the chain of components which are providing the support of both liner and baffle can generate an axial misalignment between the two, altering the cooling performance: in the baffle design enough clearance between liner and baffle shall be guaranteed to avoid any contact of the components.

4.1 Gap uncertainties estimation

In addition to the thermal deformation of liner and baffle from cold to hot operating condition, which can be deterministically analyzed when the metal temperature distribution is known, there are different kind of uncertainties which are affecting the estimation of the relative gap as well: uncertainties in the components metal temperature estimation, as well as, the liner and baffle shape tolerances and the chains of mechanical tolerances of connected parts, as illustrated in Figure 4-3.

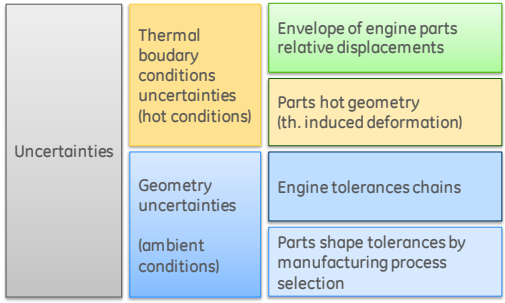

Figure 4-3, Gap estimation uncertainties

It is worth to mention that some of these uncertainties, as the manufacturing tolerances, are proportional to the combustor size, while the gap value, being selected on the basis of the desired cooling performance, is constant among different size of combustors: their percentage impact on the overall gap value is increasing with the combustor size.

These uncertainties shall be carefully considered in the design, since, increasing the combustor size, can be considered as an upper boundary for this kind of cooling architecture.

To opportunely consider all these aspects, the first attempt baffle geometry is defined as nominal condition, then two worst cases of maximum and minimum gap are evaluated.

The minimum gap condition of the outer gap is obtained combining statistically the mentioned uncertainties to have increased axial and radial coordinate of liner and decreased axial and radial coordinates of baffle, vice versa the maximum gap condition

of the outer gap is obtained combining statistically the uncertainties to have decreased axial and radial coordinate of liner and increased axial and radial coordinates of baffle.

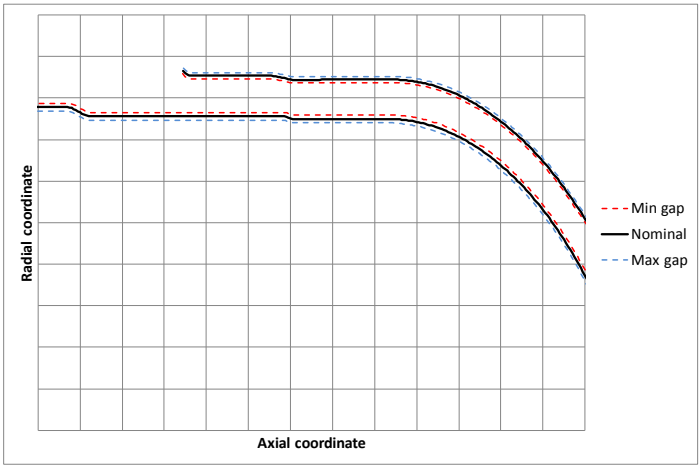

Figure 4-4, Outer gap nominal, minimum and maximum gap

Nominal			Min gap				Max gap			
axial	OL nom	OB nom	OL min gap		OB min gap		OL max gap		OB max gap	
Xnom	**OLnom**	**OBnom**	X+UxL	OL+UrL	X-UxB	OB-UrB	X-UxL	OL-UrL	X+UxB	OB+UrB

Table 4-1, Outer gap nominal, minimum and maximum gap combination

Liner and baffle metal temperatures are affected by the uncertainty inherent the estimation of the thermal boundary used to compute it.

In particular, liner temperature distribution can be considered affected by an important error until these are not obtained from validated models: any combustor development strategy relies on an experimental validation of the liners hot side thermal boundary.

In the early phase of design, once tests are not yet performed, these uncertainties are estimated performing sensitivity analyses: nominal HTC and bulk temperature are changed respect to the expected values in a range of confidence, which is acquired in the frame of precedent developments and tests or combining different kind of simulations. Hypothesis used in the setting phase of the sensitivity analyses are

subjected to the analyst experience and sometimes it's difficult that these are demonstrated in a rigorous way: the uncertainties connected to the uncertainty estimation are typically accepted as a second order, negligible error.

Liners and baffles linear dimension tolerances can affect the global cross-sectional passage area of the coolant, significantly altering the cooling performance, linked to coolant velocity, and pressure drop.
Liners and baffles shape tolerances instead can affect locally the cooling performance, generating locations where the gap results more close or open than desired. Nevertheless, the impact of larger shape tolerances can lead, in the worst case, to a undesired contact between liner and baffle: for this reason, a careful evaluation of both linear dimension and shape tolerances shall considered in the design development.
The liner and baffle manufacturing process selection is an iterative process, based on the research of the best solution fitting all the product requirements coming from the manufacturing, sourcing, quality and design intent points of view, as described in chapter 2.6.

Since all the tolerances derive from the selection of the manufacturing processes for liners and baffles, they can change along the design process, later during the engine production phase and also during the maintenance and repair activities.
Availability of manufacturers change in time, because of the natural commercial turnover and the research toward cheaper business partners.
Availability of technological processes, as well as, change in time for the evolution of the process itself, for research toward cheaper solution, for change of the relevant legislative normative and other casual event and accidents.
These aspects shall be carefully considered in a mature design: a design tolerant for larger ranges of manufacturing tolerances more likely can establish as best solution.

The relative axial and radial position between liner and baffle, during the engine assembly, can change as function of the linear and shape tolerances of the components which are providing the axial support of both liner and baffle. Even if it cannot be

provided a general statement about the possible combinations of such tolerances, being strictly related to the adopted engine architecture, anyway it is possible define the approach could be used to opportunely consider them in the design process.
Equation 4-1 is a simple rule, suitable for the preliminary design phase, to combine statistically the chain of tolerances.

$$x_{tot} = 1.5 * \sqrt{\sum_i x_i^2}$$

Equation 4-1, Stack-up of tolerances for preliminary design

A good practice to minimize the undesired uncertainties caused by the components tolerances is devise the combustor assembly sequence such that the baffle relative position respect to liner is obtained by means of a final regulation, supported by direct measurements and dedicated tools, if required.
A clever assembly sequence, partially compensating the negative effects of these uncertainties, can improve the baffle cooling performance maintaining the same manufacturing capability of the liner and baffle. Another way to underlying this advantage, thinking to a design to cost approach, could be to achieve same cooling performances, while reducing the combustor manufacturing cost. The increased time and tooling required in the shop for the combustor assembly, as well as the required higher experience of the involved manpower, can marginally impact the overall cost estimation, while leading, in some cases, to a commercial strategical advantage as exclusive fleet service operations.

4.2 Nominal gap selection

Design of the baffle profile, following the first attempt criteria of an axial constant velocity in hot condition, starts from the geometry of the liner, already defined in the design process. The selection of the most appropriated value for the gap is performed considering the two worst cases of minimum and maximum gap, which are bounding the selection respect to the maximum available pressure drop and the maximum acceptable liner temperature respectively.

The selection of the nominal gap value, over all the ones satisfying both worst cases, is based on the figure resulting equispaced from the two extreme bounds.

The nominal baffle profile is generated executing the GA code optimization routine, described in chapter 5.9, setting the objective function to the constant velocity option.

The final baffle profile is obtained after a manufacturability assessment of the proposed geometry, since the selected technological processes can introduce some limitations in the desired profile.

An explicative example is the limitations which the metal sheet forming processes, typically the cheapest technology to obtained thin body component, introduce in the baffles design. Rate of slope change of the baffle profile shall be lower than a typical value of 6 degrees, to obtain acceptable metal deformation during the forming process.

After the manufacturability assessment, the modified baffle profile is analyzed again with the GA code, to quantify the impact of required changes and finally confirm that the gap is respecting the two extreme bounds.

The condition of minimum cooling of the liner is obtained performing the GA code analysis adding the estimated uncertainties listed in chapter 0 to the nominal liner / baffle gap (maximum gap condition) and using the minimum coolant mass flow, according to the engine secondary flow variability. In this worst case, the metal temperature prediction shall be lower than the maximum acceptable one. Figure 4-5 shows an example of nominal, minimum and maximum liner and baffle metal temperatures compared with the maximum acceptable liner temperature.

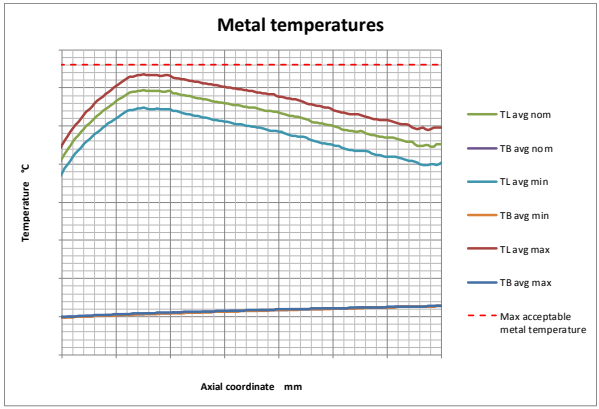

Figure 4-5, Metal temperature as function of gap variation

The condition of maximum cooling of the liner is obtained performing the GA code analysis subtracting the estimated uncertainties listed in chapter 0 to the nominal liner / baffle gap (minimum gap condition) and using the maximum coolant mass flow, according to the engine secondary flow variability. In this worst case, the coolant pressure losses prediction shall be lower than the maximum available pressure drop. Figure 4-6 shows an example of nominal, minimum and maximum coolant pressure losses compared with the maximum available pressure drop.

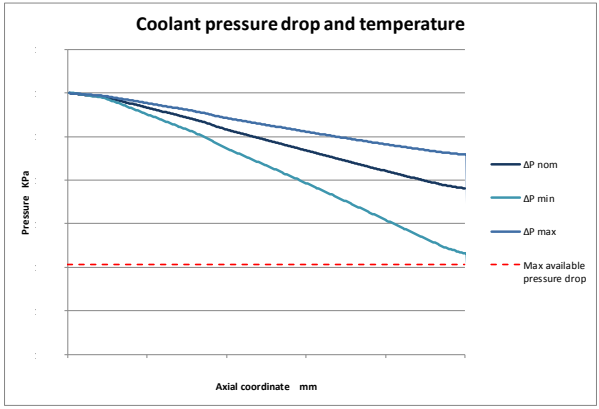

Figure 4-6, Coolant pressure losses as function of gap variation

During the design progress, some of the uncertainties assumed during the preliminary design phase can be reduced.

The uncertainties in the components metal temperature estimation can be reduced after accurate assessment with CFD simulation and experimental measurement comparison. At the same way, liner and baffle tolerances estimation, after the first prototypes manufacturing, can be reduced based on measurements of the components dimensions. Thanks to reduced uncertainties, the nominal gap selection could be updated with latest predictions, improving the cooling performance, if needed, by further reducing the gap value, while respecting the worst cases conditions mentioned in chapter 0.

4.3 Optimized gap

Liners durability is typically limited by the number of cycles to crack initiation, which, in turn, is proportional to the level of temperature reached by the material. In addition, local gradients of temperature can reduce further the number of cycles to crack initiation for the same temperature level.

Considering that, an optimization of the cooling system can be realized to minimize the local temperature gradients, obtaining a more effective cooling action in the locations where higher is the heat exchange with the hot gases.

A gap reduction leads to a local increase of the coolant speed, reaching a more effective cooling, while in all the remaining positions, the gap shall be larger, to bound the coolant pressure losses to an acceptable value.

The optimization problem could be expressed as: for all the design operating conditions, maintaining the coolant pressure losses within the available pressure drop threshold, minimize the liners metal temperatures gradients along the combustor axis direction. Design intent is to minimize thermal induced stresses so that the resulting liners durability can be significantly enhanced, without penalize engine performance or introduce risks for other turbine cooling systems.

The optimized baffle profile is generated executing the GA code optimization routine, described in chapter 5.9, setting the objective function to the flat temperature option.

Also in this case, the final baffle profile is obtained after a manufacturability assessment of the proposed geometry, since the selected technological processes can introduce some limitations in the desired profile. After the manufacturability assessment, the modified baffle profile is analyzed again with the GA code, to quantify the impact of required changes and finally confirm that the gap is respecting the two extreme boundaries.

5 GA Code Description

The Gap Analysis (GA) code [Ref. 97 and Ref. 98] predicts liner and baffle axisymmetric metal temperature and deformation by means of one-dimensional conjugate aero-thermal-strain analysis, while improving, both in the design and analysis phases, the prediction of heat transfer coefficient on liner cold side region of forced convection with turbulators. Pressure losses of the coolant flowing in the gap between liner and baffle are predicted as well.

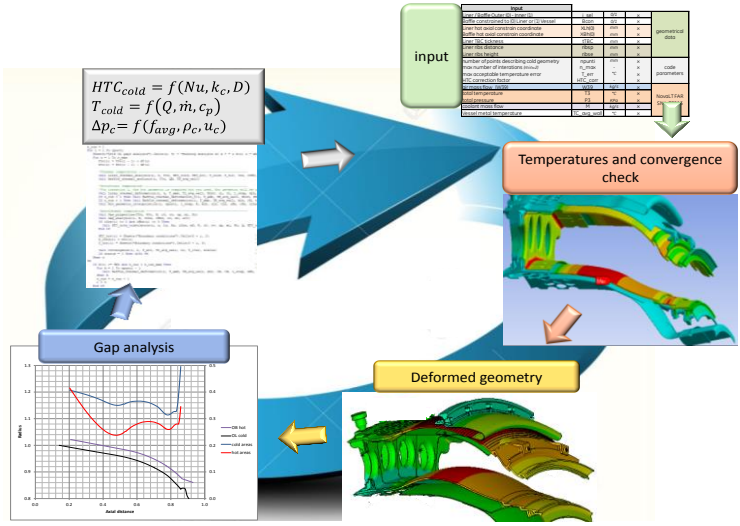

Figure 5-1, Computational loop schema

The code computational loop (see fig. Figure 5-1 and Figure 5-2) generates the liner and baffle temperature distribution and the cooling passages deformed geometry from the results of a thermal heat balance. The passage area formed by couple of liner and baffle deformed surfaces, influences the local coolant velocity, leading to changes in the evaluation of heat transfer coefficients and coolant pressure losses. Adiabatic wall temperatures are evaluated considering the progressive increase of coolant temperature along the passage; coolant thermodynamic properties are computed as a function of its local temperature.

Figure 5-2 summarizes the GA code flow chart: first a computational grid in the meridian section of the combustor is generated, interpolating the liner and baffle cold geometry for a parametric number of axial control volumes.

Then, sequentially for each axial control volume *i*, it executes the computational loop of Figure 5-2: liner and baffle temperature prediction, thermal strain evaluation and hot deformed geometry interpolation on the computational grid, then coolant passage area estimation and coolant thermodynamics properties updating. The computation loop involves the prediction of the cold side heat transfer coefficient and a convergence check, done on control volumes metal temperature at each iteration.

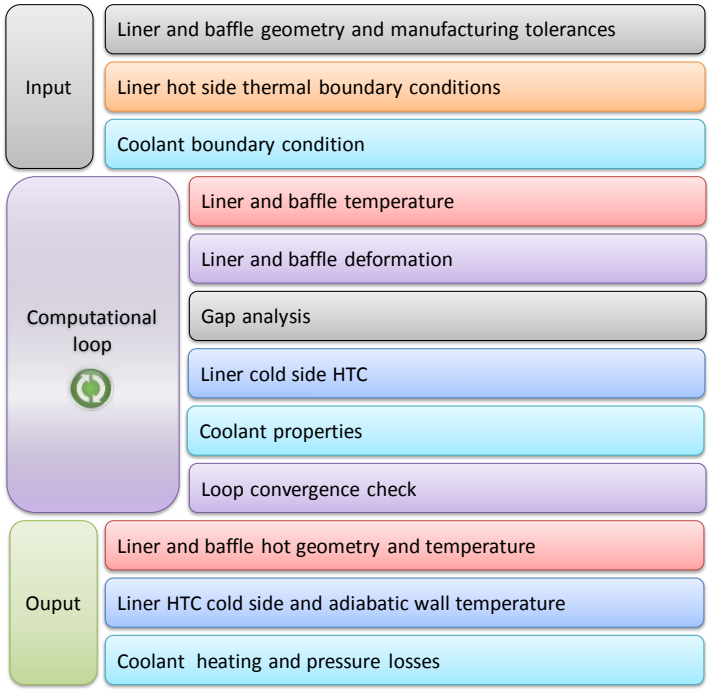

Figure 5-2, GA code flow chart

5.1 Input data

GA code requires three groups of input data:

- Geometrical inputs: the nominal liner and baffle geometry, provided as a couple of points in the meridian section of the combustor, and their manufacturing tolerances;
- Thermal boundary conditions: the distribution on the liner hot side of the heat transfer coefficients and adiabatic wall temperatures;
- Coolant boundary condition: the combustor flow split, the coolant inlet total pressure, temperature and the mass flow.

The GA code executes the conjugate analysis with given total coolant mass flow: this choice is determined by the adoption of an external tool for the engine flow split prediction, which receive pressure losses estimation generated by the GA code as feedback.

Input				
Liner / Baffle Outer (0) - Inner (1)	i_sel	*0/1*		geometrical data
Baffle constrained to Liner (0) or Vessel (1)	Bcon	*0/1*		
Liner hot axial constrain coordinate Baffle hot axial constrain coordinate	XLh(0) XBh(0)	*mm* *mm*		
Liner TBC tickness	tTBC	*mm*		
Liner ribs distance Liner ribs height	ribsp ribse	*mm* *mm*		
Axial length step max number of interations *(min=2)* max acceptable temperature error HTC correction factor	l_step n_max T_err HTC_corr	*mm* - *°C* -	1 200 1.E-04 1.0	code parameters
air mass flow (W39)	W39	*kg/s*		Cycle deck data
total temperature total pressure	T3 P3	*°C* *KPa*		
coolant mass flow	M	*kg/s*		

Figure 5-3, GA code input data

Figure 5-3 shows the GA code user interface. The boolean variable *i_sel* defines if the gap analysis shall be performed on outer or inner liner/baffle gap.

The boolean variable *B_con* defines which kind of baffle mechanical constrain is selected: fixed to liner or fixed to vessel.
The next two variables *XLh(0)* and *XBh(0)* set the hot axial constraint location respectively for liner and baffle, in chapter 5.3 more details about are provided.
The variable *tTBC* defines the thickness of the liner hot side thermal barrier coating.
The variable *ribsp* defines the mutual distance between liner cold side rib, while the variable *ribse* their height.
In the code parameter section, there are:

- the definition of spatial resolution: *l-step* defining length of each analysis step;
- limiter to the maximum number of conjugate loop calculation: *n_max*;
- max acceptable liner temperature error for the convergence check: *T_err*;
- the HTC correction factor, obtained by the code calibration with experimental data, in details described in chapter 6.2: *HTC_corr*.

In the cycle deck data section, there are the required inputs, coming from the engine hydraulic network model:

- air mass flow;
- total temperature;
- total pressure;
- coolant mass flow.

Being an 1D axisymmetric code, it handles one gap profile at a time: nevertheless, non-axisymmetric features, like geometrical and shapes tolerances, can be assessed by a sensitivity analysis playing with the *Geometrical inputs* set of data.

The cold geometry of the cold side of the outer liner (i_sel=0) is provided by a list of points, as couple of X, Z coordinates, expressed in the system of reference frame. In addition, the liner thickness is provided for each of the point provided.
The cold geometry of the hot side of the outer baffle is also provided by a list of points, as couple of X, Z coordinates, expressed in the system of reference frame. In addition, the baffle thickness is provided for each of the point provided.

Similar input data are required in case of Inner liner / baffle gap analysis (i_sel=1).

The geometrical system of reference is orthogonal with:

- X axis coincident with engine axis: X=0 coincident with Combustor interface with engine casing;
- Y axis in tangential direction;
- Z axis in radial direction.

In order to specify the starting point of the geometry object of the gap analysis the corresponding axial coordinate shall be specified in the Cold geometrical data table.

Cold geometrical Data			
Point	X	R	
	mm	mm	
0	0	-	*start of heat shield impingement area*
1	50	-	*end of heat shield impingement area*
2	251	-	*end of forced cold side convection with turbolators*
3	296	-	*end of nugget 1*
4		-	*end of nugget 2*
5		-	*end of nugget 3*

Figure 5-4, GA code "Cold geometrical Data" table

The code is structured to be integrated with additional cooling features which can be affecting different parts of the same liner.

5.2 Liner and baffle temperature

Liner temperatures are obtained solving the steady state heat balance for conduction in the liner metal and convective and radiative heat exchange with hot gases and coolant (Equation 5-1 and Equation 5-2). Conduction in axial direction is neglected. As per schema of Figure 5-5, thickness and thermal conductivity are evaluated as a function of the average metal temperature. The thermal barrier coating applied on liner hot surface is considered. The hot side heat transfer coefficients *HTChot* are obtained from already

experimentally verified external correlations and CFD analyses; it considers both convective and radiative heat exchange with hot gasses.

$$\frac{Q}{A} = \frac{T_{hot} - T_{cold}}{\frac{1}{HTC_{cold}} + \frac{t_l}{k_l} + \frac{t_{TBC}}{k_{TBC}} + \frac{1}{HTC_{hot}}}$$

Equation 5-1, Steady state heat balance

$$T_l = T_{cold} + \frac{Q}{A\, HTC_{cold}}$$

Equation 5-2, Liner metal temperature

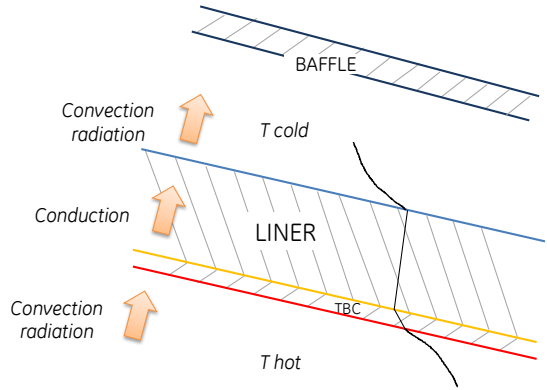

Figure 5-5, Thermal heat balance

The radiative heat exchange between liner and baffle *Qrad* is computed with Equation 5-3 after the Equation 5-2 solution and introduced as *pr* multiplier of the cold side HTC (Equation 5-4 and Equation 5-5). Emissivity values have been assumed from analogous metal surface properties measurements. Being the liner cold side fully enclosed by the baffle, view factor is assumed 1.0.

$$\frac{Q_{rad}}{A} = \sigma\, VF\, \varepsilon_l\, \varepsilon_b\, (T_l^4 - T_b^4)$$

Equation 5-3, Radiative heat exchange between liner and baffle

$$pr = \frac{Q + Q_{rad}}{Q}$$

Equation 5-4, Pr multiplier

$$T_l = T_{cold} + \frac{Q}{A\ HTC_{cold} pr}$$

Equation 5-5, Update liner metal temperature

Baffle temperatures are obtained solving the steady state heat balance in Equation 5-6 considering radiative heat flux with liner and surrounding structures and the convective heat exchange with the coolant on both the sides: the resulting equation, implicit in the baffle temperature variable, is numerically solved.

$$\sum Q = Q_{rad\ liner} + Q_{rad\ vessel} + Q_{conv\ liner\ side} + Q_{conv\ vessel\ side} = 0$$

where:

$$Q_{rad\ liner} = A * \sigma * VF * \varepsilon_l * \varepsilon_b * \left(T^4_{liner\ cold\ wall} - T^4_{baffle}\right)$$

$$Q_{rad\ vessel} = A * \sigma * VF * \varepsilon_v * \varepsilon_b * \left(T^4_{vessel} - T^4_{baffle}\right)$$

$$Q_{conv\ liner\ side} = A * HTC_{liner\ side} * \left(T_{coolant} - T_{baffle}\right)$$

$$Q_{conv\ vessel\ side} = A * HTC_{vessel\ side} * \left(T_{coolant} - T_{baffle}\right)$$

Equation 5-6, Baffle steady state heat balance in radial direction

5.3 Liner and baffle deformation

Liner and baffle strain are computed for each control volume *i* (Equation 5-7 and Equation 5-8) considering the thermal expansion coefficients as a function of the metal temperature: each of the two bodies is approximated as a sequence of annular rings with thickness equal to the axial control volume length, neglecting the deformations induced by congruence displacements of the adjacent rings and the external loads due to pressure differentials.

The liner and baffle axial length increase is computed considering the cumulative length increase starting from their axial constrain location. The code is structured to allow the imposition of different liner and baffle constraining points, to be fully representative of the mutual deformations.

$$\Delta x_i = s\,[1 + CTE_i\,(T_i - T_{amb})]$$

Equation 5-7, Liner and baffle axial strain

$$\Delta r_i = r_i\,CTE_i\,(T_i - T_{amb})$$

Equation 5-8, Liner and baffle radial strain

5.4 Gap analysis

The equivalent hydraulic diameter *D* of the gap between liner and baffle and the passage area *Ac* (Figure 5-6) are computed for each control volume *i* respectively by Equation 5-9 and Equation 5-10, considering in hot deformed geometry the normal direction to both the metal surfaces: αl and αb are the local tangents to the curvature profiles of liner and baffle.

$$D_i = 2\left|r_{b,a} - r_{l,a}\right| cos(\frac{\alpha_l + \alpha_b}{2})$$

Equation 5-9, Equivalent hydraulic diameter

$$A_{c,i} = cos\left(\frac{\alpha_l + \alpha_b}{2}\right) \pi \left(r_{b,a}^2 - r_{l,a}^2\right)$$

Equation 5-10, Passage area

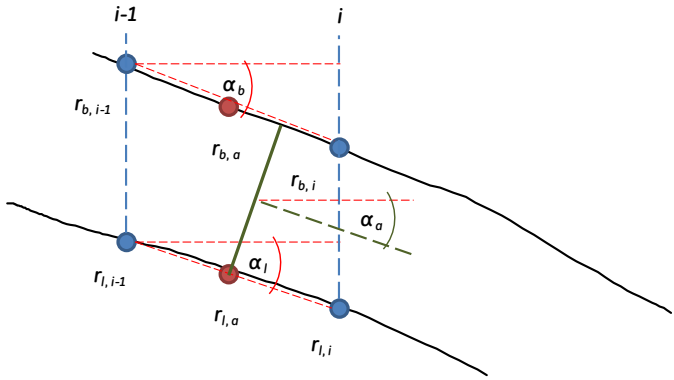

Figure 5-6, Passage area Ac

5.5 Liner cold side HTC

Liner cold side HTC in the region of turbulated forced convection are evaluated adopting the formulation proposed by Han: a comprehensive description of such type of methodology has been proposed by Han et al., [from Ref. 99 to Ref. 103].

First coolant velocity u_C and the related Reynolds number are computed. The friction coefficient is computed according to the well-known equation of Colebrook and White for the smooth wall condition and by a verified correlation for the turbulated wall: an average of the two obtained friction coefficients *fa* is adopted for the pressure losses computation in Equation 5-12.

Then turbulated Reynolds, Stanton and Nusselt numbers are computed as a function of the ribs distance *ribsp*, height *ribse* and angle respect to normal direction *β*.

Finally, in the HTC cold side computation (Equation 5-11) the term *HTCcorr* has been introduced during the code calibration with the experimental data.

$$u_c = \frac{\dot{m}_c}{\rho_{0c} * A_c}$$

$$Re = \frac{D * u_c * \rho_{0c}}{\mu_{0c}}$$

$$Rer = \frac{ribse}{D} * Re * \sqrt{\frac{f_s}{2}}$$

$$gh = \frac{ribsp}{10 * ribse}^{0.14} * 2.83 * \frac{\beta}{90}^{0.3} * Rer^{0.28}$$

$$rm = \frac{ribsp}{10 * ribse}^{0.35} * \left(15.6 - 31.6 * \frac{\beta}{90}\right) * 21.1 * \frac{\beta}{90}^{2}$$

$$St = \frac{f_s}{(gh - rm) * \sqrt{2f_s + 2}}$$

$$Nu = \frac{\rho_{0c} * u_c * c_p * St * D}{k_c}$$

$$HTC_{cold} = \frac{Nu\ k_c\ HTC_{corr}}{D}$$

where:

- $\dot{m}_c$, ρ_{0c} and μ_{0c} are the coolant mass flow, density and dynamic viscosity;
- c_p and k_c are thermal capacity at constant pressure and thermal conductivity of the coolant.

Equation 5-11, Liner HTC cold side computation

For the estimation of the baffle heat exchange with coolant, HTC is computed considering the smooth wall condition.

5.6 Coolant properties

Coolant pressure loss Δp_c is computed as a function of average friction f_a on liner and baffle wet surfaces and considering also the loss of velocity term at gap exit (Equation 5-12), having C_D equal to 0.95. Coolant temperature increase ΔT_c in Equation 5-13 is computed considering liner and baffle convective heat exchange.

$$\Delta p_c = \sum_i f_{a,i} \frac{\Delta x_i}{D_i} \frac{1}{2} \rho_{c,i} u_{c,i}^2 + \frac{1}{2} \rho_{c,end} \frac{{u_{c,end}}^2}{c_D}$$

Equation 5-12, Coolant pressure loss

$$\Delta T_c = \sum_i \frac{Q_{conv,l_i} + Q_{conv,b_i}}{\dot{m}_i c_{p_i}}$$

Equation 5-13, Coolant temperature increase

5.7 Code convergence

Being coolant and metal properties, as well as the geometrical dimensions, computed as a function of the temperature, a numerical relaxed loop for convergence purpose has been introduced: convergence check is performed on liner metal temperature results for each axial control volume *i*.

Few iterations for each control volume *i* are needed to achieve convergence criteria, while maintaining prompt execution feature.

5.8 Conjugate vs Not conjugate analysis

A sensitivity analysis on effect of the conjugate analysis, compared with the not conjugate approach, on the predicted liner metal temperature and hot geometry as well as on coolant velocity and pressure drop has been performed, based on a realistic design case, as described in chapter 4.

Figure 5-7 shows the percentage variation between the two analyzed cases of the physical characteristics as function of the cold gap between liner and baffle; all the presented results are evaluated as an average along the axial coordinate.

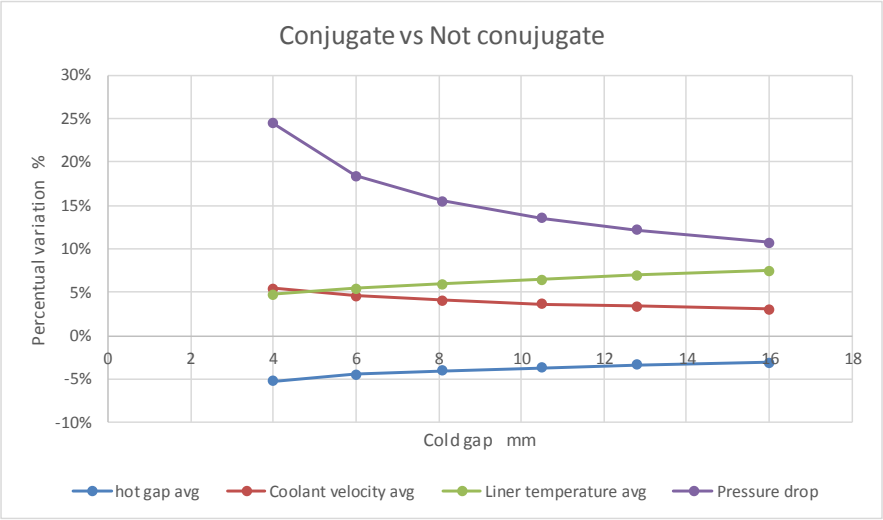

Figure 5-7, Conjugate vs Not conjugate analysis

The most affected physical characteristic is the total pressure drop estimation, being a quadratic behavior respect to the coolant velocity, as per Equation 5-12.

Analyzing the absolute variation between the two analyzed cases of liner metal temperature as well as pressure drop, we can conclude that the difference between the conjugate and not conjugate approach cannot be considered negligible, since can significantly affect the liner durability evaluation by one side and the engine secondary flow distribution by the other side.

5.9 Optimization routines

The objective of each of the two optimization routines is the generation of a baffle profile, at ambient condition, satisfying the gap sizing criteria in hot condition, as described in chapter 4.3.

The two routines, adopting an optimization gradient method, are based on the iterative GA code execution, altering the baffle geometry and evaluating the resulting effects in terms of liner metal temperatures and pressure losses. Figure 5-8 summarizes the optimization routines flow chart.

The inputs required are the same of the GA code, except for the baffle geometry not required, and with the additional definition of the gap sizing criteria.

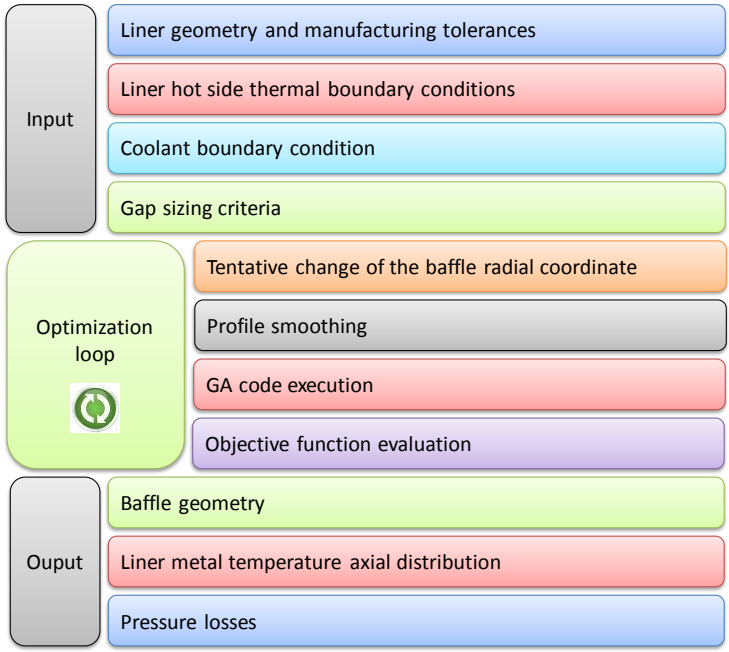

Figure 5-8, Optimization routines flow chart

Then the optimization routines execute the computational loop of Figure 5-8: for each axial control volume, a tentative change of the baffle radial coordinate is estimated and checked if acceptable respect to minimum and maximum radial coordinate limits. If required, a baffle profile smoothing is performed. Then the GA code is executed and the objective function is evaluated. Based on the GA code results, the tentative baffle radial change is rejected or implemented, defining a new tentative baffle geometry.
The optimization loop ends when the objective function variation is less than the minimum value defined or the maximum number of iterations is exceeded.

5.9.1 Gap sizing criteria

Since the GA code is executed at given coolant mass flow, the selection of the possible baffle radius change $r_{i,j}$, for each iteration j of the optimization routines loop, is subordinated to the respect of the constrain in Equation 5-14: coolant pressure losses shall be equal to the one obtained with the initial geometry within a tolerance of ±5%.

$$\Delta p_{c,initial} * 0.95 \leq \Delta p_{c,j} \leq \Delta p_{c,initial} * 1.05$$

Equation 5-14, Optimization constrain on coolant pressure loss

The constrain in Equation 5-14 for the optimization problem is assuring that the optimized baffle profiles, obtained for each of the available gap sizing criteria, are respecting the available pressure drop and the maximum acceptable liner temperature conditions, described in chapter 0.
When the nominal gap geometry is analyzed, as well as the worst cases configurations obtained adding the gap estimation uncertainties described in chapter 0, optimization routines will modify the baffle geometry maintaining the same pressure drop.

5.9.2 Tentative change of the baffle radial coordinates

The first step of the optimization loop is the evaluation, for each control volume used to discretize the geometry, of the tentative change of the baffle radial coordinates.

In the routine for the axial constant velocity gap objective, the change of the baffle radial coordinate Δr_j, as per Equation 5-15, is proportional with a coefficient *kf* to the coolant velocity difference, respect to the target value, with the exponential coefficient *e*.

$$\Delta r_j = -s \; kf \; \left(v_{c,j} - v_{c,target}\right)^e$$

where:

- *s* is the sign: *s* = -1 for outer baffle, while *s* = +1 for inner baffle;
- *kf* is a proportional coefficient;
- $v_{c,j}$ is the local coolant velocity at control volume *j*;
- $v_{c,target}$ is the coolant velocity target value;
- *e* is the exponential coefficient.

Equation 5-15, Axial constant velocity gap - changes of baffle radial coordinates

The change of the baffle radial coordinates, being evaluated respect to a defined liner geometry, has a negative sign for the outer gap, while positive for the inner gap.
In the outer gap case, if the coolant velocity difference with respect to the target value is positive, means that in the local control volume velocity is higher than the target one, therefor a local gap increase is required: the local baffle radial coordinate will be increased. In the inner gap case, the similar condition of required local gap increase is obtained by decreasing the local baffle radial coordinate.
In the routine for the optimized gap objective, the change of the baffle radial coordinate Δr_j, as per Equation 5-16, is proportional with a coefficient *kf* to the temperature difference, respect to the target value, with the exponential coefficient *e*.

$$\Delta r_j = s \; kf \; \left(T_j - T_{target}\right)^e$$

where:

- T_j is the local temperature at control volume *j*;
- T_{target} is the temperature target value;

Equation 5-16, Optimized gap - changes of baffle radial coordinates

Also in this case, the change of the baffle radial coordinates, being evaluated respect to a defined liner geometry, has a negative sign for outer gap, while positive for inner gap. In the outer gap case, if the temperature difference with respect to the target value is positive, means that the local control volume has a temperature higher than the target one, therefor to change the solution with the aim to reduce it, an increase of local coolant velocity is needed, requiring a local gap reduction: the local baffle radial coordinate will be reduced. In the inner gap case, the similar condition of required local gap reduction is obtained by increasing the local baffle radial coordinate.
To decrease the computational time, the optimization process starts with an initial value of the *kf* proportional coefficient equal to the 25% of the expected gap,
Then, the initial value will be decreased every time a local optimum condition is reached for the current *kf* value, as described in chapter 5.9.4.
The computed change of the baffle radial coordinates is subjected to the satisfaction of a constrain for the optimization problem: the tentative baffle geometry, at iteration *j*, shall be included within the minimum and maximum baffle radius. This constrain is required to respect in all the local parts of the new proposed baffle profile the minimum gap distance with liner and the surrounding engine components, to avoid undesired contacts in the worst combination of uncertainties and operative conditions.

$$r_{b\,min,j} \leq r_{b\,i,j} \leq r_{b\,max,j} \quad \forall j$$

Equation 5-17, Optimization constrain on minimum and maximum baffle radius

5.9.3 Profile smoothing

The tentative baffle geometry can present a sharp profile, due to sudden variation of the thermal boundary condition in axial direction, typically during the preliminary design phase, or related to the iterative geometrical changes in case of high value of the proportional coefficient *kf*. For this reason, an option can be activated on the optimization process to introduce a profile smoothing, after the estimation of the tentative change of the baffle radial coordinates and before the GA code execution.

The profile smoothing is obtained by linearly interpolate adjacent control volume radial coordinates, to limit the radius variation to a maximum 3% of the control volume axial length.

5.9.4 Objective function evaluation

In the routine for the axial constant velocity gap objective, the objective function of the optimization, which shall be minimized, is defined as:

$$F_{obj,j} = \frac{\sum_i \left| v_{i,j} - v_{i,target} \right|}{i}$$

where:

- $v_{i,j}$ is the liner metal temperature distribution at iteration *j*;
- $v_{i,target}$ is the liner target temperature;
- i is the number of control volumes.

Equation 5-18, Axial constant velocity gap - objective function

The target coolant velocity is obtained averaging the coolant velocity axial distribution obtained analyzing the not modified baffle profile with the GA code: a correction of the first value assumed is performed in case of the pressure losses obtained are not respecting the Equation 5-14.

In the routine for the optimized gap objective, the objective function of the optimization, which shall be minimized, is defined as:

$$F_{obj,j} = \frac{\sum_i \left| T_{i,j} - T_{i,target} \right|}{i}$$

where:

- $T_{i,j}$ is the liner metal temperature distribution at iteration *j*;
- $T_{i,target}$ is the liner target temperature;

Equation 5-19, Optimized gap - objective function

The liner target temperature is obtained averaging the liner cold side axial temperature distribution obtained analyzing the not modified baffle profile with the GA code: a correction of the first value assumed is performed in case of the pressure losses obtained are not respecting the Equation 5-14.

The objective function value at the j iteration of the optimization computational loop is used to decide if the tentative baffle radial change shall be rejected or implemented.
If the value is lower than the one obtained in the previous step, then the tentative radial change is applied, passing to the next iteration, while if the objective function value is increasing, then the tentative radial change is rejected and the proportional coefficient kf is reduced by a 10%.

6 GA Code Validation

As part of the GA code development, a validation of the tool has been performed during the code writing phase and finally before the first official release as predictive tool in the design of new combustors cooling system.

The strategy of validation has been structured in three steps: first a comparison of the predicted temperature for the liner and baffle has been performed respect to results obtained from a thermal analysis of a detailed tridimensional finite element model.

Then, using the same detailed FE model, a comparison of the liner and baffle predicted strain has been executed respect to a structural analysis results.

The verifications obtained from these two comparisons demonstrate the GA code capability to correctly manage the discretization of the cold geometry and the mechanical constraints of liner and baffle, as well as their hot deformed shape and evaluate the mutual clearance between the two components. Steady-state temperature estimation of both liner and baffle, described in chapter 5.2, is verified by the comparison with the FEM results for an axisymmetric set of thermal boundaries.

In addition, the hypothesis of simplification introduced in components strain evaluation, described in chapter 5.3, is quantified and justified in its reduced model formulation.

Finally, in the third step of validation, the GA code capability to correctly predict the liner cold side heat transfer coefficient in the conjugate analysis formulation has been demonstrated, by means of an extensive comparison with available experimental data and the calibration activity followed, as described in the chapter 6.2.

6.1 Comparison with FEM analysis

A first validation has been performed comparing the temperature and thermal strain estimated by the GA code with the results obtained by a detailed FEM thermo-structural analysis, using the same liner and baffle geometry and with the same hot and cold boundary conditions.

The computational mesh, shown in Figure 6-1, has been generated considering the requirements, coming from the expected thermal and structural analysis execution, in terms of element typology, sizing, aspect ratio and quantity. Hexa elements, with at least two elements in the thickness, has been used for both liners and baffles.

The high number of elements of the detailed mesh, needed for proper stress capturing, guides the choice of meshing just a sector of the full annular combustor, applying symmetry boundaries to the section planes.

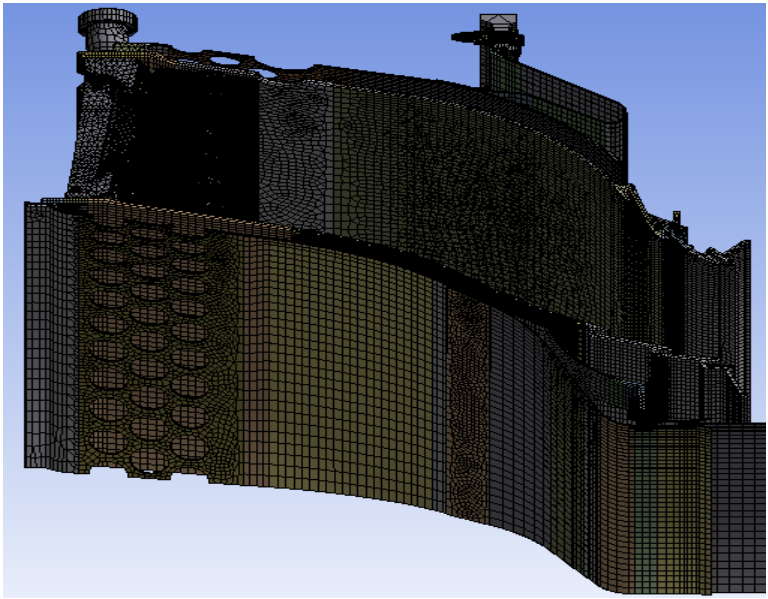

Figure 6-1, Detailed FEM mesh

The model setup has been performed assuming realistic combustor configuration and operating conditions.

Material properties applied for all the components have been selected from a company database: for each material, the relevant mechanical characteristics are measured from a statistically relevant number of times and provided as function of temperature and delivery state. Elastic-plastic formulation has been applied in the region of high level of stresses.

Mutual constraints and contacts between the different components have been applied: in the analyzed case, the baffle is axially fixed to the liner in a location located after the forced convection region, which is objected of the comparison and also to the engine vessel. The liner is axially and radially constrained by the forward side to the combustor domeplate.

Pressure loads, due to differential pressure in the combustor volumes, have been applied on both liner and baffle.

The thermal boundary conditions applied have been calibrated by means of available liner and baffle temperature measurements, obtained in a full annular rig, as described in chapter 6.2; not axisymmetric features, as staging effects, have not been considered.

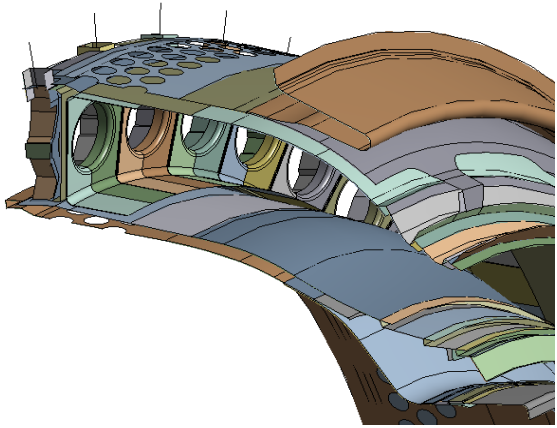

Figure 6-2, View of the sector FE model

Figure 6-3 shows the results of thermal analysis: the temperature distribution on the whole combustor, while Figure 6-4 reports the extraction of the outer liner cold side metal temperature along the axial coordinate.

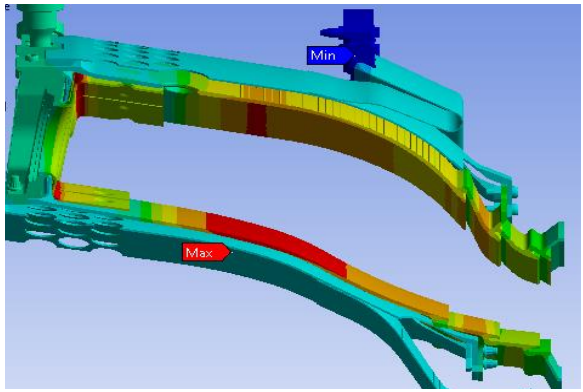

Figure 6-3, Combustor temperature results

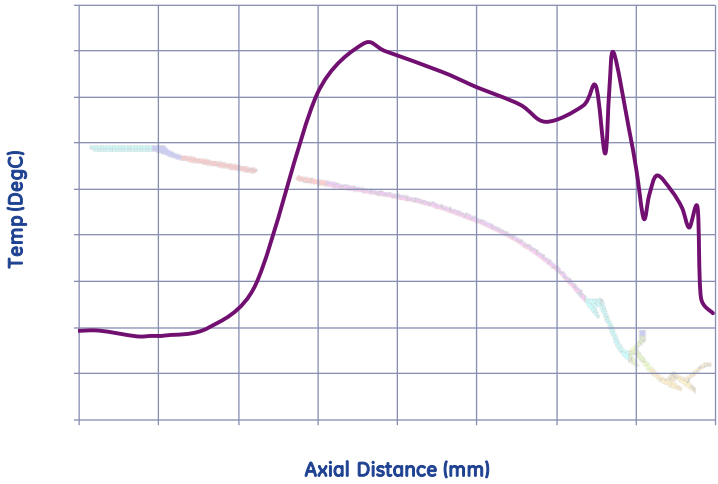

Figure 6-4, Axial distribution of liner cold side metal temperature

Figure 6-5 and Figure 6-6 show the results of structural analysis in terms of total deformation (vectorial sum of axial and radial) of the whole combustor and outer liner cold side metal temperature.

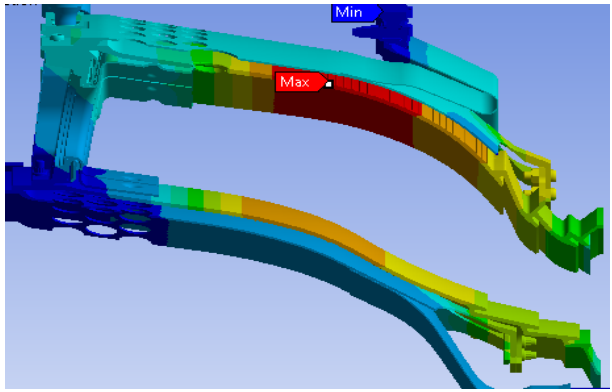

Figure 6-5, Combustor total deformation results

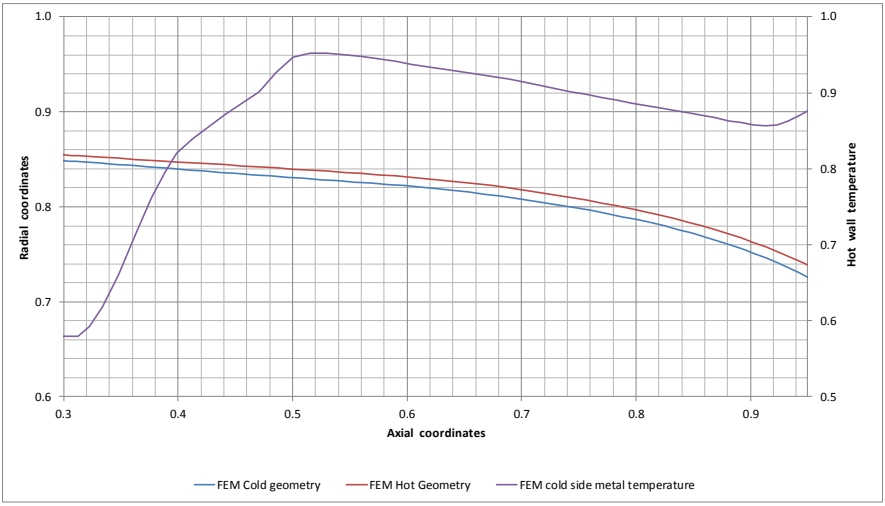

Figure 6-6, Outer liner deformation and metal temperature

6.1.1 FEM comparison results

The maximum error of temperatures estimation obtained by the thermal heat balance embedded in the GA code, described in chapter 5.2, respect to a detailed FEM thermal analysis is about 0.6%: the lack of fit is due to the neglected axial conduction, in a region where a noticeable axial temperature gradient is present.

The maximum error of deformation estimation obtained by the simplified structural approach embedded on the GA code, described in chapter 5.3, respect to the detailed FEM structural analysis is about 0.2%: such result justifies the negligibility of the deformations induced by congruent displacements of the adjacent rings and the external loads due to pressure differentials (Equation 5-7 and Equation 5-8).

Figure 6-7 shows the good agreement obtained from the GA code and the FEM results. Since the good agreement obtained, the GA code can be used as a reduced model allowing in the design phase the execution of sensitivity analyses, typically time expensive with the detailed methodology, in a negligible amount of time.

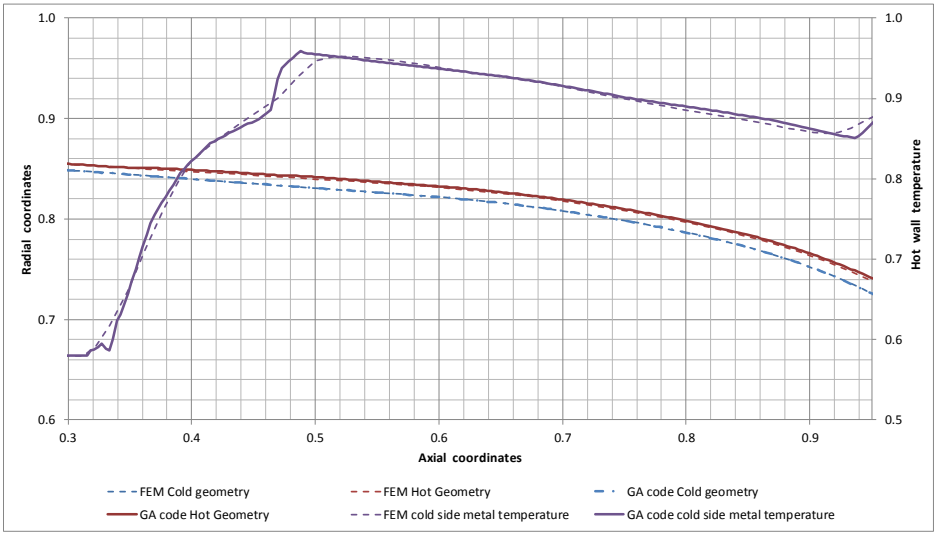

Figure 6-7, FEM / GA code liner temperature and deformation comparison

An additional advantage during the preliminary design phase is worth to be mentioned: the interaction between structural FE model, one-dimensional correlation and CFD model typically need to be carefully verified and it leads to some inefficiency in the repeated execution of the analysis sequence: an intrinsic advantage in the adoption of the GA code is the robust and fixed procedure established between the conjugate aero-thermal-strain analyses.

6.2 GA code calibration

In the frame of the NovaLT16 gas turbine combustor development, a series of test campaigns have been executed in a dedicated full annular rig.

Thanks to experimental data availability, an activity of verification of the GA code correlations accuracy for the cold side heat transfer coefficient computation has been performed. First a comparison between the acquired experimental data and the GA code results has been realized, then the correction factor *HTCcorr*, used in Equation 5-11, has been tuned in a calibration process with the available measurements, as schematically represented in Figure 6-8.

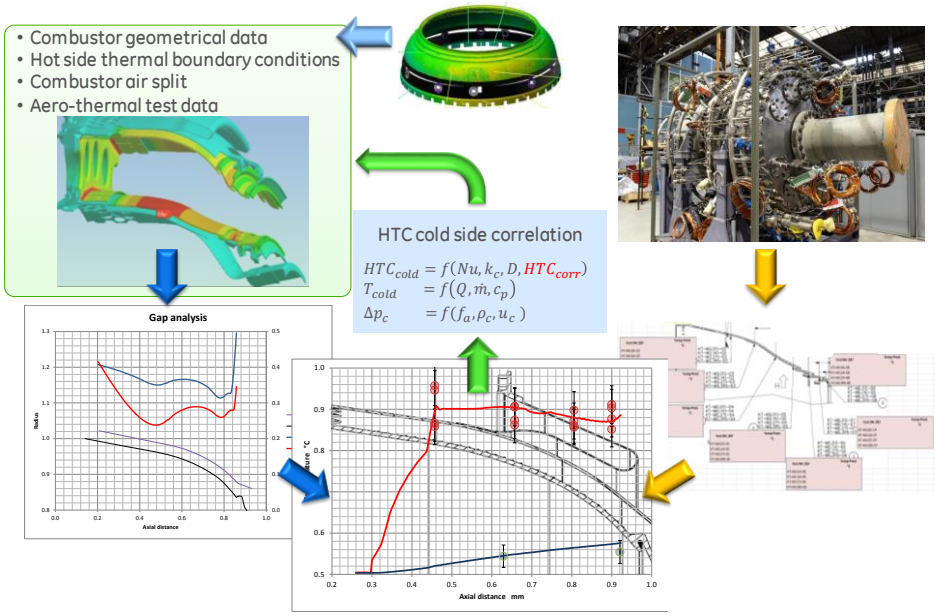

Figure 6-8, GA code calibration process

The experimental data have been acquired in more than 500 fired hours and 6 different combustor configurations in a dedicated full annular rig, designed to validate combustion chamber performances of the NovaLT16 gas turbine.

The full annular rig, schematically described in Figure 6-9, is composed by a compressor diffuser, combustor and burners interfaces replicating the engine one, a first stage nozzle simulacrum with equivalent throat area, pressure barriers, hot gas exhaust quenching and discharge volume.

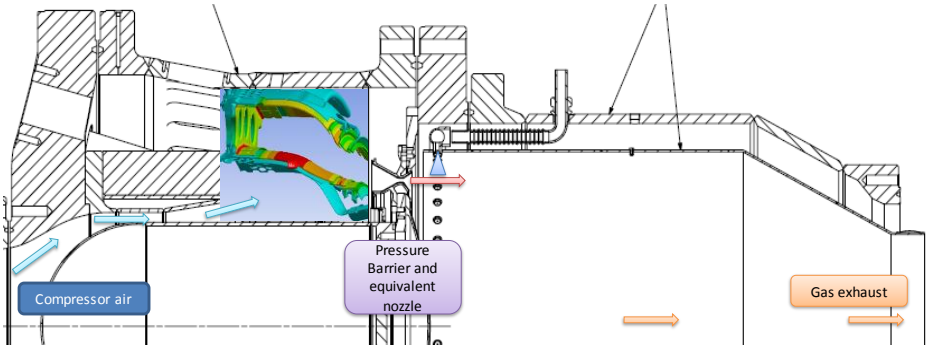

Figure 6-9, NovaLT16 full annular rig cross-section

Test setup is supplied with cooling water lines for the pressure casing instrumentation, emission and temperature probes. Pressure barriers cooling system has been designed using minimum coolant to meet the test bench durability requirements, by means of detailed FEM analyses. Secondary cooling flows can be adjusted as required by replication of engine operating conditions.

Since the presented calibration process was not the aim of the test rig development, quantity and accuracy of measurements have not been optimized for this purpose. Nevertheless, comparing the wide database of measurements acquired and making relative comparisons between different operating conditions as well as combustor tested configurations, mutual dependency of the physical parameters involved can be accurately estimated. For this reason, the calibration process here after described has an important validation role for the GA code.

Among all the measurements acquired and all the tested combustor configurations, a subset has been individuated to verify the GA code capability to correctly estimate effects of:

- Geometrical changes of liner and baffle (3% variation);
- Combustor inlet temperature (38% variation);
- Flame temperature (8% variation);
- Coolant mass flow (12% variation).

The test cases for the calibration process, reported in Table 6-1, have been selected to envelop the conditions of extreme variation of above parameters; values reported in the table have been scaled respect to SN3, TP145 case.

Validation test points							
Test campaign	SN	3	3	3	4	5	6
Test Point	TP	119	135	145	12	48	9
Average gap liner / baffle	gap	100%	100%	100%	101%	99%	102%
Outlet compressor temperature	TCD	80%	63%	100%	100%	100%	100%
Flame temperature	FT	102%	106%	100%	98%	100%	99%
Coolant mass flow	m	103%	103%	100%	91%	93%	95%

Table 6-1, Test cases for calibration process

Liner metal temperatures have been measured, for the part relevant to the gap analysis, in 4 axial locations with 4 circumferential positions each, as shown in Figure 6-10 for the outer liner in the sections named 2, 3 ,4 and 5; similar distribution has been realized for the inner liner.

Baffle metal temperatures have been measured in 3 axial locations with 2 circumferential positions each, as shown in Figure 6-11 for the outer baffle in the sections named 1, 2 and 4; similar distribution has been realized for the inner baffle.

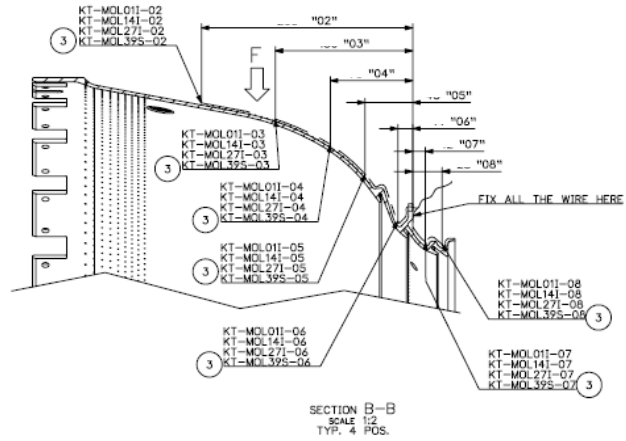

Figure 6-10, NovaLT16 outer liner thermocouples instrumentation

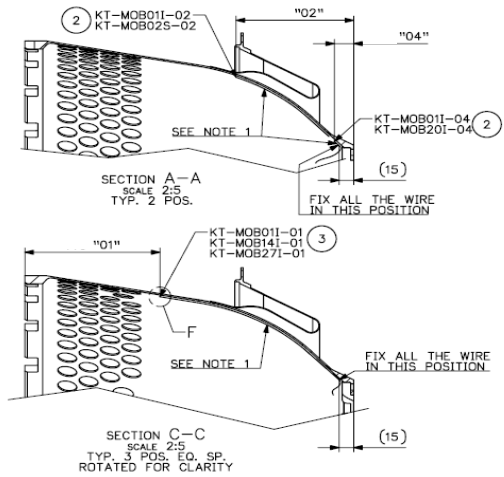

Figure 6-11, NovaLT16 outer baffle thermocouples instrumentation

Coolant air temperatures have been measured in 2 axial locations with 3 circumferential positions each; in Figure 6-12 the exit position of the measurements for the outer baffle is shown; similar distribution has been realized for the inner baffle.

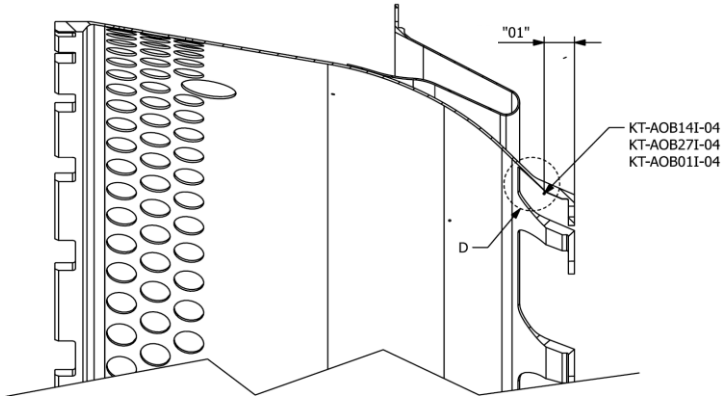

Figure 6-12, NovaLT16 outer baffle coolant thermocouples instrumentation

Coolant air pressure have been measured in 2 axial locations with 4 circumferential positions each; in Figure 6-13, the exit position of the measurements for the outer baffle is shown; similar distribution has been realized for the inner baffle.

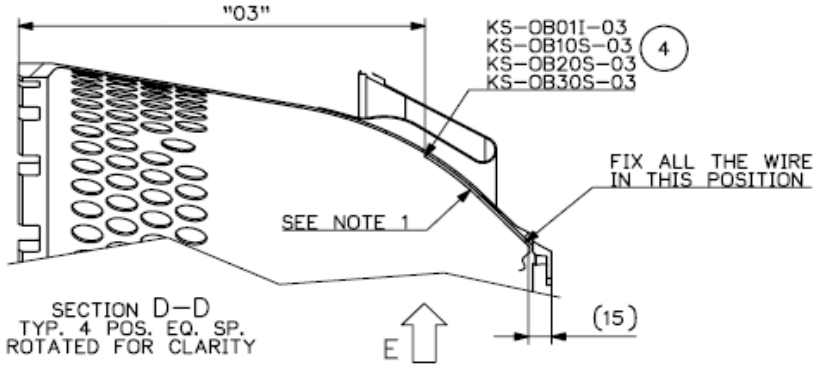

Figure 6-13, NovaLT16 outer baffle coolant pressure probes instrumentation

Accuracy of the measurements, reported in following figures are:

- ±2 °C for thermocouples (about 0.25% of the absolute value);
- ±0.12 kPa for pressure probes (about 0.5% of the absolute value).

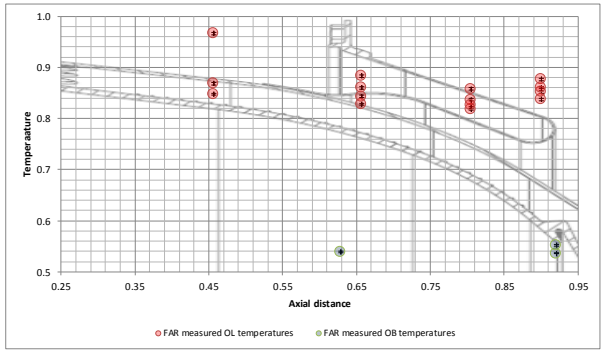

Figure 6-14, FAR (SN3, TP145) metal temperature measurements

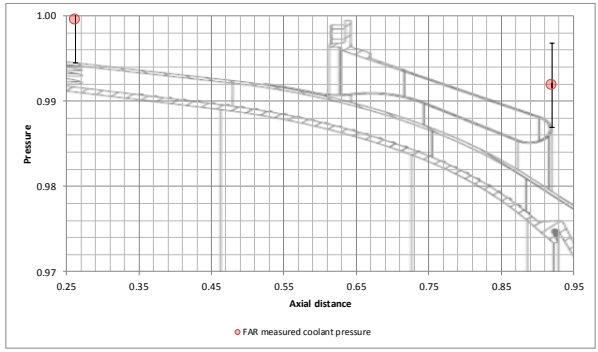

Figure 6-15, FAR (SN3, TP145) coolant pressure measurements

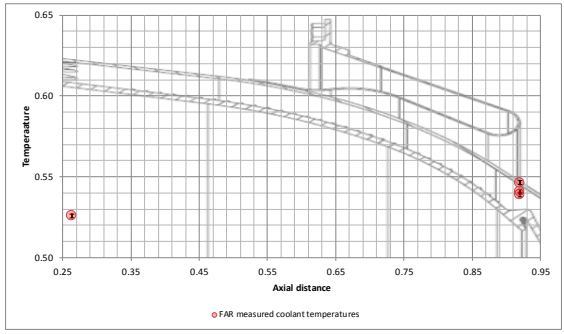

Figure 6-16, FAR (SN3, TP145) coolant temperature measurements

GA code has been used imposing from each of the tested configurations the liner and baffle geometry, liner hot side thermal boundary conditions and combustor flow split, coolant total pressure, temperature and mass flow and vessel metal temperature.
Same imposed data, as the coolant total pressure, temperature and mass flow and vessel metal temperature, are directly coming from the acquired data during the tests.
The remaining inputs have been obtained as described in the following chapters.
The liner hot side thermal boundary conditions have been obtained, starting from the reference distribution, by scaling the heat transfer coefficient and adiabatic wall temperature values. Hereafter the scaling formulas:

$$HTC(T,x_i) = HTC_{ref}(x_i) * Func\left[C(T,x_i)^{0.8} * \left(\frac{\mu}{\mu_{ref}}\right)^{-0.8} * \left(\frac{k}{k_{ref}}\right)^{1} * \left(\frac{Pr}{Pr_{ref}}\right)^{1/3}\right]$$

Equation 6-1, HTC scaling formula

$$T_{aw_i} = \frac{\left(T_{aw_{0i}} - T_{ref_0}\right)}{\left(T_{TCD_0} - T_{ref_0}\right)} * \left(T_{TCD_1} - T_{ref_1}\right) + T_{ref_1}$$

Equation 6-2, Adiabatic wall temperature scaling formula

To increase the accuracy of the GA code prediction, liner and baffle real geometries have been introduced and evaluated in the calibration process, thanks to available measurements, realized by CAM touch probes and laser scans (Figure 6-17), of the combustor parts manufactured for the full annular rig test.

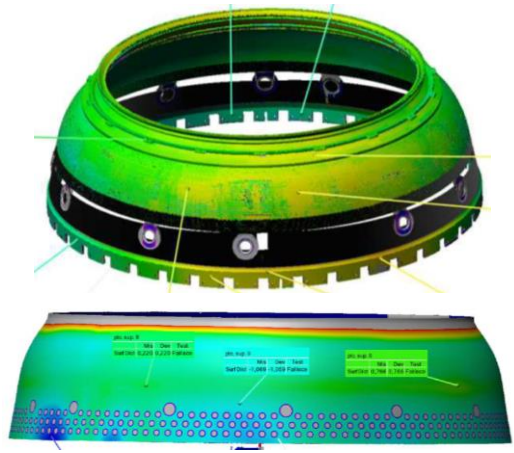

Figure 6-17, Liner and baffle surfaces laser scan

The combustor flow split has been obtained from a dedicated model developed for the full annular rig tests execution and independently calibrated with the measurements collected in the first phase of each test campaign.
Before the execution of fired tests, an initial calibration phase of the rig flow split is usually performed, without flame, to verify the proper correspondence between the required flow split in the combustor and the surrounding structures and the pressure measurements. The distribution of the pressure probes is realized specifically to check all the relevant pressure jump inside the test rig: in same components, holes are present to be plugged or unplugged to eventually compensate a flow split not meeting the requirements with enough accuracy.

Results predicted by GA code have been compared with the available measurements acquired during the tests: liner and baffle metal temperatures and coolant temperature and pressure before and after the forced convection section.
Six cases are documented in the following chapters, showing the comparison between results obtained from the GA code and the measured data under the same conditions.

6.2.1 SN3-Test Point 119

Test campaign 3, point 119 is an acquired set of measurements having an operating condition with low combustor inlet temperature, high flame temperature and coolant mass flow among the test cases. The assembly condition gap between liner and baffle is the nominal one. Following graphs report the obtained comparison with the predicted liner and baffle metal temperatures and coolant temperature and pressure losses, with the *HTCcorr* parameter equal to 1.15 (condition of minimum difference between measured temperatures and predicted ones: 13 °C average value).

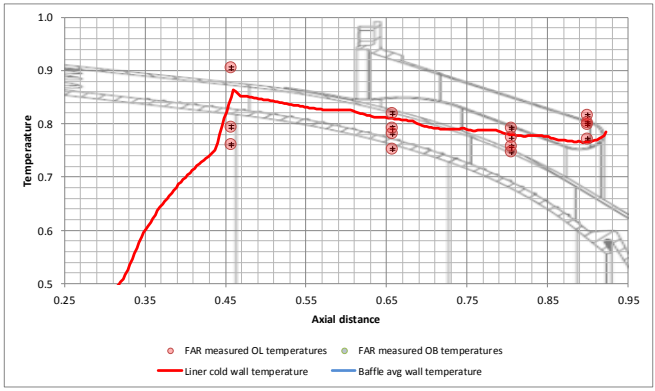

Figure 6-18, SN3-TP119 Liner and baffle metal temperature comparison

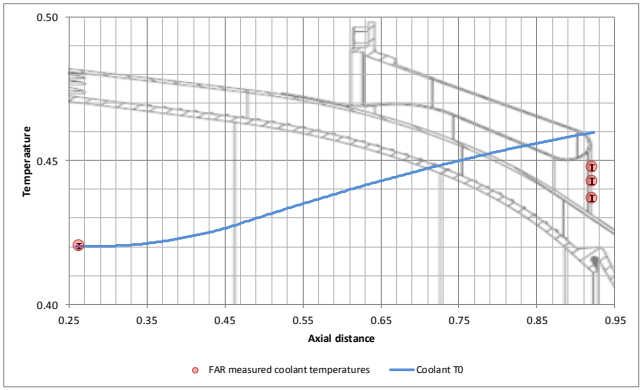

Figure 6-19, SN3-TP119 Coolant temperature comparison

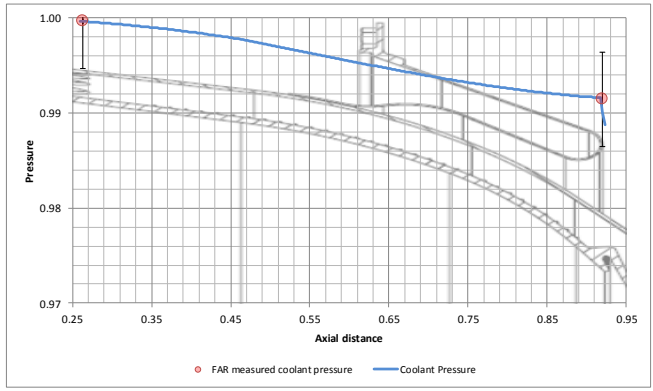

Figure 6-20, SN3-TP119 Coolant pressure comparison

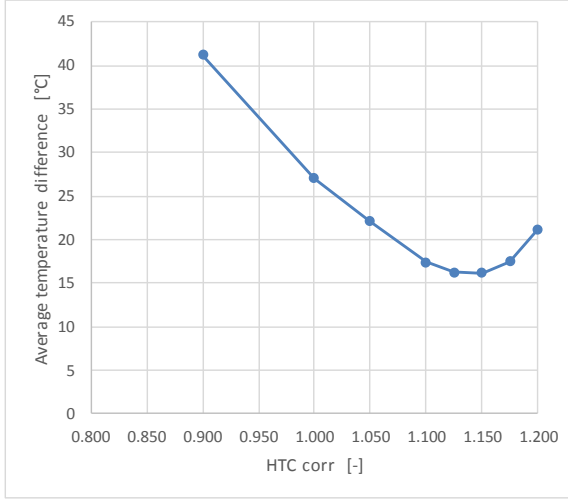

Figure 6-21, SN3-TP119 *HTCcorr* factor vs average temperature difference

6.2.2 SN3-Test Point 135

Test campaign 3, point 135 is an acquired set of measurements having an operating condition with minimum combustor inlet temperature, highest flame temperature and coolant mass flow among the test cases. The assembly condition gap between liner and baffle is the nominal one. Following graphs report the obtained comparison with the predicted liner and baffle metal temperatures and coolant temperature and pressure losses, with the *HTCcorr* parameter equal to 1.10 (condition of minimum difference between measured temperatures and predicted ones: 15 °C average value).

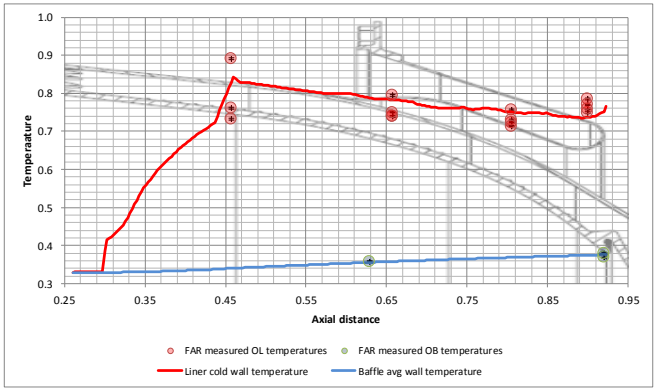

Figure 6-22, SN3-TP135 Liner and baffle metal temperature comparison

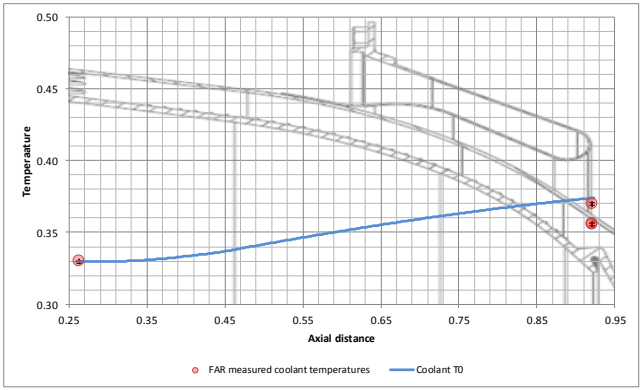

Figure 6-23, SN3-TP135 Coolant temperature comparison

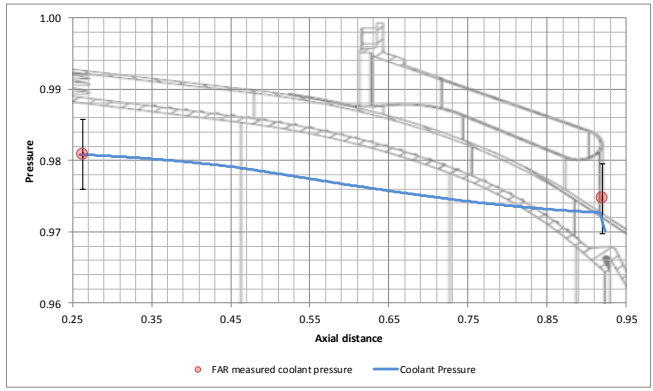

Figure 6-24, SN3-TP135 Coolant pressure comparison

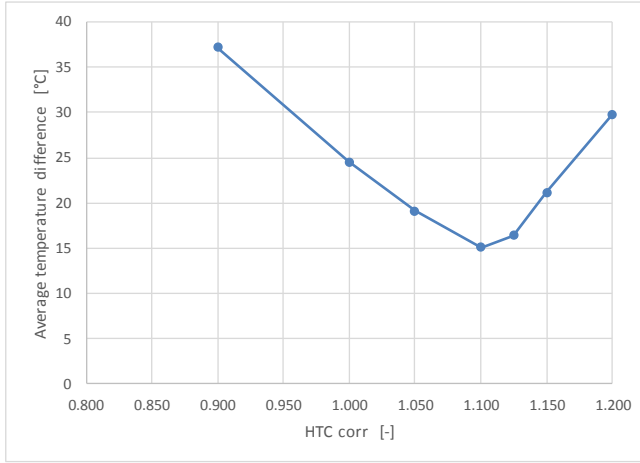

Figure 6-25, SN3-TP135 *HTCcorr* factor vs average temperature difference

6.2.3 SN3-Test Point 145

Test campaign 3, point 145 is the acquired set of measurements taken as reference condition, having nominal combustor inlet temperature, nominal flame temperature and coolant mass flow among the test cases. The assembly condition gap between liner and baffle is the nominal one. Following graphs report the obtained comparison with the predicted liner and baffle metal temperatures and coolant temperature and pressure losses, with the *HTCcorr* parameter equal to 1.08 (condition of minimum difference between measured temperatures and predicted ones: 16 °C average value).

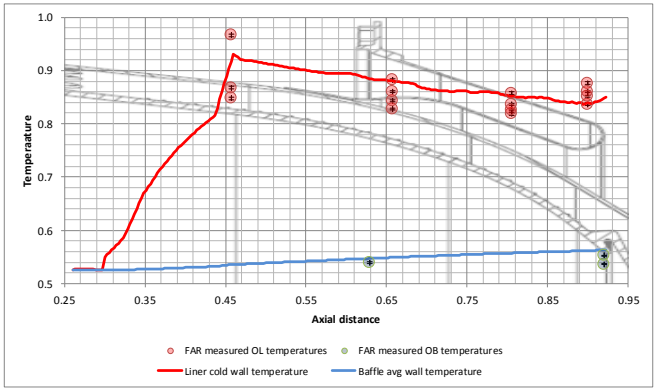

Figure 6-26, SN3-TP145 Liner and baffle metal temperature comparison

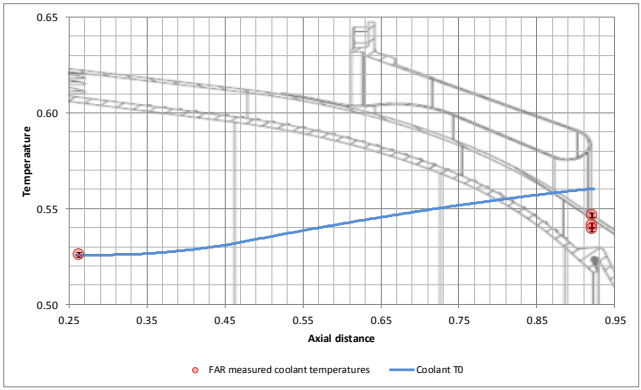

Figure 6-27, SN3-TP145 Coolant temperature comparison

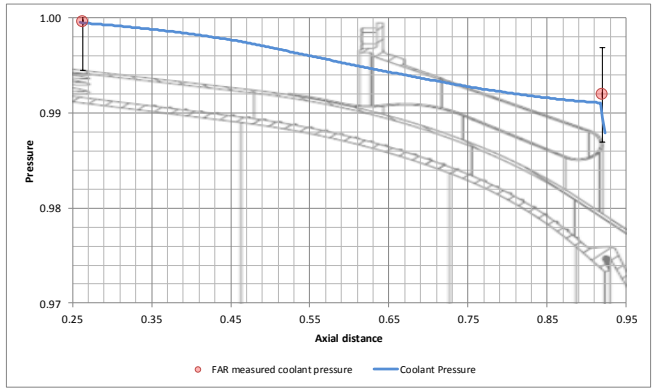

Figure 6-28, SN3-TP145 Coolant pressure comparison

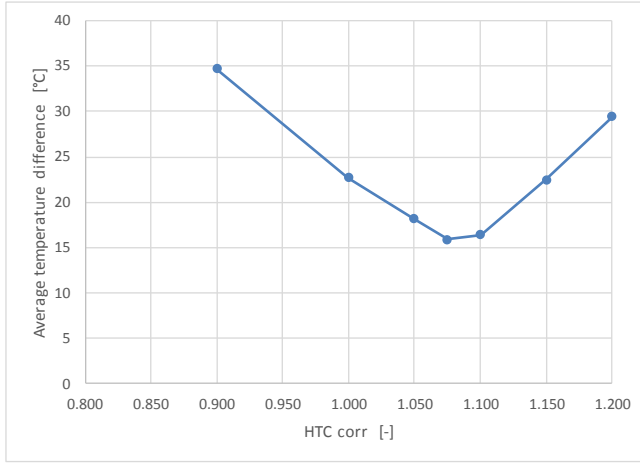

Figure 6-29, SN3-TP145 *HTCcorr* factor vs average temperature difference

6.2.4 SN4-Test Point 12

Test campaign 3, point 119 is an acquired set of measurements having an operating condition with low combustor inlet temperature, high flame temperature and coolant mass flow among the test cases. The assembly condition gap between liner and baffle is the nominal one. Following graphs report the obtained comparison with the predicted liner and baffle metal temperatures and coolant temperature and pressure losses, with the *HTCcorr* parameter equal to 1.00 (condition of minimum difference between measured temperatures and predicted ones: 20 °C average value).

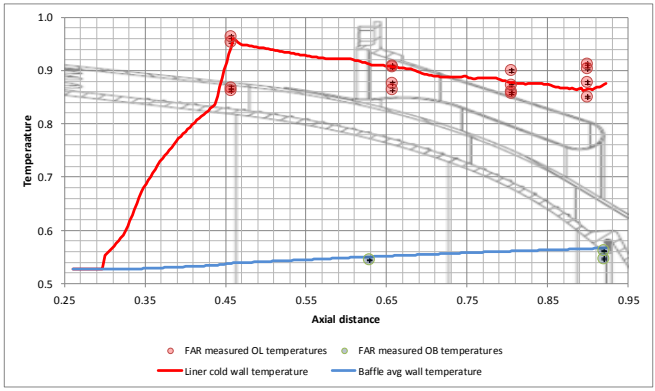

Figure 6-30, SN4-TP012 Liner and baffle metal temperature comparison

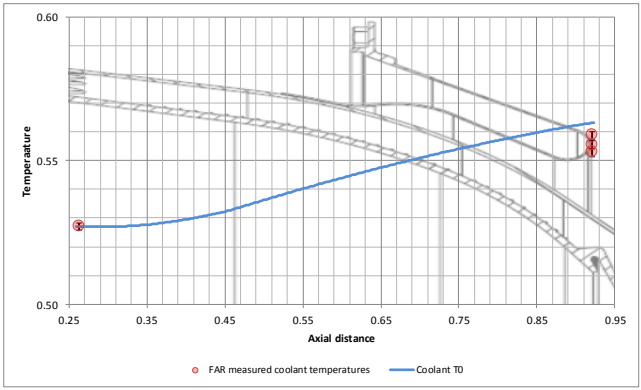

Figure 6-31, SN4-TP012 Coolant temperature comparison

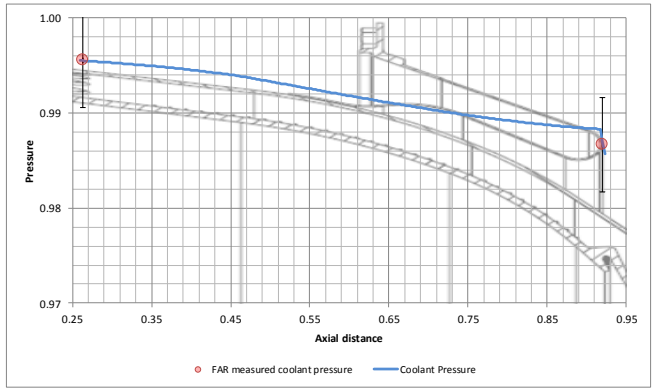

Figure 6-32, SN4-TP012 Coolant pressure comparison

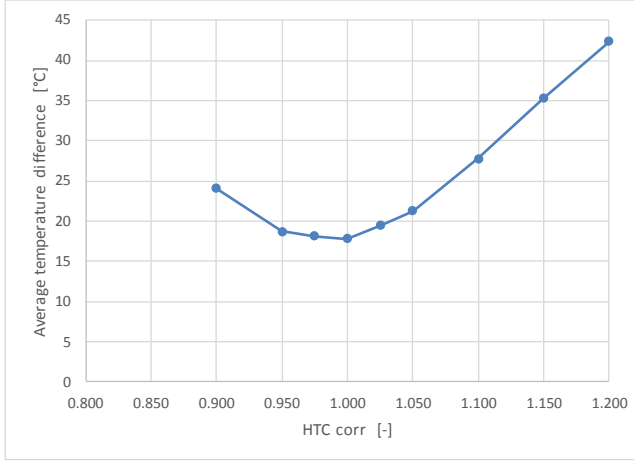

Figure 6-33, SN4-TP012 *HTCcorr* factor vs average temperature difference

6.2.5 SN5-Test Point 048

Test campaign 3, point 119 is an acquired set of measurements having an operating condition with low combustor inlet temperature, high flame temperature and coolant mass flow among the test cases. The assembly condition gap between liner and baffle is the nominal one. Following graphs report the obtained comparison with the predicted liner and baffle metal temperatures and coolant temperature and pressure losses, with the *HTCcorr* parameter equal to 0.90 (condition of minimum difference between measured temperatures and predicted ones: 9.2 °C average value).

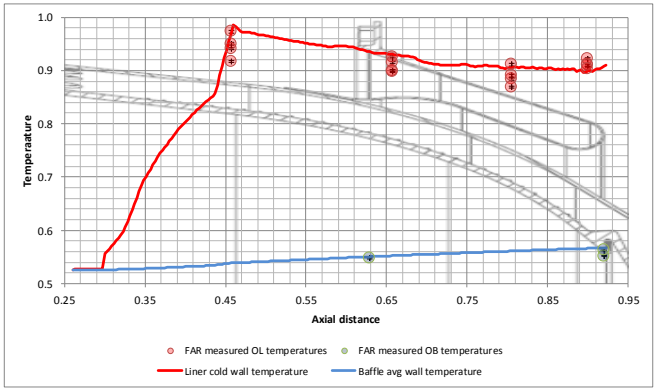

Figure 6-34, SN5-TP048 Liner and baffle metal temperature comparison

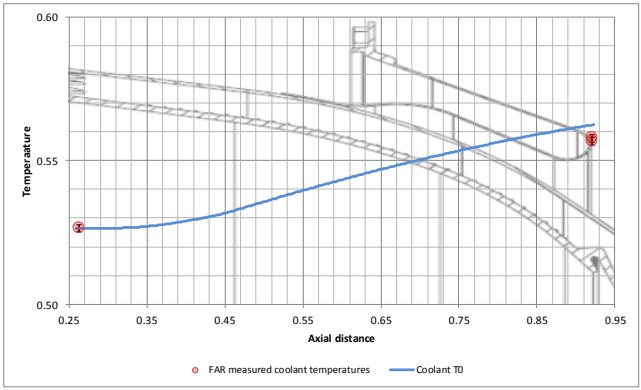

Figure 6-35, SN5-TP048 Coolant temperature comparison

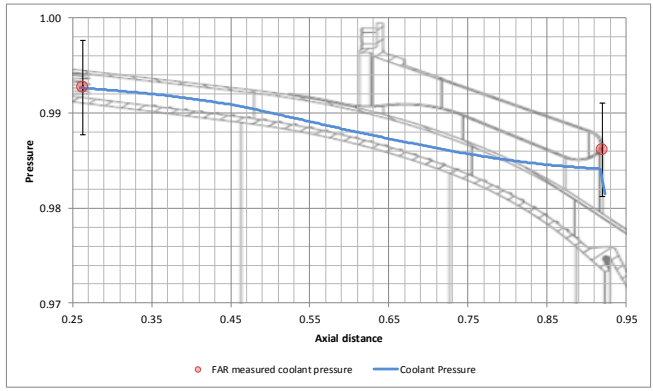

Figure 6-36, SN5-TP048 Coolant pressure comparison

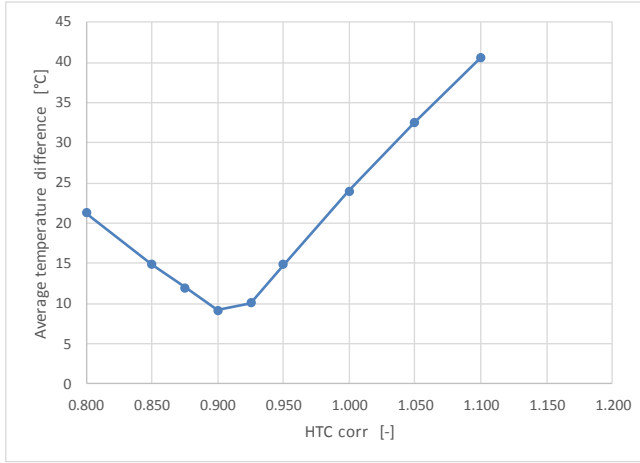

Figure 6-37, SN5-TP048 *HTCcorr* factor vs average temperature difference

6.2.6 SN6-Test Point 009

Test campaign 6, point 009 is an acquired set of measurements having an operating condition with high combustor inlet temperature, low flame temperature and nominal coolant mass flow. The assembly condition gap between liner and baffle is the maximum among the tested ones. Following graphs report the obtained comparison of predicted liner and baffle metal temperatures and coolant temperature and pressure losses, with the *HTCcorr* parameter equal to 1.00 (condition of minimum difference between measured temperatures and predicted ones: 20 °C average value).

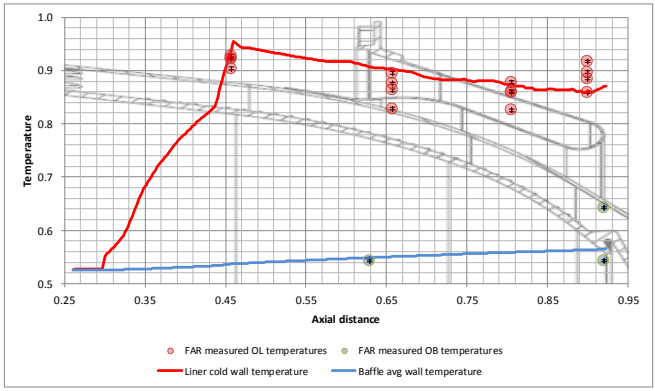

Figure 6-38, SN6-TP009 Liner and baffle metal temperature comparison

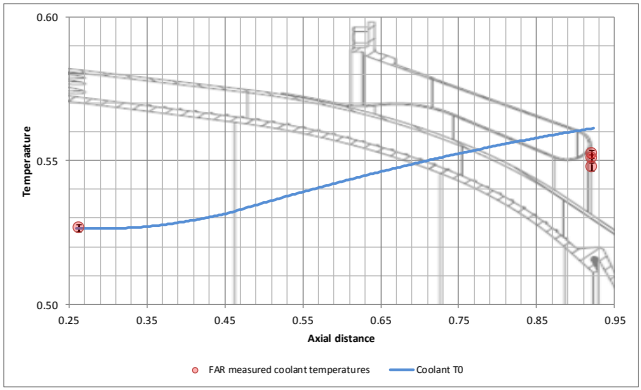

Figure 6-39, SN6-TP009 Coolant temperature comparison

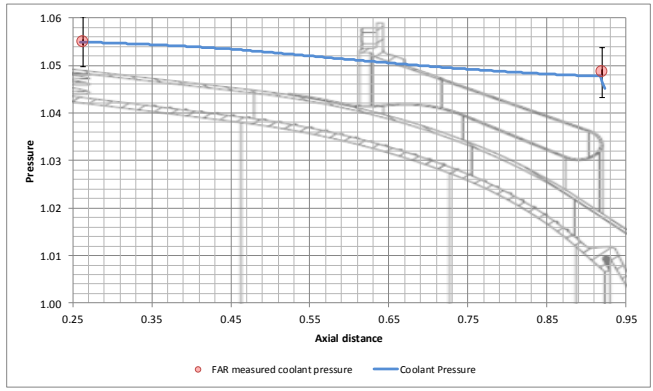

Figure 6-40, SN6-TP009 Coolant pressure comparison

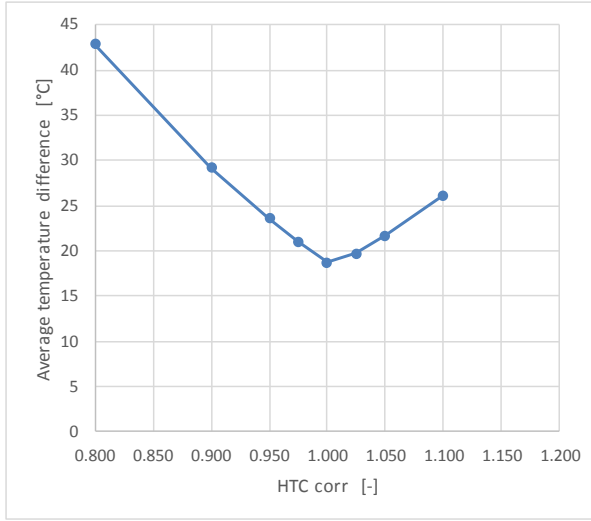

Figure 6-41, SN6-TP009 *HTCcorr* factor vs average temperature difference

6.2.7 Calibration results

The correction factors *HTCcorr* obtained for each calibrated test point, such that differences between experimental temperatures and predicted ones are minimum, are ranging within 0.90 – 1.15 values; maximum temperatures difference over the cases is within 20 °C, as summarized in Table 6-2 and shown in Figure 6-42.

These results confirm the GA code capability to properly simulate the main physical phenomena involved in the problem.

Validation test points							
Test campaign	SN	3	3	3	4	5	6
Test Point	TP	119	135	145	12	48	9
Average gap liner / baffle	gap	100%	100%	100%	101%	99%	102%
Outlet compressor temperature	TCD	80%	63%	100%	100%	100%	100%
Flame temperature	FT	102%	106%	100%	98%	100%	99%
Coolant mass flow	m	103%	103%	100%	91%	93%	95%
GA code datamatching parameter	HTCcorr	1.15	1.10	1.08	1.00	0.90	1.00
Average temperatures differences	ΔT	13.1	15.1	15.9	17.8	9.2	18.7

Table 6-2, Validation test points and results

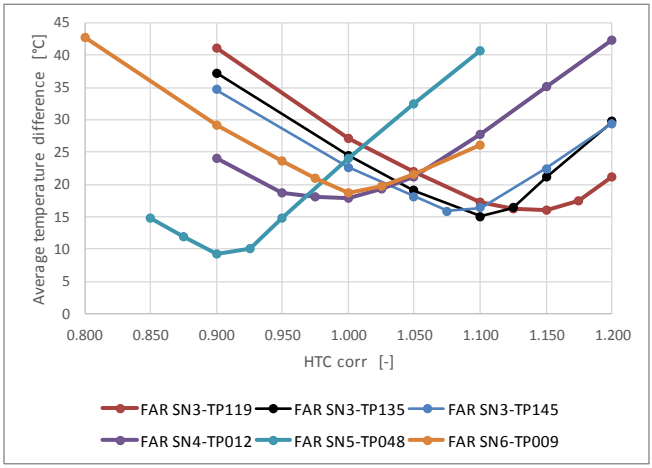

Figure 6-42, Overview of *HTCcorr* factor vs average temperature difference

The minimum error condition over all the calibration cases results centred in the 1.04 figure: such value is finally assumed as optimum value to be used for any prediction application of the GA code (e.g. during preliminary design phase of similar architecture combustors).

Performing an analysis of all the calibration cases setting the optimum value 1.04 of *HTCcorr* calibration factor, a final estimation of the temperature prediction error has been obtained: ±26 °C, as shown in Figure 6-43, corresponding to about 3% of the measured temperatures range.

The standard deviation of the temperatures comparison is 16.7 °C, corresponding to about 2% of the measured temperatures range.

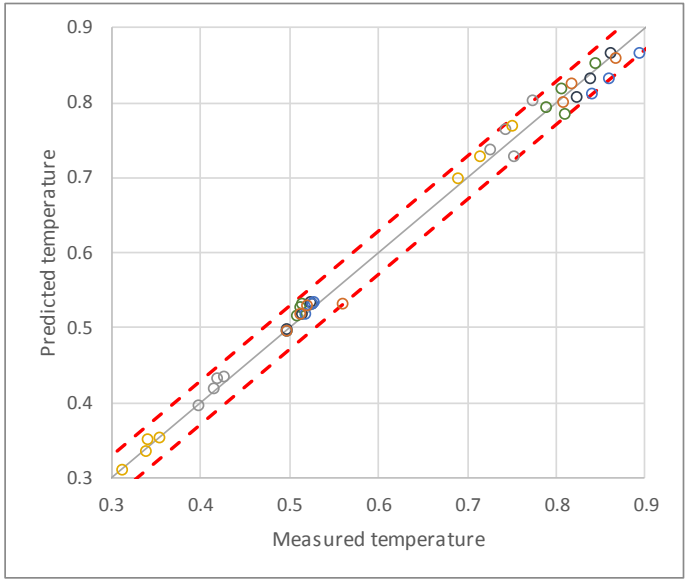

Figure 6-43, Error estimation

7 GA Code Application

The baffles design process, described in chapter 4, has been adopted in the combustor development of a new industrial gas turbine: the NovaLT12.

The engine overall architecture has many points in common with the NovaLT16 gas turbine already developed: it is a two-shafts engine configuration with variable NGV at power turbine inlet, adopting the well consolidated scaling process of the GE gas turbine design philosophy [Ref. 104].

About the combustor architecture changes have been introduced with respect to the NovaLT16 schema: the most relevant, related to the mechanical configuration, are the different set of constraints of the baffles and a different sealing system between liners and first turbine nozzle. Both these two architecture evolutions are based on the studies presented in this thesis. In the present chapter, the description of the baffles design will be presented.

7.1 Preliminary design phase

The baffle design started after the definition of the following design data (Figure 7-1):

- Maximum acceptable temperature: this reference value is function of the liners material. The first attempt adopted material is based on the selection already performed in the frame of NovaLT16 engine combustor development.
- Available pressure drop, as well as coolant mass flow, pressure and temperature are all obtained from the engine secondary flow estimation, considering a cooling architecture similar to the one of the NovaLT16 engine, depicted in chapter 3.1. In particular, the constraining value for both inner and outer gap of the available pressure drop is dictated by the first stage nozzle pressure drop requirement.
- Liners geometry, obtained as the best compromise between the derived requirements of typology, number and size of burners, combustion gasses residence time, aerodynamic profile indications, interfaces with surrounding components and assembly sequence.

- Liners hot side thermal boundaries: this set of data is the most affected by the uncertainties in the preliminary design phase until experimental data can be acquired to limit, by means of correlative 1D models and CFD model validation, the inherent difficulty in an accurate prediction of hot gasses heat exchange. The liners hot side thermal boundaries depend to the flame temperature axial distribution (hot side adiabatic wall temperature) and the fluid flow field inside the liners. Thanks to the scaling approach adopted for the burners and their surrounding structures, the same typology of burner already validated in the frame of NovaLT16 combustor design and testing, the Double Annulus Counter Rotating Swirler (DACRS), has been adopted, achieving a substantial reduction of these uncertainties in the preliminary design phase.

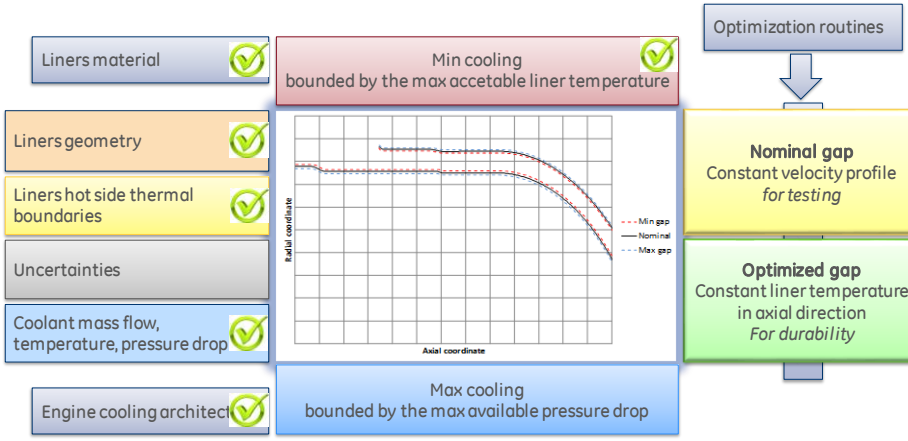

Figure 7-1, Baffles design process advancement

The uncertainties estimation taken a considerable amount of time, spent in design iterations with the selection of technological processes to manufacture the baffles and the resulting pressure drop estimation, which initially was not meeting the requirement of maximum available pressure drop.

The first family of manufacturing process selected for the baffles body was the metal sheet fabrication; this means a selection of a variety of processes, as bending, bulge forming, deep draw forming, double action expansion forming, draw forming, expansion forming, folding, hot forming, hydroforming, punching, rolling, roll forming, and shearing. This selection was based on the expectation of a cheaper direct material cost, compared with the conventional machining of forged parts.

The preliminary analysis of the linear and shape tolerances for the baffles body, also supported by the experience collected measuring some of NovaLT16 baffles with CAM touch probes and laser scans (Figure 6-17), generates values so high that the subsequent gap analysis was not able to meet the requirement of the maximum available pressure drop. In this manufacturing analysis was also assumed the first piece production condition: this means for the metal sheet fabrication processes that the worse results in terms of final geometry tolerances has been considered respect to the ones obtained with a full developed production line.

Critical for the quality of the bended, formed or punched components is the initial investment in the stamps and tools production and optimization, since typically at least two or three iterations in the tool design and adjustment are required.

Since the first nozzle cooling requirement was not satisfied, then the conventional machining of forged parts has been considered as manufacturing process. The baffles geometry, for annular combustor diameter dimension of about one meter, as order of magnitude, leads to a flexible behaviour of the component. When the machining process shall be applied on component of such typical diameters, it is fundamental to adopt enough thickness to provide the stiffness required to maintain the cut process stable as well as needed to obtain the desired shape tolerances. The minimum thickness required was higher than the typical values obtained by metal sheet fabrication processes and higher also than the minimum one required for avoiding baffle buckling and oxidation failure modes. Then the design of the baffles was modified to consider the incremented thickness requirement of the new manufacturing process selected and, consequently, also the others geometrical changes devoted to decoupling the baffles resonance frequencies from the expected exciters.

An additional aspect changing the design from the conventional machining to the fabrication manufacturing process is the rate of the geometrical slope change along the axial direction: conventional machining is not posing limitations about this aspect, while fabrication is limited to the plastic deformation of the adopted material during the different intermediate phases of metal sheet forming, bending or punching.
Being components not exposed to significant temperature gradients in all the operative conditions, thermal loads do not leaded to additional design requirements.
The design presented in this thesis has been based finally on the conventional machining of forged parts for the baffles manufacturing process.
It is worth to mention that, in parallel, an additional design effort has been put in place to convert again the design to the version consistent with the fabrication processes. This design iteration is justified, following a design to cost approach, by the expected saving in direct materials costs, assuming a volume of gas turbine unit production enough large to justify the initial investments in stamps and tools and making the fabrication process able to reach a level of tolerances acceptable for the first nozzle cooling requirement.
The resulting uncertainties estimation for both outer and inner baffle is reported respectively in Table 7-1 and Table 7-2.
In the tables, the term "worst relative displacements" is considering the deformation of the different engine parts during the worst engine transient phases, belonging to the chain of supporting structures for both liners and baffles. This term, as well as the thermal boundary conditions uncertainties, is affected by the hypotheses assumed to estimate these uncertainties. There are accurate methodologies based on MonteCarlo like analyses or the more recent technics of Uncertainty Quantification to be adopted to execute this investigation in the most robust way. For the preliminary design phase, the effort to introduce such methodologies has been considered not advantageous respect to assume directly components temperature variations in the range of the worst measurements acquired during the NovaLT16 engine tests.

Outer Baffle	Tolerances (cold gap)				Thermal bounday conditions uncertainties			Worst relative displacements
	Tolerances chain		Shape tolerances		Parts hot geometry			
	Liner	Baffle	Liner	Baffle	Liner	Baffle	HPT Vessel	
	mm	*mm*	*mm*	*mm*	*mm*	*mm*	*mm*	*mm*
axial	0.2	0.1	0.2	0.2	0.1	0.0	0.1	0.4
radial	-	-	0.5	0.5	0.5	0.2		

Table 7-1, NovaLT12 outer baffle uncertainties estimation

Inner Baffle	Tolerances (cold gap)				Thermal bounday conditions uncertainties			Worst relative displacements
	Tolerances chain		Shape tolerances		Parts hot geometry			
	Liner	Baffle	Liner	Baffle	Liner	Baffle	CDC	
	mm	*mm*	*mm*	*mm*	*mm*	*mm*	*mm*	*mm*
axial	0.2	0.5	0.2	0.2	0.1	0.1	0.4	0.6
radial	-	-	0.5	0.5	0.4	0.1		

Table 7-2, NovaLT12 inner baffle uncertainties estimation

It must be noticed that, comparing Table 7-1 and Table 7-2 values, the most relevant difference is in the inner baffle tolerances chain estimation: reason of the worse value is in the long mechanical path from the inner baffle axial fixation point, located on the compressor discharge chamber, and the corresponding one for the inner liner.
In addition, also the estimation of the worst relative displacement is affected by a larger uncertainty for both the longer axial length and the higher number of components.

The most obvious selection of the baffles constrain architecture was the one already known and tested in the NovaLT16 engine. Nevertheless, with the aim to reduce the manufacturing and installation costs, a trade-off of the possible alternatives architectures of baffles constraints has been performed.
Fundamental support in the estimation of different kind of constraints has been provided by the design of experiments analyses executed by means of the GA code: indeed, the

code has been structured to allow the imposition of different liner and baffle constraining points, to be fully representative of the mutual deformations, as described in chapter 5.3. The design of experiment assessment has been performed assuming an initial position of the baffle constraints and checking the effect of such assumption in the relative variation of the gap with the liner.
Outer baffle constraint point has been moved from the initial location on the outer liner to the HPT vessel, having evaluated the gap variation during the transient phases acceptable. Similarly, the inner baffle constraint point has been moved from the initial location on the inner liner to the CDC component.

The assembly sequence is based on the relative centering between the baffle and its relative liner: during the assembly, a dedicated tool is used to verify the concentricity of the two bodies, unless the shape tolerances effect, which can introduce local an out of concentricity condition.
The adopted criteria for the first attempt baffles geometry definition, accordingly to the validation strategy based on the combustor testing in a full annular rig, has been based on the axial constant velocity gap in hot condition. The desired cross-sectional area has been computed using the available coolant mass flow and its density, estimated on the assumed temperature and pressure at the compressor discharge from the turbine thermodynamic cycle.

Using the GA code routine for the axial constant velocity gap objective, described in chapter 5.9, the first attempt baffles geometry has been generated. In Figure 7-2 the hot predicted deformed geometry of outer liner and baffle are reported for the nominal case. Minimum and maximum gap cases then have been defined combining the uncertainties estimated respect to nominal case.
To individuate a nominal gap value, respecting both the requirements of maximum acceptable liner metal temperature and maximum available pressure drop, as in Figure 7-1, a sensitivity analysis, varying the nominal gap value has been performed.

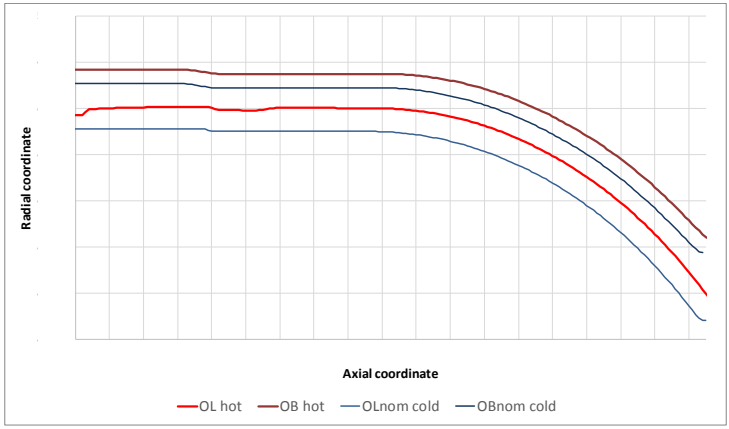

Figure 7-2, Outer baffle - Cold to hot prediction

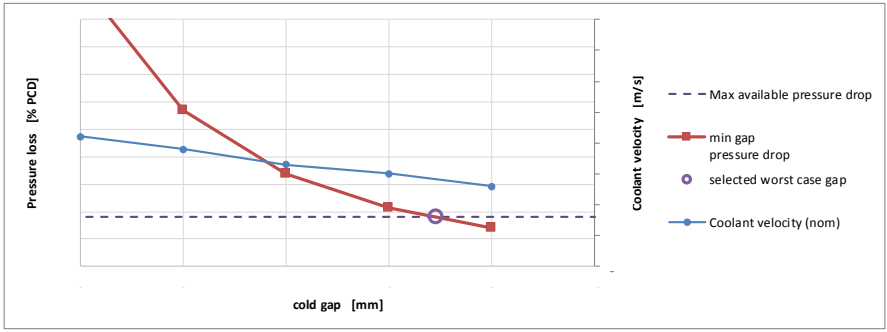

Figure 7-3, Outer baffle gap sensitivity analysis

Since the higher source of uncertainties is in the liner hot side thermal boundary conditions, the nominal value selection has been based on the first acceptable value, meeting the pressure drop requirement posed by the first nozzle cooling system.

Figure 7-4 reports the predicted metal temperatures, averaged in the thickenss, for outer liner and baffle in the 3 cases nominal, minimum and maximum gap, while Figure 7-5 and Figure 7-6 report respectively the coolant pressure drop, its flow temperature and velocity.

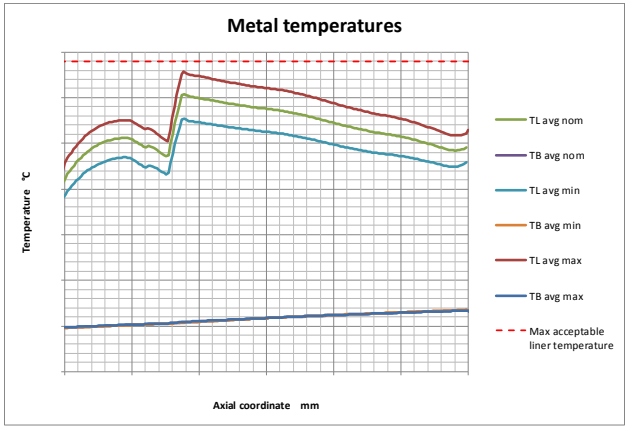

Figure 7-4, Outer baffle average metal temperatures predicted

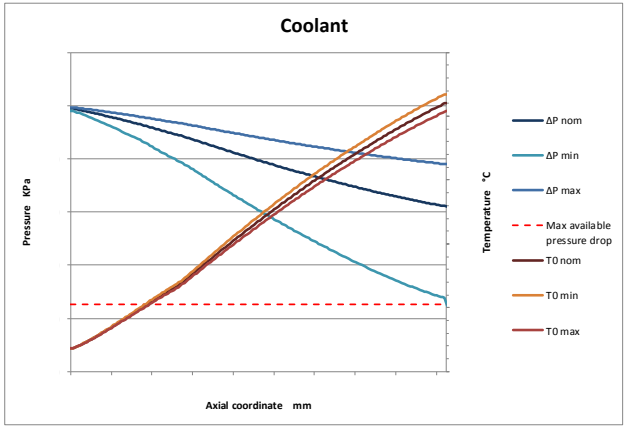

Figure 7-5, Outer baffle coolant pressure and temperature predicted

From Figure 7-4 and Figure 7-5, it is demonstrated that the selected design, considering all the mentioned uncertainties, is meeting both the requirements of maximum acceptable liner metal temperature and maximum available pressure drop.

It is worth to be mentioned that the coolant pressure drop, proportional to the square of the coolant velocity (Equation 5-12), increases proportionally more for the minimum gap case respect to how much reduces in the maximum gap case. This condition broke

the symmetry of the two worst cases respect to the nominal condition, since the cooling effectiveness is substantially proportional to the coolant velocity (Equation 5-11).

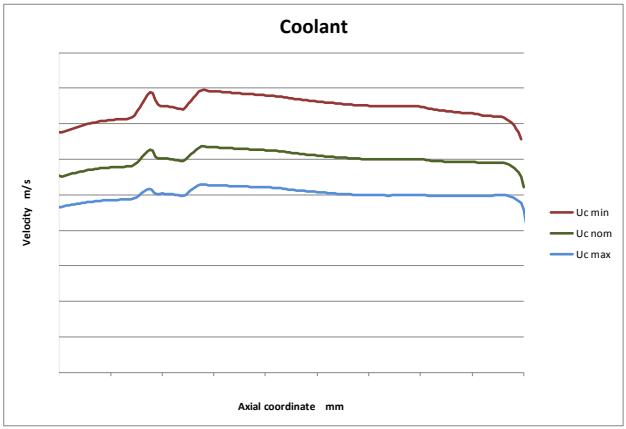

Figure 7-6, Outer baffle coolant velocity predicted

Comparing the outer liner metal temperature profile in Figure 7-4 with the coolant velocity profile in Figure 7-6, can be observed that the cold side cooling is about constant along the axial direction, while the hot side thermal boundaries, varying significantly, produce an axial temperature distribution with an important gradient in the metal temperatures.

Same design steps of the outer baffle have been performed for the inner baffle gap selection. Figure 7-7 reports the predicted metal temperatures, averaged in the thickness, for inner liner and baffle in the 3 cases nominal, minimum and maximum gap, while Figure 7-9 and Figure 7-10 report respectively the coolant pressure drop, its flow temperature and velocity.

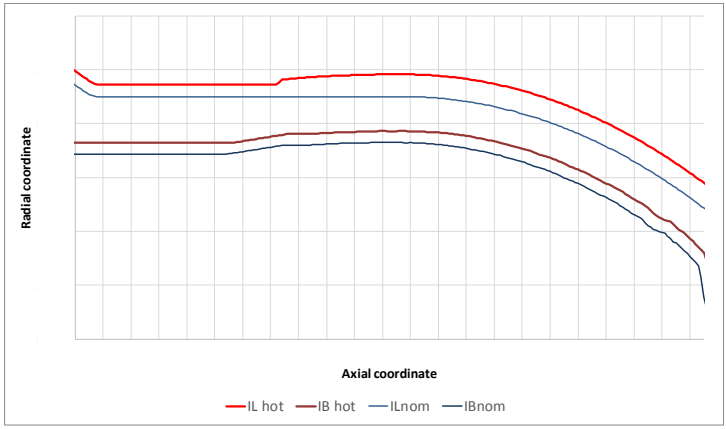

Figure 7-7, Inner baffle - Cold to hot prediction

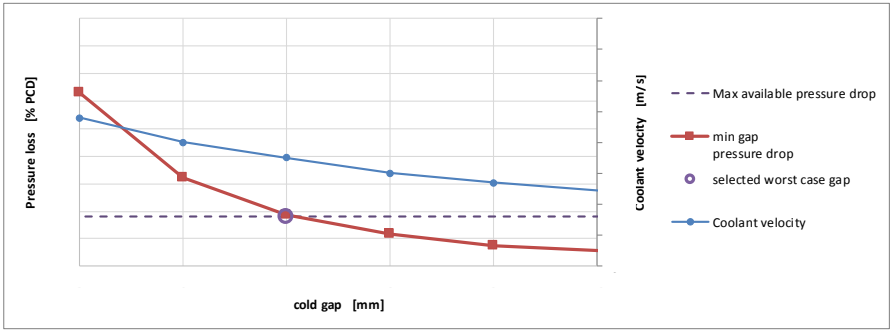

Figure 7-8, Inner baffle gap sensitivity analysis

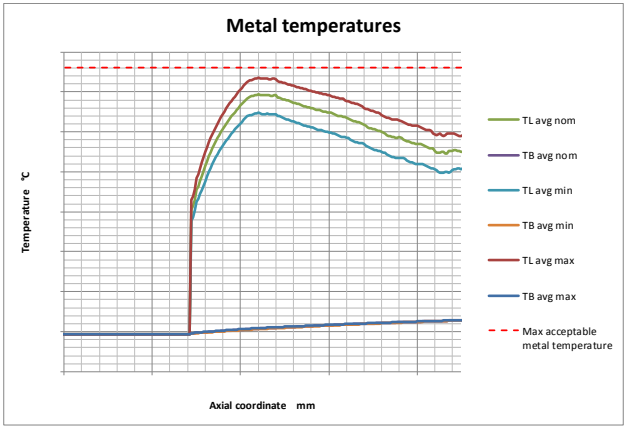

Figure 7-9, Inner baffle average metal temperatures predicted

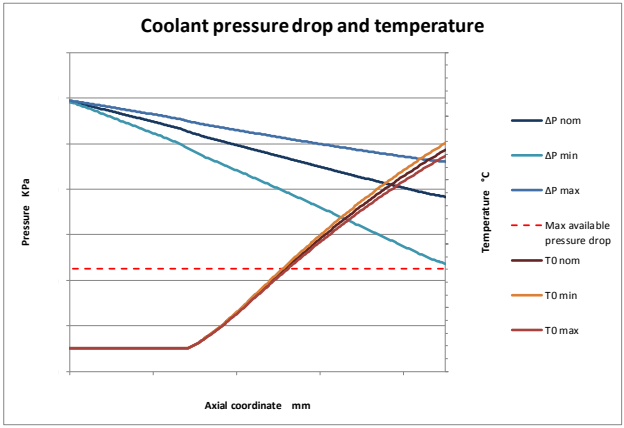

Figure 7-10, Inner baffle coolant pressure and temperature predicted

From Figure 7-9 and Figure 7-10, it is demonstrated that the selected design, considering all the mentioned uncertainties, is meeting both the requirements of maximum acceptable liner metal temperature and maximum available pressure drop.

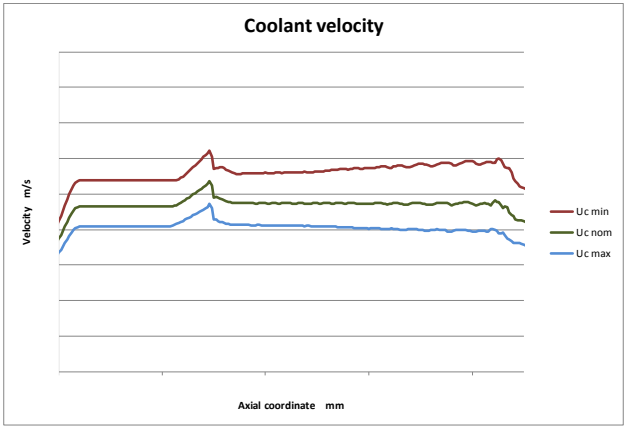

Figure 7-11, Inner baffle coolant velocity predicted

Also for the inner case, comparing the liner metal temperature profile in Figure 7-9 with the coolant velocity profile in Figure 7-11, can be observed that the cold side cooling is about constant along the axial direction, while the hot side thermal boundaries, varying significantly, produce an axial temperature distribution with an important gradient in the metal temperatures. Starting from this observation, the baffle design optimization has been introduced, as described in the next chapter 7.2.

Once defined the geometry of the full combustor, a two-dimensional axisymmetric finite element model has been prepared, as shown in Figure 7-12, aimed to simulate under the thermal and pressure loads, the deformation of liners and baffles, to verify the critical stress regions and, on these, analyse the number of cycles to crack nucleation.
The use of this kind of model, despite the not fully representativeness of the stress on the tridimensional structures, has the advantage of predicting the stresses in the liners and baffles along the engine axis direction in a quick and accurate way. During the preliminary design phase, the two-dimensional axisymmetric FEM can help a clear understanding of the thermal induced stresses impact mainly on the liners LCF life.
The predicted temperature maps, depicted in Figure 7-13, are consistent with the results of the GA code.

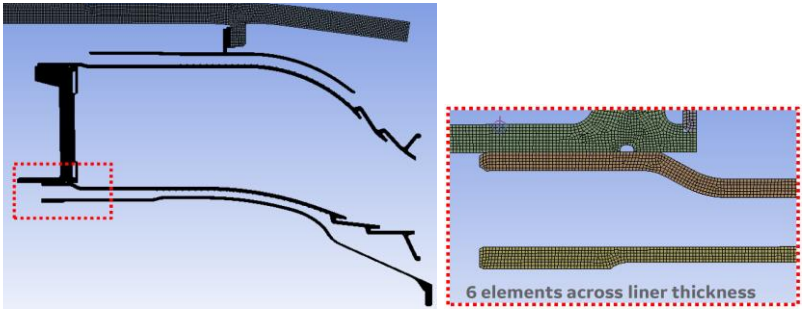

Figure 7-12, NovaLT12 combustor 2D axisymmetric FE model

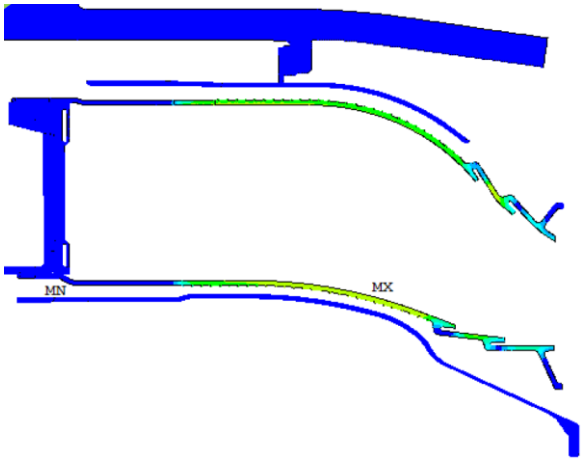

Figure 7-13, NovaLT12 combustor thermal map

Being a 2D axisymmetric model, a setting of the areas where every kind of holes are located, as shown in Figure 7-14, shall be performed altering the material characteristics to properly consider the reduced material sections: orthotropic material characteristics are then used instead of the isotropic ones.

Due to the fully tridimensional geometry of the domeplate, the correction introduced just with orthotropic material characteristics could be not enough to properly capture the

component stiffness. For this reason, a comparison with a tridimensional FEM has been performed, verifying both axial and radial deformations under a similar load.
Such check demonstrates the goodness of the initial assumption, justifying then the use of the axisymmetric domeplate model for the combustor deformation and stress analysis. In Figure 7-15 the constrained areas of baffles are represented.

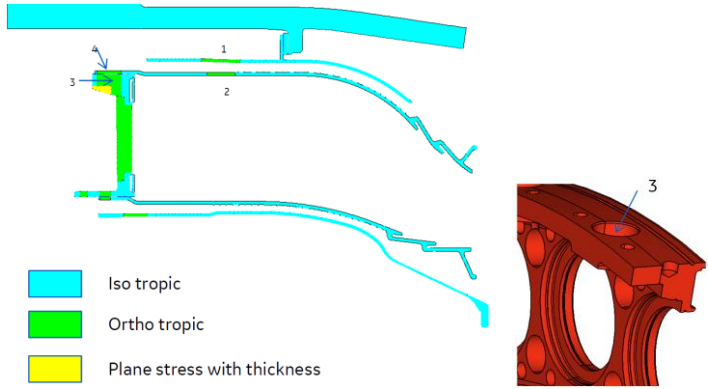

Figure 7-14, 2D axisymmetric model orthotropic regions

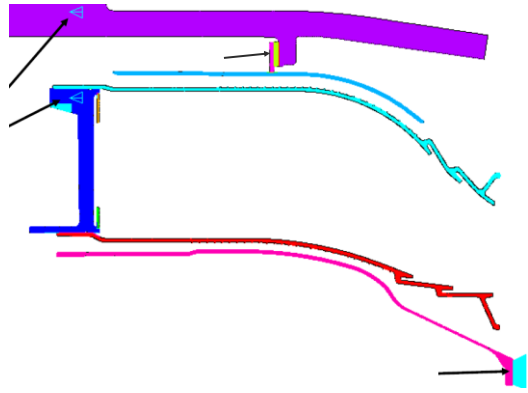

Figure 7-15, 2D axisymmetric model constraints

The resulting stress distribution in Figure 7-16 shows clearly that the areas of relevant stress are located where there are important temperature axial gradients. Such first

results have been updated once highlighted that in some regions the Von-Mises stress was exceeding the yield limit. Adopting the elastic-plastic formulation of the material characteristics in temperature, a more accurate strain estimation has been obtained, despite of the higher computational time required for the not linearity introduced.

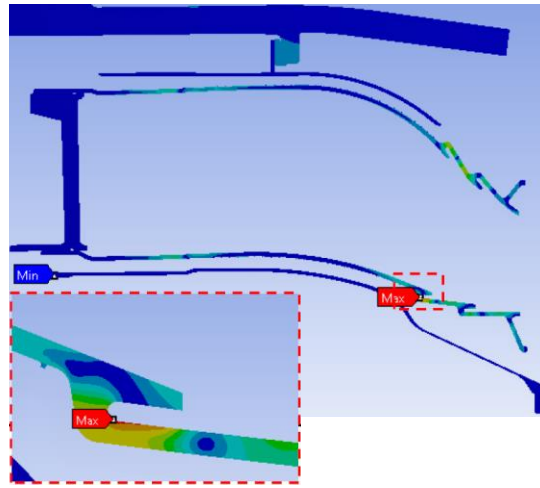

Figure 7-16, NovaLT12 combustor stress distribution

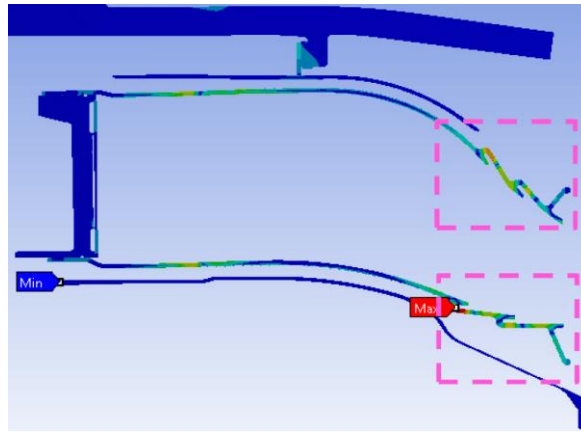

Figure 7-17, NovaLT12 combustor strain prediction

Figure 7-17 reports the resulting strain on the combustor components: maximum level of strain is in the nuggets region. Also in the region of forced convection, obtained thanks to the baffles design, there is a significant amount of strain, where stronger axial temperature gradient is present. For what concern the baffles, the design optimization is to find the way to decrease such significant level of strain.

7.2 Baffle design optimization

As described in chapter 4.3, an optimized geometry of the baffles can be obtained minimizing the liners metal temperatures gradients along the combustor axis direction, while maintaining the same coolant pressure losses of the original design.
Design intent is to minimize the axial temperature gradient, directly proportional to the thermal induced stresses, so that the resulting liners durability in terms of cycles to crack nucleation can be significantly enhanced.
Using the GA code routine for the optimized gap objective, described in chapter 5.9, the baffles geometry has been modified, starting from the same inputs used to design the axial constant velocity gap profiles. In Figure 7-18 the optimized outer baffle profile is compared with the initial obtained one, while in Figure 7-19 the resulting outer liner average metal temperature profiles are shown.

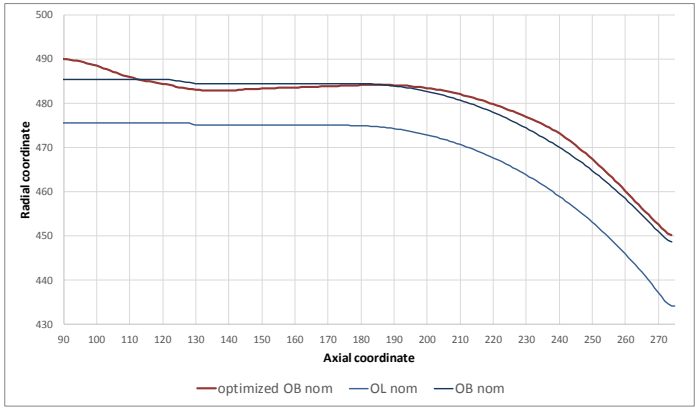

Figure 7-18, Outer baffle cold profile comparison

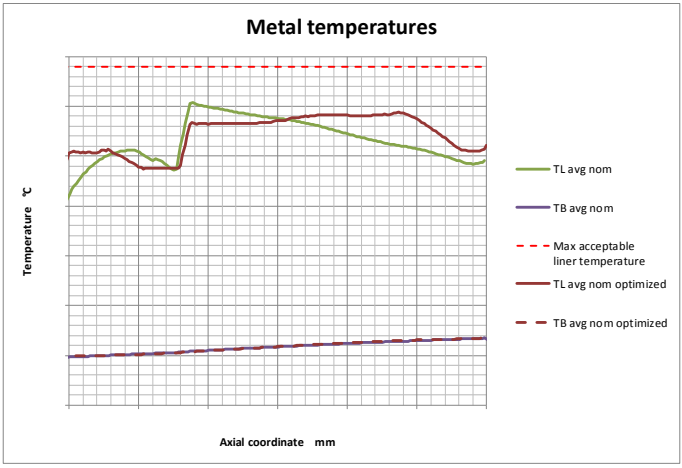

Figure 7-19, Outer liner average metal temperature profile comparison

The obtained reduction in the outer liner axial temperature gradient of about 38%, is leading to a local LCF life increase, strongly not linear for the selected material at the expected temperature, of more than 3 times the initial design prediction.

In Figure 7-20 the optimized inner baffle profile is compared with the initial obtained one, while Figure 7-21 shows resulting inner liner average metal temperature profiles.

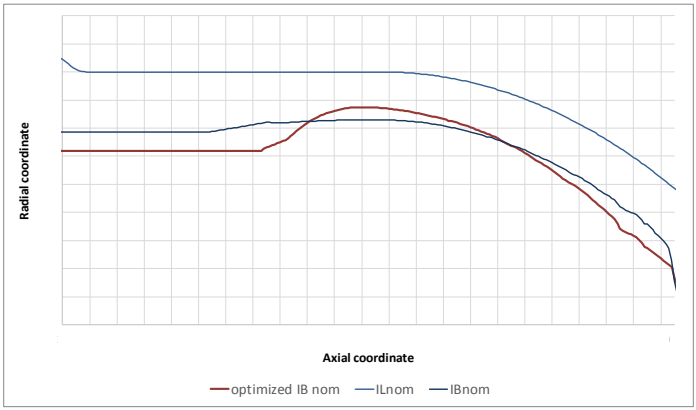

Figure 7-20, Inner baffle cold profile comparison

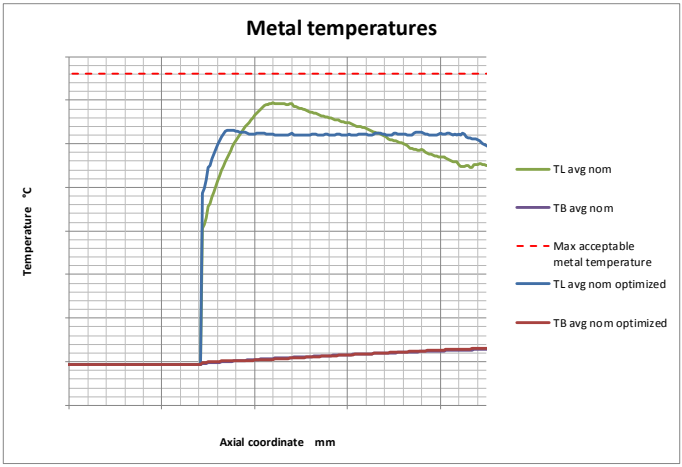

Figure 7-21, Inner liner average metal temperature profile comparison

The obtained reduction in the inner liner axial temperature gradient of about 29%, is leading to a local LCF life increase of more than 2 times the initial design prediction.

It can be observed, referring to Figure 7-19 and Figure 7-21, that there are some factors which are posing limits in the achievement of an ideal liner flat temperature distribution: by one side there are the technological constrains of the selected manufacturing process, which are locally imposing a minimum slope value for the geometry, and the cost reduction aspects, which act on the oversize material reduction of the raw forged parts. By the other side, the optimized baffle shall have a good enough cooling effectiveness in many different operating conditions: a geometrical optimization tailored just in a reference condition does not represent the optimum for the cooling design. Then the optimum profile is defined as envelop of the optimized profiles obtained under different worst cases thermal boundary conditions.

Some constraints in the available room for the geometrical modifications are imposed by the engine structures surrounding the baffles, as reported in Equation 5-17, but, in addition, some others functional constraints can be derived from the specific engine

architecture: in the arrangement of the NovaLT12 engine compressor, for example, the inner baffle back side surface is having a functional role in the diffuser section, being in fact a more stringent condition to the optimization problem.

Finally, it is worth to mention that, once the liner and baffle geometry is released, an optimization of the required mechanical tolerances has been performed as well. Using a design of experiment approach, the nominal geometry has been distorted with the assumed errors: the GA code results quantify the effect of the liner and baffle manufacturing tolerances, showing the critical regions, on which concentrated the manufacturing effort.

8 Liners – first stage nozzle sealing systems

The present chapter describes the studies performed on the leaf seals sealing system and on the alternative sealing solutions between combustor liners and turbine first stage nozzle. Aim of these studies is the increase of reliability of the combustor flow split prediction and to identify areas of improvement of the sealing between liners and S1N.

A reliable model of the leakage across the liners-S1N interface over the engine operating conditions allows a more accurate estimation of the engine secondary flow system and particularly of the combustor flow split. As described in chapter 3.1, the flow split estimation affects mainly liners and S1N cooling systems and the combustion air/fuel ratio: the reason of the high interest in the sealing performance between liners and S1N is in the impact on design compliance with requirements on the combustor and S1N durability, operability and emissions.

In particular, NOx emissions value is the most sensible engine parameter highlighting changes in the burners AFR and, being subjected to the stringent legislative requirements introduced in chapter 2.3, shall be maintained in the acceptable values range also in partial load operating conditions.

At the same time, also the reliability of the liners cooling system depends on the correct estimation of the leakage between liners and S1N: the coolant mass flow, which is one of the input parameters for the baffles design, as mentioned in chapter 4, is estimated solving a hydraulic network model having the liners-S1N leakage data as input.

Of primary importance for the sealing system design, as well as reaching the minimum possible leak rate, is the achievement of a constant sealing performance over the engine operative life or, at least, over the maintenance interval, since, changes in the expected air distribution can affect the reliability of others sealing or cooling systems.

The selection of the most appropriate sealing system shall be based on all the relevant requirements coming from the secondary flow design, engine operating conditions, cost and manufacturing constraints, assembly procedure and expected life.

The most important criterium for the sealing system selection is the estimation of the axial and radial relative displacements between the two components shall be interfaced and sealed: liners and S1N platforms.

The relative displacements between the sealed parts, are estimated since the early phase of design by means of the thermal and structural analyses of all the components involving the mechanical chains of components supporting the interfacing ones.

For the liners / S1N interface, the analysis dominium is comprising the combustor assembly, the high-pressure turbine assembly and also the compressor discharge structure. For all the involved components, an initial estimation of the deformations is performed typically by means of hand calculations or FEM 2D axial symmetric models, where the required thermal boundaries are estimated by the components thermal analysis. Such analyses are iterated and refined from initial assessments all along the development of the project up to the validation with the experimental data coming from prototype engine and dedicated test rig for validate some specific aspects, as leak areas or durability for the most critical sealing components.

The envelope of the positions assumed by liners and S1N platforms over the engine expected mission is reported in Figure 8-1 and Figure 8-2 for both the outer and inner sealing system, plotting in the meridian section view axial and radial relative displacements between liners and first stage nozzle platforms, where the axial and radial red bars around the assembly condition individuate the worst tolerance stack up during the assembly.

Looking to the axial relative displacements for both outer and inner interface, it can be observed that the maximum positive variation happens during the engine start-up: liners thermal inertia is sensible less than the one of the structure supporting it, then when the flame heat release increases their temperature, the associated thermal expansion shall be compensated by the sealing systems. Looking to the radial relative displacements, can be observed instead that outer and inner interface has an opposite direction moving from assembly to engine start-up condition: the inner liner thermal growth reduce the radial distance with the S1N inner platform, while the outer liner thermal growth increase the radial distance with the S1N outer platform.

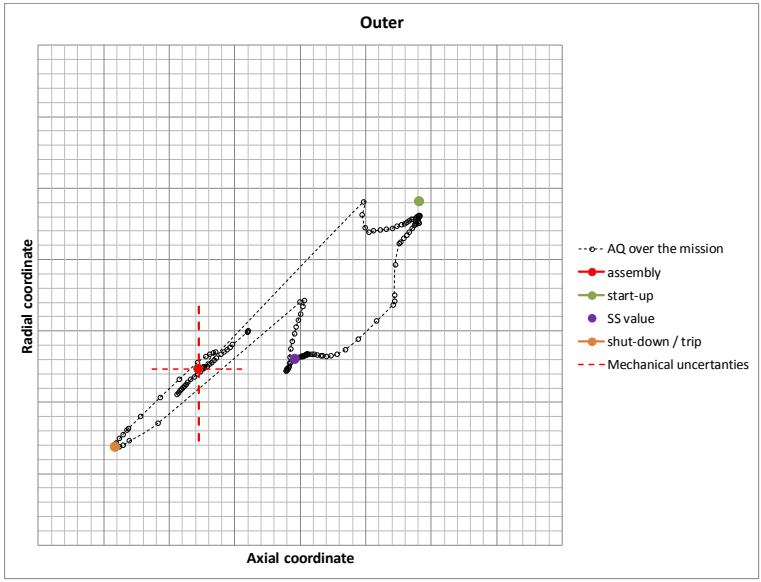

Figure 8-1, Outer sealing interface, relative displacements over expected mission

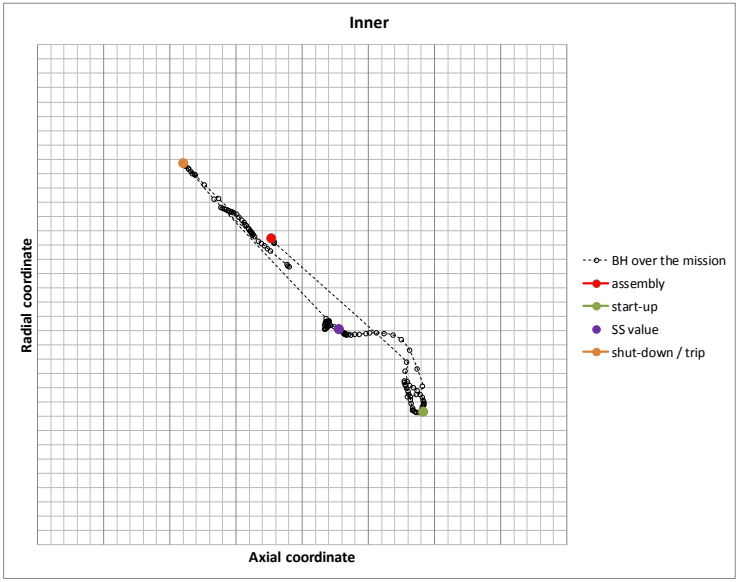

Figure 8-2, Inner sealing interface, relative displacements over expected mission

To individuate the worst conditions can occur in the sealing interface, two different types of uncertainties are considered with respect to the nominal geometry scenario: the components linear and shape tolerances and the assembly tolerances stack-up, which are constant over the expected mission (red dotted bars in Figure 8-1) and the steady state temperature maps prediction uncertainties, which are proportional to the expected temperature in steady state hot operating condition.

The start-up and the trip phases, being the worst conditions over the mission, constrain the design of the sealing system.

The tridimensional deformations of the involved interfaces for the sealing system are evaluated as superimposition of the effects respect to the 2D axial symmetric analysis.

One of the most important effect on the tridimensional shape of the liners is the burners staging phase during the engine load increase up to FSFL operating conditions: the worst staging scenario is represented by a continuous arc of fired burners, involving about half of the burners. An example of the tridimensional liners deformation is obtained by the finite element model analysis of the worst case burners staging sequence analyzed and reported in the Figure 8-3.

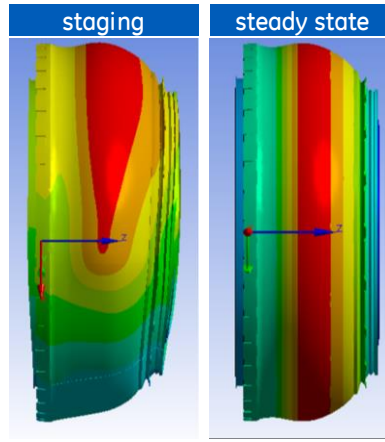

Figure 8-3, Staging effect on Liners deformation

The thermal induced deformation of the turbine S1N has been obtained by means of a finite element model analysis, see Figure 8-4, with focus on the platforms deformations, zones where the sealing system interface is located. In axial direction, both outer and inner platform increase their dimension in the middle part with respect to the edges. In radial direction, both outer and inner platform edges increase their dimension with respect to the central part of the S1N sector.

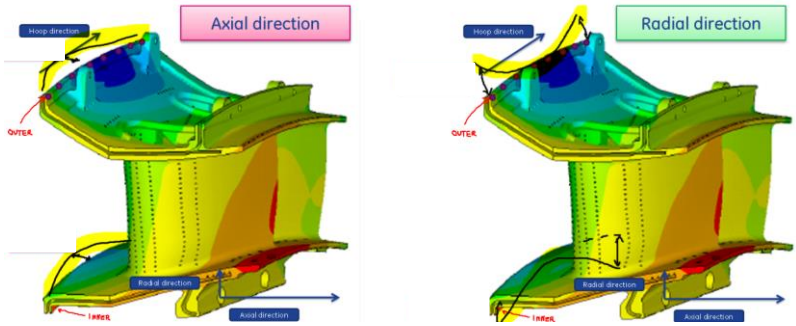

Figure 8-4, S1N platform deformation

Whole S1N sector rotations, due to external aero loads acting on the airfoils, are typically negligible with respect to thermal induced deformations, but are considered in their role of altering the nominal position of the sealing system interface.

Adding the estimated uncertainties of the boundaries adopted in the thermal FEA, as well as for the mechanical tolerances stack-up, the worst relative displacements for liners / S1N interfaces with respect to assembly position can be determined: all the alternative sealing concepts shall be able to withstand such extended range of axial and radial displacements.

The engine assembly sequence, involving the sealing system between liners and S1N, is realized assembly the combustor with a dedicated setup and tools, in order to guarantee all the assembly tolerances and, in particular, the concentricity of the liners and their aft-end axial distance respect to the reference plane of the combustor. Once assembled, the combustor is then installed in the HPT vessel. Compressor is connected with the HPT vessel and the S1N assembly, composed by the sectors and a supporting

ring, is installed on the compressor discharge chamber interface. During this last step, the sealing system is axially compressed. The assembly of the sealing system shall be realized acting only with an axial relative movement between the liners already in fixed position and S1N, which shall be inserted and fixed by means of the S1N ring to CDC interface. An eventual access to the sealing parts for specific assembly adjustments is guarantee only to outer part and with limited available room.
Considering the variation of the operative conditions, the sealing system shall withstand a continuous working temperature ranging typically from the 500 to 700 °C, whit eventual maximum transient working temperature of 800 °C for short period of time (less than one minute).
As mechanical loads, the sealing system shall withstand a continuous working pressure drop ranging from 20 to 100 KPa, with a maximum transient pressure drop increase of 10 KPa, due to combustion dynamics.

8.1 Leaf seals

Leaf seals is a sealing system between liners and S1N typically adopted for aero and aero-derivative gas turbine engines, thanks to its limited mass and the good level of sealing can realize. This sealing system has been analyzed and designed for the NovaLT16 combustor, since the positive heritage accumulated in others gas turbine.
As highlighted in the combustor design development, the leaf seal application for the NovaLT16 engine is out of the range of experience collected in similar sealing application, manly for the amount of the relative displacements between liners and S1N and for the required MTBM, typically more severe for industrial application.
Therefore, in addition to the aim of increasing the reliability of the combustor flow split prediction, models have been developed to predict also the sealing system reliability.
In this chapter, a detailed analysis of this sealing solution is reported, for a deeply understanding of the main aspects influencing their design.
The leaf seals are metal sheets with a thickness of some tenths of the millimeter, as order of magnitude, as shown in the Figure 8-5.

Figure 8-5, NovaLT16 outer and inner leaf seals

The leaf is constrained to the S1N sector by means of two pivots inserted in a corresponding hole and slot-hole and in a machined cavity on the S1N cold side platform, as represented in Figure 8-6; two conical springs, coaxial with the pivots, provide a soft trust, pushing the leaf toward the liner aft-end during the assembly.
The conical type spring allows a relative rotation between the two extreme spring faces, while maintaining the axial preload, for small rotation angles.
The S1N sectors assembly with leaf seals is positioned in front of the combustor liners aft-end during the HPT integration, by means of a translation parallel to the engine axis.

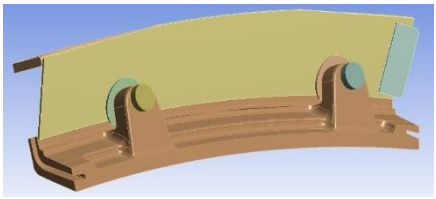

Figure 8-6, Outer S1N platform with leaf seal and liner aft-end

The pressure in the hot gas path volume is less than the pressure in the liner and S1N cold sides, mainly due to combustor pressure losses. When the delta pressure increases from zero to the full speed engine operating condition, the leaf seals are strongly pushed against liners aft-end, obtaining by their deformation an improvement of the sealing.
A study of the kinematic can help the understanding of the mechanism realized by the assembly of liner aft-end, leaf seal and S1N: a hypothesis assumed in this analysis is the perfectly rigid behavior of the leaf seal. This hypothesis will be then removed introducing the real flexural deformation of leaf seal under the applied pressure loads.

The leaf seal positions, assumed in function of the axial relative displacement between liner aft-end and S1N, are shown in Figure 8-7 for the outer one: the leaf seal movement is a roto-translation, where the contact positions with both liner aft-end and S1N platform are changing in function of the angle sign.

Analyzing the contact points variation along the radial direction, the outer leaf seal, for negative angles, is touching the external diameter of liner aft-end and S1N platform, while for positive angles is touching the inner diameters of both. Inner leaf seal, vice versa, is touching inner diameter of liner aft-end and S1N platform for negative angles, while for positive angles is touching the outer diameters of both.

Analyzing the contact points variation along the axial direction, when the worst positive angle is reached: the leaf is in contact in the two extreme circumferential edges both with liner aft-end and S1N; maximum clearance is in the middle of the two contact areas. When the worst negative angle is reached: the leaf is in contact in the middle point of both the two contact areas with Liner aft-end and S1N; maximum clearance is in the two extreme circumferential edges.

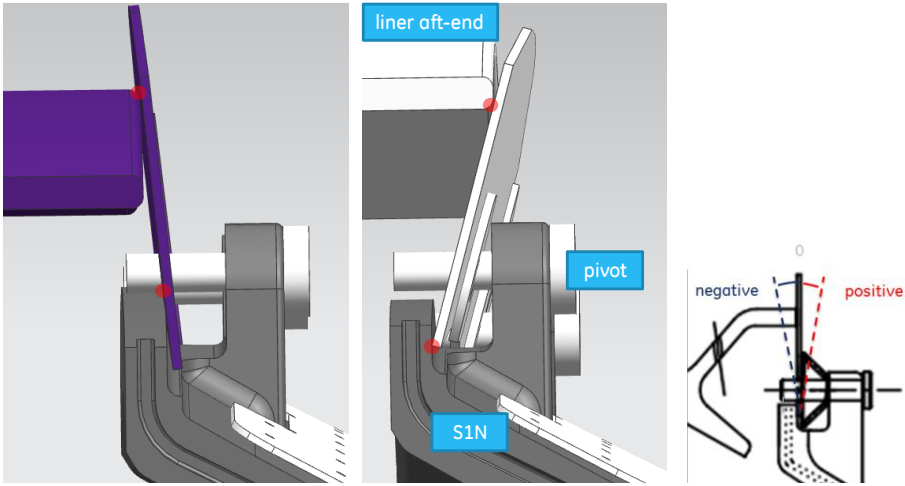

Figure 8-7, Sketch of outer leaf seal positions

The leaf seal angle for the outer sealing system, can be evaluated by means of Equation 8-1, supported by the sketch in Figure 8-8.

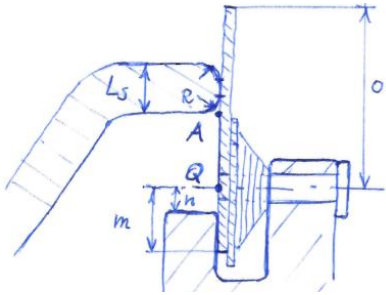

Figure 8-8, Outer leaf seal angle computation

$$\alpha_{nom} = tg^{-1}\left(\frac{AQ_x}{D}\right)$$

$if\ AQ_x > 0 \qquad D = AQ_r + R + m$
$if\ AQ_x < 0 \qquad D = AQ_r + L_s - R + n$

where:
AQ_x is the relative axial displacements between liner aft-end and S1N;
AQ_r is the relative radial displacements between liner aft-end and S1N;
R is the liner aft-end radius;
L_s is the liner aft-end thickness;
m is the radial distance between pivot axis and the leaf lower edge;
n is the radial distance between pivot axis and the S1N edge.

Equation 8-1, Outer leaf seal angle computation

To understand the relation involving the angular positions can be assumed by the leaf seals and the relative displacements over the engine mission of liners and S1N, the graphs in Figure 8-1 and Figure 8-2 has been plotted in terms of leaf seal angle in function of the mission time.

In Figure 8-9 a conceptual of the outer and inner leaf seal positions variation over the mission are reported; at start-up condition the leaf seal reaches the worst positive angle, while at shut-down or trip condition, it reaches the worst negative angle.
Being the achievable sealing function of the leaf seals angle, the leak rate estimation is nominally computed in steady state condition.

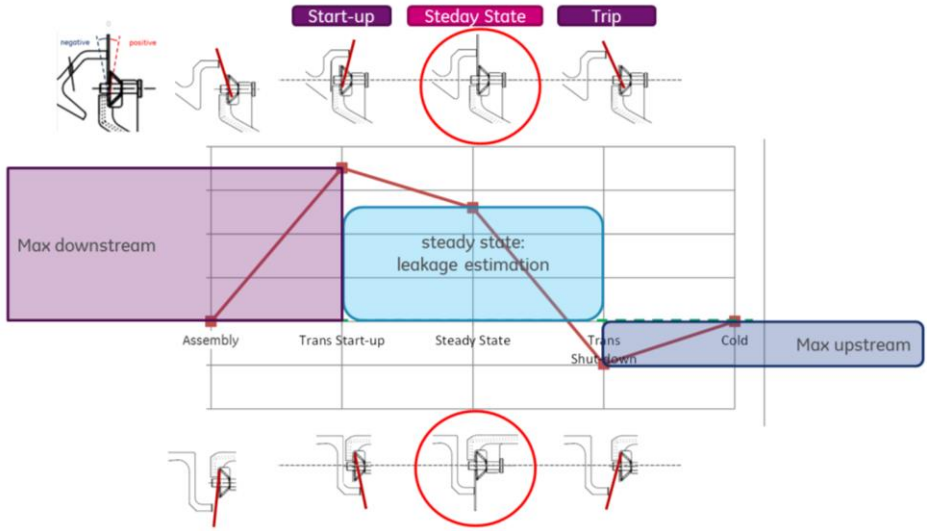

Figure 8-9, Leaf seal kinematic evolution over the mission – details

The interface between leaf seal holes and its assembly pivots realizes in fact an imperfect joint, allowing relative leaf roto-translation with respect to the fixed pivots, which are welded on the S1N during the leaf seals integration.
Performing a tolerances stack-up analysis of the geometrical dimensions of pivots and S1N and leaf holes, it can be obtained that the leaf seals, assumed as rigid bodies, can tilt from a minimum of -36% to a maximum of +64% of their angular range.
Minimum angle is limited by the contact between leaf seal holes and pivots, while maximum angle, as depicted in Figure 8-7, is limited by the contact between leaf seal and S1N structures supporting pivots and springs.

Leaf seal angle measurements have been performed on the sealing system prototypes during the assembly, in ambient condition and without pressure load applied: corresponding to the rigid body behavior of the seals.
Collecting leaf seal angle measurements for 8 different sealing systems, each composed by 22 elements, a statistical distribution of the angular capability of the leaf seals have been acquired: average angular range is 76% of nominal one, while the 3σ angular range is limited 52% of nominal one.
An accurate assembly procedure has been introduced during the welding of the pivots to the S1N sector, allowing a reduction of the uncertainties in the pivot angular position respect to the S1N sector. The obtained advantage has been an increase of the leaf seal angular range: average value equal to 91% and 3σ value equal to 60% of nominal one.
Collected measurements evidence a significant reduction leaf seals angular capability with respect to the nominal expected one: such reduced values shall be assumed to the design and verification of the leaf seals.
Furthermore, the angular range, depending to the interface between leaf seals and S1N, can be used as an invariant parameter in the leaf seals design, allowing a geometrical scaling of this sealing solution for different required relative displacements between liner and S1N.
The leaf seal main geometrical design parameters are reported in Figure 8-10.

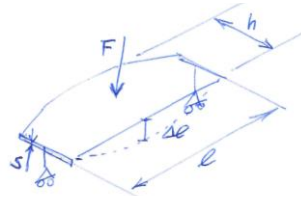

Figure 8-10, Leaf seal geometrical parameters

The leaf length *l*, function of the S1N sectors number *n*, the S1N pivot hole radial distance wrt engine axis R_Q and the gap between adjacent leaf in hoop direction *gap*, is computed by the Equation 8-2.

$$l = \frac{2\pi R_Q}{n} - gap$$

Equation 8-2, Leaf seal length computation

About the leaf thickness s, assuming a simple model as depicted in Figure 8-11, a range of acceptable thickness between s_{min} and s_{max} can be defined, considering the relation between pressure loads, leaf deflection and yield stress and maximum sagittal distance leaf / liners aft-end, applying the Equation 8-3.

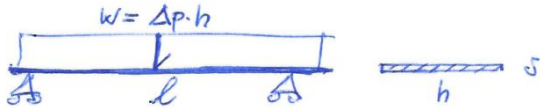

Figure 8-11, Leaf seal thickness assessment

$$s_{min} = \sqrt{\frac{\Delta P_{max}\, l^2}{192\, \sigma_y}} + t_{ox}$$

$$s_{max} = \sqrt[3]{\frac{60\, \Delta P_{min}\, l^4}{384 \quad E \quad \bar{x}}}$$

where:

- ΔP_{min} and ΔP_{max} are the minim and maximum pressure drop across the sealing system, evaluated respectively to FSNL and FSFL operating conditions, respect to the nominal value, specified in Equation 8-4;
- E, σ_y and t_{ox} are the material characteristics, respectively Young's modulus, yield stress -3σ and total oxidation (on two sides) evaluated to expected operating temperature and for the required MTBM.
- $\bar{x}$ is the axial sagittal distance between the not deformed leaf tilted at the maximum positive angle and the liner aft-end, as depicted in Figure 8-12.

Equation 8-3, Leaf seal length computation

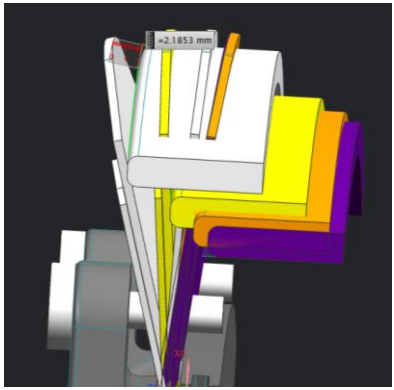

Figure 8-12, Axial sagittal distance

$$\Delta P_{nom} = PCD * (\Delta P\%_{burner} - \Delta P\%_{liner\ /\ baffle\ \ gap})$$

where:

- PCD is the compressor discharge pressure;
- $\Delta P\%_{burner}$ is the pressure drop across the burner;
- $\Delta P\%_{burner}$ is the pressure drop after the liner / baffle gap.

Equation 8-4, Leaf seal nominal pressure drop

The radial relative position between liner aft-end and S1N platform at the assembly is defined considering two possible undesired conditions: when liner reach the contact with S1N pivots or when the leaf seal is free, since liner overcomes the leaf eight.
Considering all the relative displacements depicted in Figure 8-1 and Figure 8-2, and once the S1N radial distance respect to engine axis is defined by the theoretical hot gas path, liners aft-end geometry is adjusted to guarantee enough margin respect to the two mentioned undesired conditions. At the same time, also the leaf height (h) is defined, considering as additional criteria that the leaf height shall be the minimum one assuring a margin against the free condition: higher leaf seals can be affected by the aerodynamic loads on the portion of their surface exceeding in radial direction the liner aft-end profile. The required angular range can be centered in the leaf seal angular capability, acting on the axial relative distance at the assembly between liners aft-end and S1N platforms.

Based also on the experience collected in combustor tests performed in a full annular rig, the following criteria shall be respected in the leaf angular range design:

- FSFL required angle shall be within the leaf seal 3σ capability angular range. If not respected, leaf seal HCF failure can occur (chattering failure mode), as shown in Figure 8-13; leaf seal can be not in contact with liner aft-end during some transient phases, reaching in this condition a not acceptable level of dynamic response to the exciters;

Figure 8-13, Example of leaf seal HCF failure

- The maximum required angle shall be lower than the leaf seal maximum available angle: overcoming such value, permanent leaf seal deformation will occur, as shown in Figure 8-14; the excessive axial difference of deformation between liner aft-end and S1N platform, stamps the leaf seal, imposing a plastic permanent bending.
- Leaf seals shall be always in contact with liners aft-end, to avoid damage or rupture, due to high cycle fatigue induced by acoustic vibrations (chattering failure mode);
- If the condition always in contact is satisfied, leaf seals should be vertical in operating FSFL conditions, to maximize the sealing.

Figure 8-14, 3D scan of a plastically deformed leaf seal

To fulfil the above criteria, some iteration in the design process, changing the leaf seals design parameters, could be requested, to increase the available angular range. In Figure 8-15 the conceptual design flow adopted is schematically shown.

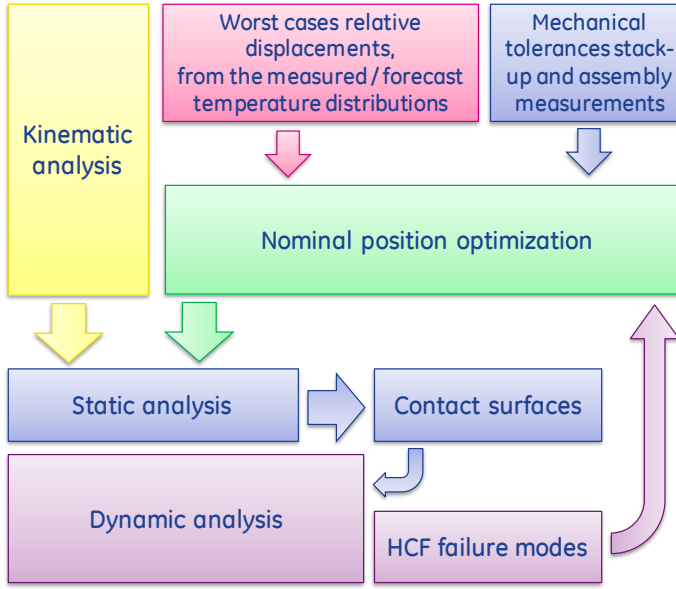

Figure 8-15, Leaf seals conceptual design flow

Applying Equation 8-1 over the expected mission, it's possible to retrieve the evolution of the required leaf seals angular range: the α_nom angle (black line) in Figure 8-16. Adding the uncertainties for mechanical tolerances and thermal maps prediction, the required angular range is extended to the minimum and maximum values over the expected mission: the α_min and α_max angles (blue and purple lines) in Figure 8-16.

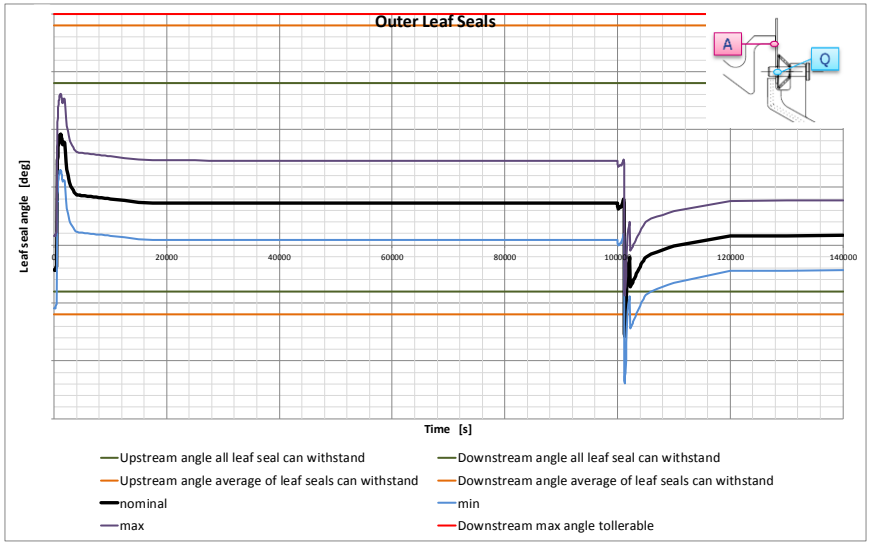

Figure 8-16, Outer leaf seal angle over the mission

In Figure 8-17 can be observed the sudden angle increase of about 9 degrees corresponding to firing up phase of the burners. Similarly, is visible in Figure 8-18 at engine trip condition the sudden angle reduction when the fuel is cut, leading to flame out. In this case the required angle is out of both the 3σ and the average leaf seal angular capability: experimentally has been demonstrated that this condition is not causing a leaf seals failure, thanks to the sudden pressure reduction happening in the engine trip case.

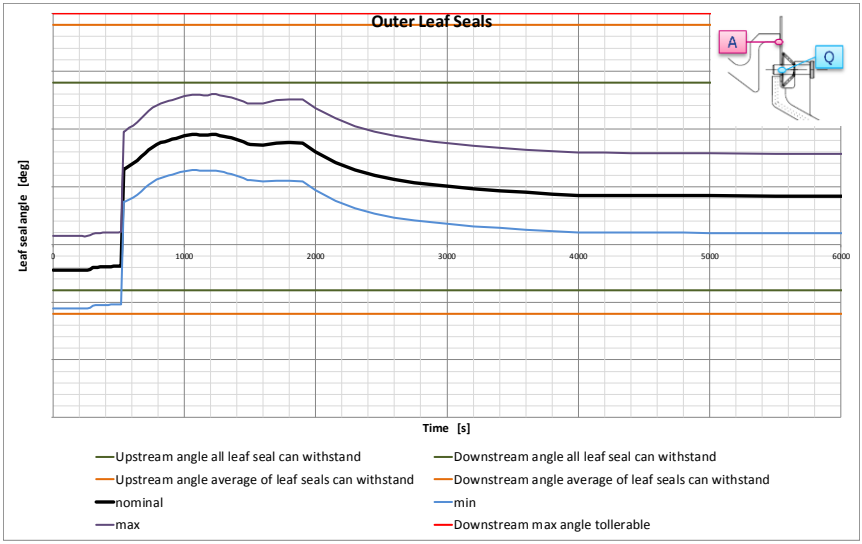

Figure 8-17, Outer leaf seal angle over the mission- engine start-up

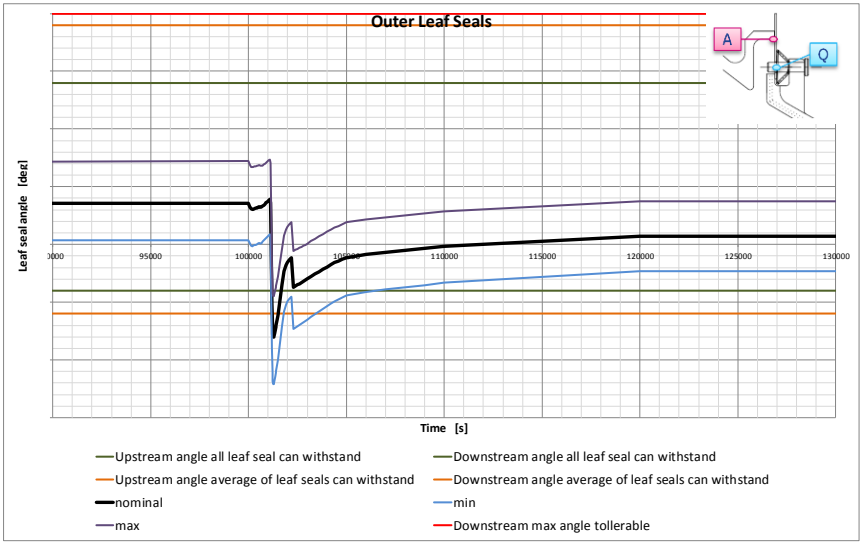

Figure 8-18, Outer leaf seal angle over the mission- engine trip

The changes over the mission of the radial position of the contact area between liner aft-end and leaf seal in Figure 8-19 are reported. Such analysis allows the evaluation of the margins respect to the free leaf seal condition, when the liner aft-end overcomes the leaf height losing the mutual contact (critical for chattering failure mode) and the condition of undesired contact between liner and pivots.

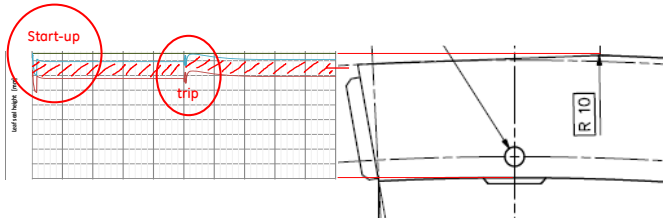

Figure 8-19, Example of outer liner / leaf seal contact area

Presence of clearances offering an air passage is a not desirable condition: clearances shall be minimized, as design goal. Listing the leaf seal clearances, there are:

- Axial flow passage between adjacent leaf seals and across the hole and hole-slot areas not fitted by pivots;
- Radial flow passage between adjacent leaf seals, considering the leaf thickness;
- 3D geometry clearances opened for tilted leaf seals conditions.

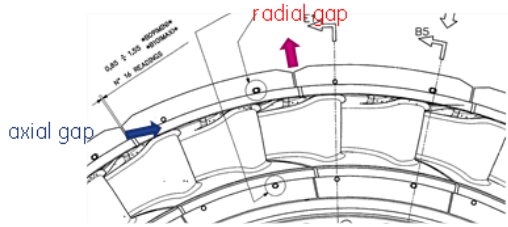

Figure 8-20, S1N assembly: example of leaf seal clearances

The axial flow passage is the most relevant term among the 3 mentioned: a clearance between adjacent leaf seals is required for the assembly tolerances on each leaf seal

position and thermo-elastic differential dilatations between leaf seal and S1N in hoop direction.

Also, the large clearance between leaf seal holes and the relative pivots diameters is required, because it should allow the rotation of leaf seal and it is also required for the differential dilatation between the S1N sectors and their supporting ring in circumferential direction.

The axial flow passage could be significantly limited, if required, introducing a cover plate: a shield brazed on each leaf seal back side, covering the adjacent leaf air passage, as depicted in Figure 8-5.

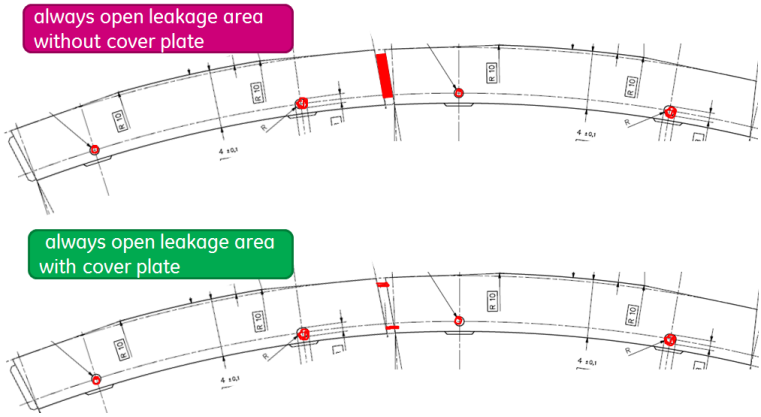

Figure 8-21, Axial flow clearances

The radial flow passage term considers the small passage areas between adjacent leaf seal in radial direction: two times (outer and inner) the leaf seals thickness multiplied by the circumferential gap between adjacent leaf seal, multiplied by leaf seals number.

To evaluate the tridimensional clearances in the tilted leaf seal conditions as function of the angle, a kinematic analysis has been performed by means of CAD software, assuming a perfectly rigid behavior of the leaf seals.

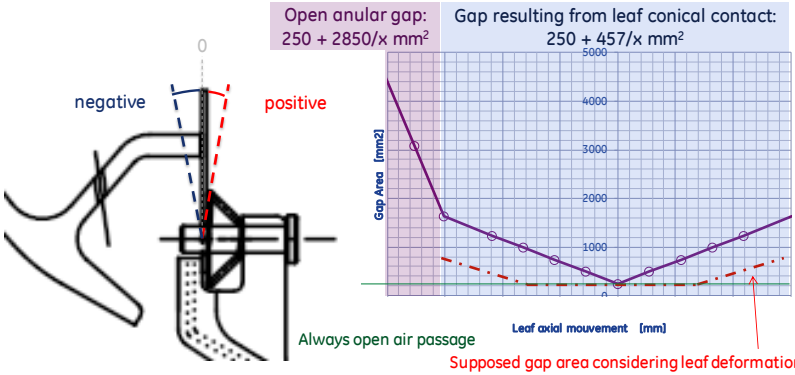

Figure 8-22, Leaf seal leak area for tilted position

In real condition, the leak area will be different from the one analyzed, as hypothesize with the red line in the following figure, considering the leaf deflection under pressure and contact loads: the FEM analysis shows that under the nominal pressure load, the leaf deflection is enough to fit the liner and S1N contact planes also in the worst tilted conditions.
The leaf seal leak area is minimum in the leaf vertical position.

The durability analyses, aimed to estimate the MTBM achievable by the sealing system, start from the leaf seals temperature prediction.
The leaf seal temperature estimation is affected by the uncertainties in the evaluation of the gas temperature within the annulus between liners aft-end and S1N: a quantitative evaluation has been done thanks to an aero-thermal model, considering that the adiabatic wall temperature seen by the leaf seals comes out from the mixing between coolant leakage and the hot gas could enter in the gap between liners and S1N platforms.

In the worst case of leakage absence, the same adiabatic wall temperature seen by the nugget at the aft-end location can be assumed for the leaf seals. The presence of additional holes feeding with coolant the annulus acts in further reducing the temperature.

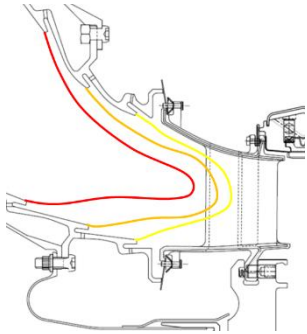

Figure 8-23, Qualitative hot gas temperature contours

The total oxidation is estimated as leaf seal both side thickness reduction, thanks to available material data based on the Equation 8-5.

$$t_{ox} = C_1 * t^{A_0 + A_1 * T/1000}$$

where:

- t is the time in hot condition;
- C_1, A_0, A_1 are constant, obtained from the material experimental data;
- T is expected leaf seal temperature.

Equation 8-5, Leaf seal total oxidation

To assess the criticality of leaf seals oxidation, the resulting temperatures measurements in the liners aft-end location coming from the Full Annular Rig test has been used to estimate the adiabatic wall temperatures; such temperatures will be assumed as leaf seal temperatures. Based on the leaf seal temperature individuated, a prediction of the leaf seal life will be performed, comparing the thickness reduction due to oxidation with the

critical value. The thickness reduction evaluated considering the MTBM requirement has been compared with the minimum thickness value, calculated according to Equation 8-3 and introduced in the FEM static and dynamic analyses.

The evaluation of long term deformation due to creep has been based on stress results, coming from the FEM analysis of the combustor 2D axial symmetric model with the only pressure loads applied (no thermal induced stress). The differential static pressure acting across the outer liner is such that it is push against the pins, therefor the creep deformation act to reduce the outer liner length. For the inner liner, the differential static pressure is pushing in the opposite direction: creep deformation act to increase the inner liner length. Figure 8-24 shows the axial deformation with only pressure loads applied.

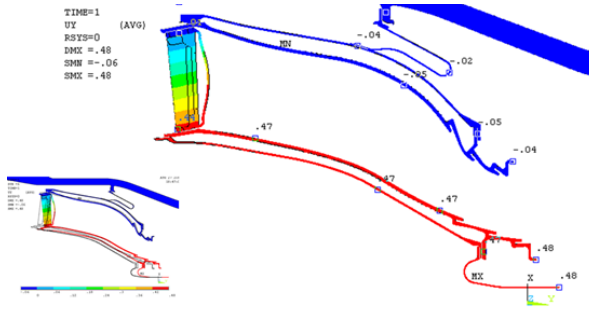

Figure 8-24, Combustor 2D axial symmetric model deformations

Combining the stress and temperature distribution on the liners with the material properties to creep, the resulting first approximation of the creep deformation is about 0.1% elongation; this result has been introduced in the estimation of the relative displacements.

To analyze the flexural deformation of the leaf seals, different analyses have been performed changing the effective contact conditions with both liner and S1N, which depends by the leaf seal angular position. The loads applied on the leaf seal FE model are the predicted uniform temperature and a static pressure drop.

Leaf seals position, deformation and reacting forces at the contact surfaces with liner and S1N are resulting from the external forces balance: forces acting on the leaf seals are the pressure loads, the springs elastic preload and the inertial force.
Each leaf seal is subjected to a static pressure drop: the static pressure inside the combustor at the liners aft-end region is resulting from the total pressure reduced by the burner pressure losses, while the static pressure outside the combustor is resulting the total pressure reduced by the aerodynamic losses in the liner / baffle gap. Such pressure load is reacted both by the liner aft-end and S1N contact surfaces in relation of the real contact status of the leaf seal in the deformed condition. The forces exchange along radial and hoop direction are negligible. Springs preload is about 2 orders of magnitude less than the delta pressure applied, while inertial forces are 3 orders of magnitude less than the delta pressure applied: both these forces are negligible.
To guarantee the independence of the solution reached by the computational mesh, a dedicated sensitivity analysis has been performed. The resulting criteria, realizing a mesh enough fine to be not influencing the results in terms of displacements in Figure 8-25, are, at least, 5 elements in the thickness of all the elements and typical elements dimension of 1 mm.

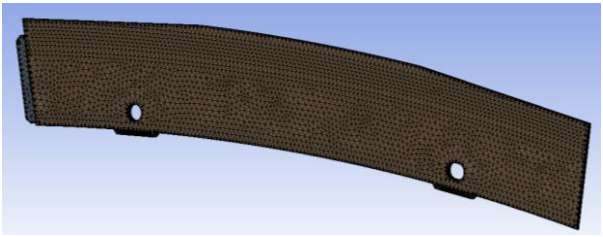

Figure 8-25, Leaf seal computational mesh

As first case, it is assumed the no contact case between liner aft-end and leaf seal, but maintaining a full contact with S1N. This condition could correspond to a couple of wrong design conditions:

- Assembly leaf seal position without liner aft-end contact;
- Hypothetical leaf seal detachment from liner during a shut-down or trip event.

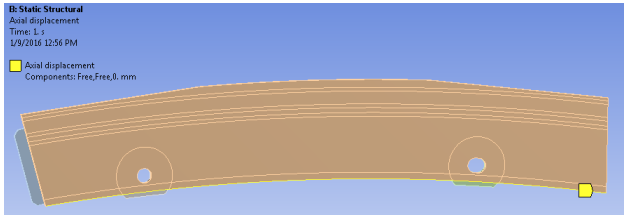

Figure 8-26, Leaf seal contact surfaces, no contact

The resulting maximum elastic axial deformation is a not representative value, since the Von Mises bulk stress obtained is quite over the 0.2% yield limit of the leaf seal material: in the right picture of for Figure 8-27, the red contour is set on the 0.2% yield limit value.

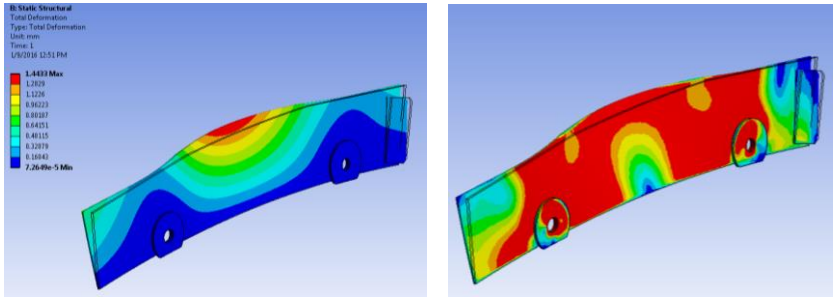

Figure 8-27, Axial deformation and Von Mises stress, no contact

In the vertical leaf seal position case, the maximum contact surfaces with liner aft-end and with S1N can be obtained, on the surfaces highlighted in Figure 8-28.

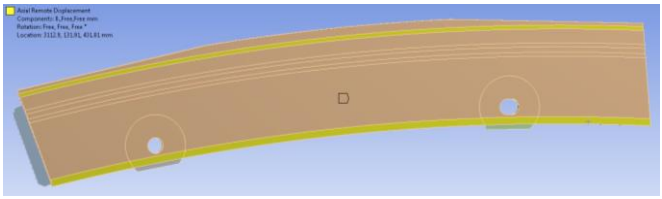

Figure 8-28, Leaf seal contact surfaces, vertical position

The resulting axial deformation is two orders of magnitude less than the leaf seal thickness, while the maximum Von Mises stress, as for Figure 3-17, is within the 0.2% yield material limit.
The vertical working condition is the best for the leaf seal in terms of durability for the minimum deformation and stress reached.

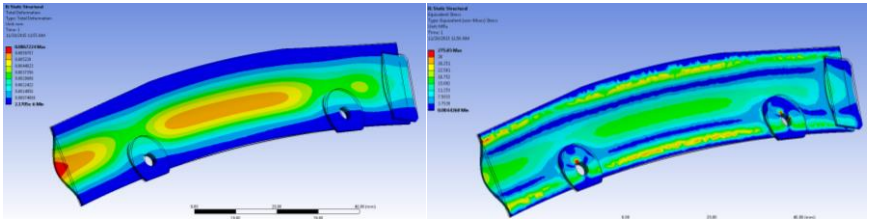

Figure 8-29, Axial deformation and Von Mises stress, vertical position

Changing the contact surfaces from the maximum condition of the leaf seal vertical position to a tilted condition, only the edges are in contact with liner and S1N, as depicted in Figure 8-30 and have been assumed in contact for the full length.

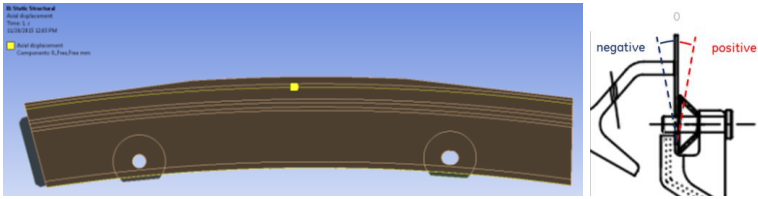

Figure 8-30, Leaf seal contacts, tilted condition, 100% edge-contact

In this case, the resulting axial deformation is one orders of magnitude less than the leaf seal thickness, while the maximum Von Mises stress, as for Figure 8-31, is still within the 0.2% yield material limit.

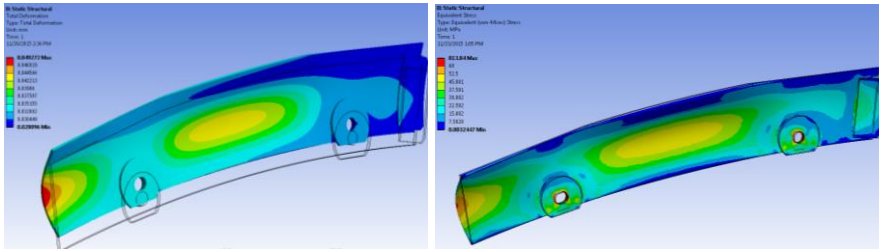

Figure 8-31, Axial deformation and stress, tilted condition, 100% edge-contact

The start-up positive tilted case represents the worst condition, having the leaf seal the minimum contact with the liner aft-end and the S1N: for the peculiar geometry of the three components, the contact happens starting from the external parts of the leaf edges for positive leaf tilting, as highlighted in the CAD kinematic study.
The deformed shape of the leaf seal increases progressively the contact surfaces starting from the external parts and moving toward the central part. In addition, for positive tilting angles, the axially constrained surfaces are at the maximum distance along the radial direction: this condition leads to higher leaf deformations.

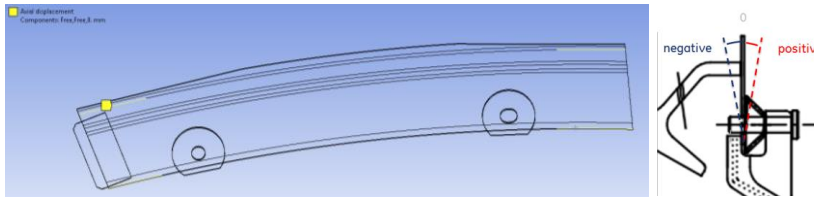

Figure 8-32, Leaf seal axial constrain, start-up tilted condition

A verification of such condition has been performed constraining the external parts of the leaf edges and checking the amount of deformation obtained: in Figure 8-33 the shape of the deformation obtained is reported.

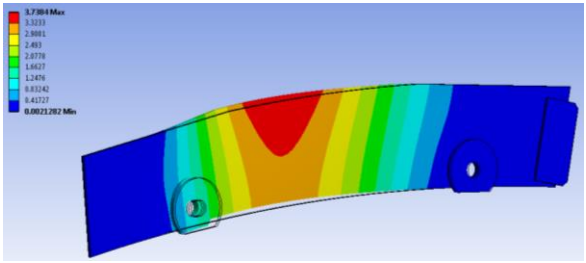

Figure 8-33, Leaf seal axial deformation, worst tilted condition

The amount of deformation in the central part is enough to generate additional contact surfaces between leaf seal and Liner and S1N structures. The leaf seals in the worst tilted condition can deflect under the applied delta pressure up to the condition of contact similar to the 100% edge-contact case, therefor the leaf seal deformed shape can fit the liner and nozzle geometry, thanks to its flexibility in hoop direction.
In conclusion, it has been observed that the contact status of the couple leaf / liner and leaf / first stage nozzle depends by:

- Leaf flexibility in hoop direction: design parameter, function of leaf length and thickness;
- Operating angular position, depending on the relative axial and radial displacement of liner and nozzle;
- Pressure drop (applied load).

The contact status is a critical point for the leaf seal durability prediction, not in terms of static stress, but in terms of dynamic behavior.
The leaf seals at assembly are free to move wrt its constraints in all the directions; by dynamic model point of view, this condition is represented by a free-free condition in a modal analysis. In addition, we can conclude also that the dynamic behavior is guided by the applied loads: leaf seals deformation and alternating stresses are result of the balance of the external forces acting on the leaf seals, namely, delta pressure load, springs elastic preload and inertial forces, where the last two are negligible respect to the pressure load.

Such forces balance determinates the real contact status on all the constraints: for the peculiar geometry of the constraints and the variability in function of the leaf seal angles, the problem is fully not linear. The complexity of a dynamic model with full not linear contacts (mono-lateral) and explicit in time solution has been considered out of the scope of the present work, so the dynamic analysis has been limited to the understanding of the dynamic leaf seal behavior, by means of modal analyses.

As first step, a free-free modal analysis has been executed: the first four natural modes, shown in Figure 8-34, have frequencies of 208, 579, 759 and 1171 Hz, located in the range of rotordynamic and acoustic exciters. This result represents a necessary, but not sufficient, condition for HCF failure, associated with potentially excessive alternating stresses generated by the leaf seals forced response to the exciters crossing the natural modes frequencies.

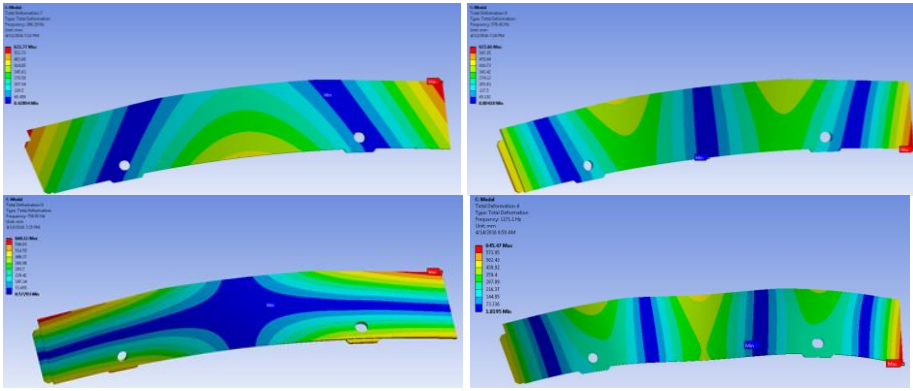

Figure 8-34, Leaf seal free-free mode shapes

Then a constrained modal analysis has been executed, assuming vertical leaf seal position and bilateral constrains for the contact surfaces. Such condition is verified under the hypothesis of a delta pressure applied on the leaf seals always positive over the mission: acoustic pressure pulsations cannot be higher than the static delta pressure.

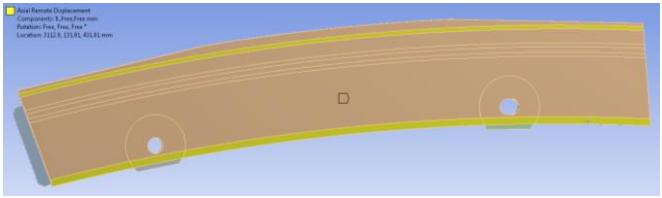

Figure 8-35, Leaf seal constrained, vertical position

The resulting first four natural modes, shown inFigure 8-36, have frequencies of 692, 834, 879 and 1610 Hz, not coupled with the ranges of rotordynamic and acoustic exciters. This result represents a necessary and sufficient condition for excluding HCF failure.

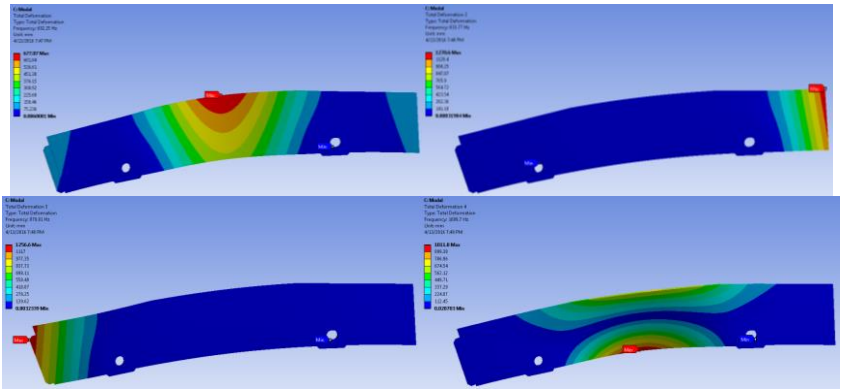

Figure 8-36, Leaf seal constrained mode shapes

A failure mode and effect analysis has been performed on the leaf seal design, as reported in Table 8-1.

Potential Failure Mode	Potential Failure Effects	S E V	Potential Causes	O C C	D E T	R P N	Actions Recommended
In what ways can the process step go wrong?	What is the impact of the Failure Mode on the customer?	How severe is the effect on the customer?	What are the causes of the Failure Mode?	How often does the Cause or Failure Mode occur?	How well can you detect the Cause or Failure Mode?	Calculated	What are the actions for reducing the occurrence, decreasing severity or improving detection?
Chattering and liberation of 1 or 2 leaf sealа due to HCF	NOX increase	1	Missed contact between leaf and liner aft end	8	10	80	Sealing design with leaf in contant during all the operative range Record the occurrence after FAR test.
	Combustion Dynamics	2				160	
	worst Pattern Factor	1				80	
	S1N Back Flow Margin	1				80	
	DOD (Domestic object damage)	8				640	
Chattering and liberation of 3 or 7 leaf seals due to HCF	NOX increase	4	Missed contact between leaf and liner aft end	5	10	200	Sealing design with leaf in contant during all the operative range Record the occurrence after FAR test.
	Combustion Dynamics	5				250	
	worst Pattern Factor	5				250	
	S1N Back Flow Margin	5				250	
	DOD (Domestic object damage)	8				400	
Chattering and liberation of more then 8 leaf seals due to HCF	NOX increase	4	Missed contact between leaf and liner aft end	2	10	80	Sealing design with leaf in contant during all the operative range Record the occurrence after FAR test.
	Combustion Dynamics	5				100	
	worst Pattern Factor	8				160	
	S1N Back Flow Margin	8				160	
	DOD (Domestic object damage)	8				160	
leaf seal hard bending	NOx increase/Back-flow margin reduction/Worst pattern factor/Dynamics increase	4	Relative axial displacement higher than allowed one	3	10	120	FAR, FETT tests and on going design improvements
wear		3		6	10	180	Hard coating on liner contact surface Take into considereation aero-elasticity investigations (analysis/test?)
acoustics-driven deformation (p' > Δp across seal)	HCF/Wear/Leakeag increase/Dynamic increase	5	p' > Δp across seal	6	10	300	FAR, FETT tests and acoustic model Take into considereation aero-elasticity investigations (analysis/test?)
hot-gas ingestion due to bow wave from nozzle and/or low pressure drop	Oxidation/Local mechanical properties degradation	8	High temperature	6	10	480	FAR and FETT tests temperature measurements at liner aft end location
seal unseating during transients	HCF/Wear/Leakeag increase/Dynamic increase/bending	5		6	10	300	
mechanical resonance in acoustics range	HCF/Wear/Leakeag increase/Dynamic increase	5		6	10	300	Design improvements (chamfer on S1N)

Table 8-1, Leaf seal FMEA

To introduce in the FMEA figures based on quantified values, in the following the relevant supporting analysis performed are reported.

Leaf seals additional leakage due to damage or release has been evaluated: with reference to the scheme of Figure 8-37, two passage areas can be identified for both outer and inner leaf release scenarios. Equivalent passage areas evaluation is reported in Figure 8-38 as a function of the number of released leaf seals. A scenario is depicted such that for a small number (about 4) of released leaf seals, only the radial area has effect on leakages: the axial one determines on the contrary the asymptotic value for a very high number of released leaf seals. The effect of leaf seals release has been evaluated onto NOx emissions and first stage nozzle back flow margin.

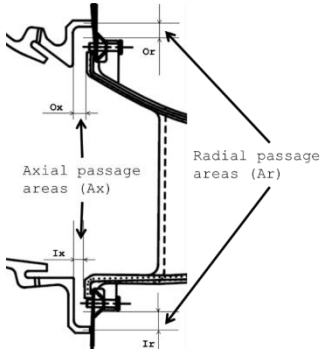

Figure 8-37, Leakages passage areas in case of leaf release

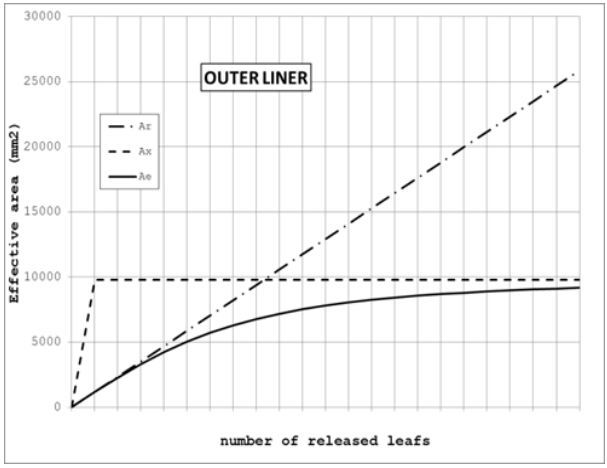

Figure 8-38, Leakages areas as a function of number of outer leaf seals released

NOx emissions increase due to leakages area increase, as shown in Figure 8-39: flame temperature increase is show as well, while the burner pressure drop decrease is shown in Figure 8-40.

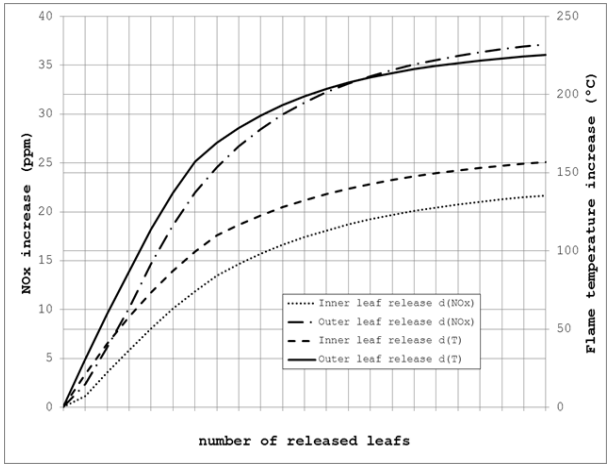

Figure 8-39, NOx and flame temperature increase

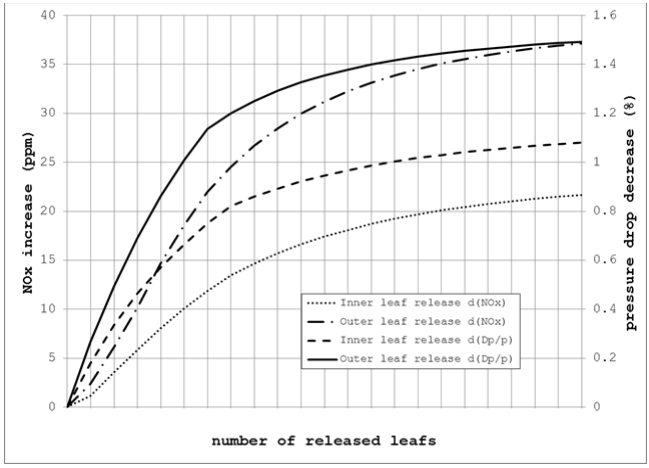

Figure 8-40, NOx increase and burner pressure drop decrease

The effect of leaf seals release onto first stage nozzle backflow margin can be determined through the evaluation of the additional pressure loss along the baffle passages generated by the additional leakage flow. Baffle passages pressure drop increase is shown in Figure 8-41.

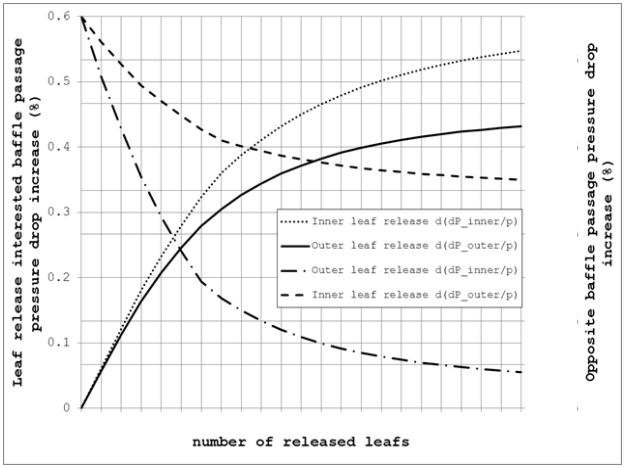

Figure 8-41, Baffle passages pressure drop increase

8.2 Alternative sealing systems

A research on publications and patents on the sealing systems between liners and high pressure turbine first stage nozzle has been performed [from Ref. 108 to Ref. 124], spanning from the 1986 to current days, to investigate possible alternative sealing solutions, which could fit the set of requirements described in chapter 8. There are few publications about sealing systems and their peculiar applications, since each OEM, typically, maintains this kind of design aspects under duties of confidentiality.
Starting from the studies performed on leaf seals and the research on the different sealing system patents a new alternative sealing design has been conceived for the NovaLT gas turbine class and tested in a full annular rig. This new alternative sealing system cannot be described in the frame of this thesis, being currently under a duty of confidentiality, as trade secret.

The sealing systems suitable to be used between combustor liner and S1N, can be sorted, using the classification approach adopted by Boyce [Ref. 105], by arrangement and configuration. Defined as axial the direction parallel to the engine axis and as radial the normal direction to the axial one, the proposed groups are:

- Axial sliding: the sealing part has a sliding contact in axial direction on one of the two surfaces to be sealed. The contact is typically preloaded in radial direction and an elastic part can withstand all the relative radial displacements.
- Radial sliding: the sealing part has a sliding contact in radial direction on one of the two surfaces to be sealed. The contact is typically preloaded in axial direction and an elastic part can withstand all the relative axial displacements.
- Double sliding: the solution includes an element moving inside a cavity in axial direction and another element moving inside a cavity in radial direction. All the sealing parts provide sealing between components having significant mutual displacements both in axial and radial directions.
- Hinge seal: sealing part is rotating respect to one of the two parts to be sealed, while it has a sliding contact with the second part both in axial and radial direction.

A distinction shall be presented between solutions which can fit the turbine first stage nozzle with annular combustor or with multiple cans combustors.
Can combustor architectures, present many advantages in design modularity, development, maintenance and operability, while suffer from higher complexity by the sealing point of view, as can be observed in Figure 8-46, Figure 8-45 and Figure 8-56.

Another fundamental distinction shall be posed is about the constrain system for the combustor: forward constrained liner (see typical Rolls-Royce combustor architecture in Figure 8-52) is subjected at the S1N interface to longer axial thermal growth than the aft constrained one, as for example the SNECMA architecture depicted in Figure 8-48.

The best example for the axial sliding group of solutions is the patent presented by Ono M. for the Mitsubishi company [Ref. 114], where the multiple configurations proposed are all combined by the capability to withstand significative relative axial displacement between liner and S1N, while negligible relative radial one.

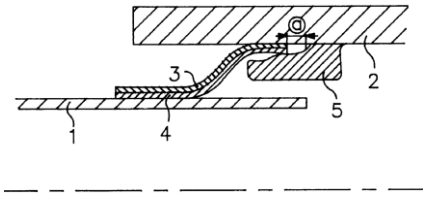

Figure 8-42, Mitsubishi patent - spring seal device for combustor

Nevertheless, due to the high temperature raised by the hog gas path components, radial displacements are typically not negligible. To maintain the relative radial displacements between liners and S1N sector to small values, over the transient phases of the engine mission, like start-up and shut-down or trip, special care shall be used in the design of the structures supporting these components, their materials and thermal inertia, mainly associated with the characteristic thickness.

One example found for the radial sliding group of solutions is the patent presented by Hash D. O. [Ref. 108] on the high excursion seal with flexible membrane design, as conceptually depicted in Figure 8-43. The flexible membrane can improve the sealing while maintaining the axial preload against the sliding surface in radial direction.

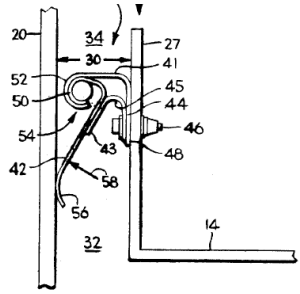

Figure 8-43, General Electric patent - High excursion seal with flexible membrane

It must be pointed out that there are many standard commercial types of sealing components, starting from simple rope seal to C, U, W section shape sealing elements, which can work between radial sliding planes with limited axial excursion, as shown in Figure 8-44.

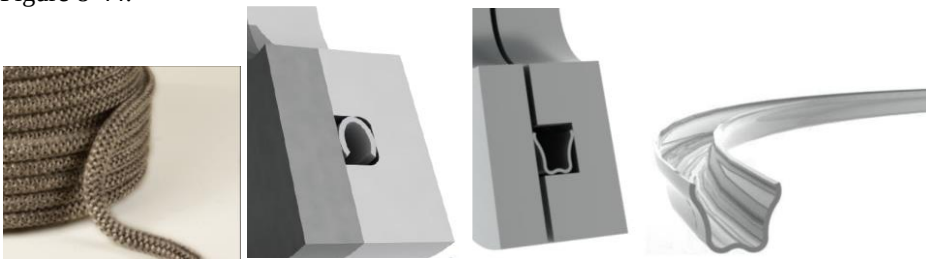

Figure 8-44, Standard commercial type of sealing system

The most common and general sealing solutions are the ones part of the double sliding group: indeed, typically liners and S1N sectors are subjected to relative axial and radial displacements and deformation over the engine missions.

One of the best example of a double sliding solution is the flexible cloth seal design [Ref. 110 and Ref. 111], as conceptually depicted in Figure 8-45. Such solution, developed to improve the sealing between first stage nozzle sectors and the combustor transition pieces, is well performing with the combustor cans configuration, as adopted in the high power size gas turbine of GE. The axial relative displacement between first stage nozzle sectors and the transition piece (so called the end part of each can of the combustor) is typically limited, since the axial constraint of the transition piece is on the cold side of the ring supporting the S1N sectors.

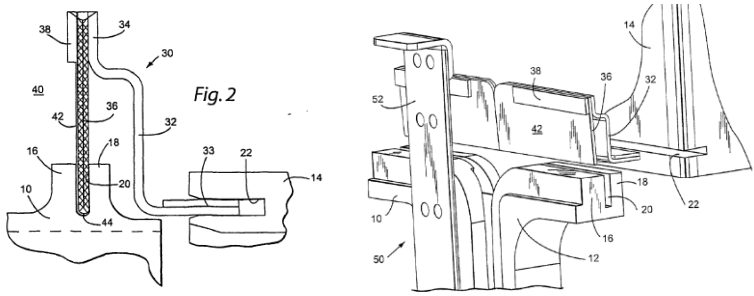

Figure 8-45, General Electric patent - flexible cloth seal

An interesting attempt to further improve the sealing between cans combustor and first stage nozzle is proposed by Bagepalli B. S. et al. [Ref. 109], introducing the brush seals use. Brush seals are utilized in many environments, usually between a stationary part and a rotating element. In US patent no. 4,781,388, there is disclosed a brush seal for use in a gas turbine for sealing between relatively stationary parts and to accommodate dimensional differences caused by thermal growth and the dynamics of the system. Disclosed brush seals require a receiving element in the form of a fork for confining the distal ends of the bristles. Figure 8-46 and Figure 8-47 are showing two potential applications of such concept with prevalent attention to axial sliding or radial sliding between the surfaces to be sealed, respectively.

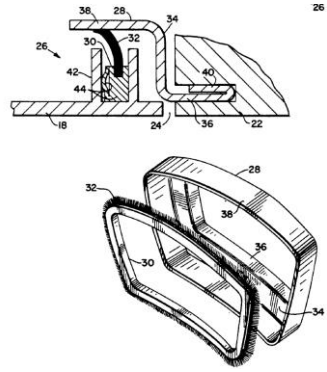

Figure 8-46, General Electric patent - self-accommodating brush seal axial sliding

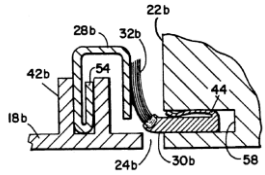

Figure 8-47, General Electric patent - self-accommodating brush seal radial sliding

In a similar context of limited relative axial displacements, but for an annular combustor architecture, there is an interesting solution, proposed by Pieussergues C. and Sandelis D. J. M. [Ref. 122], for the compact room required.

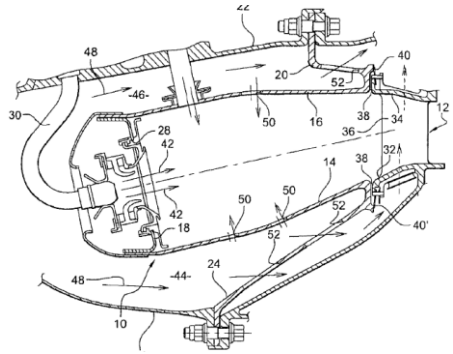

Figure 8-48, SNECMA combustor architecture – liners aft constrained

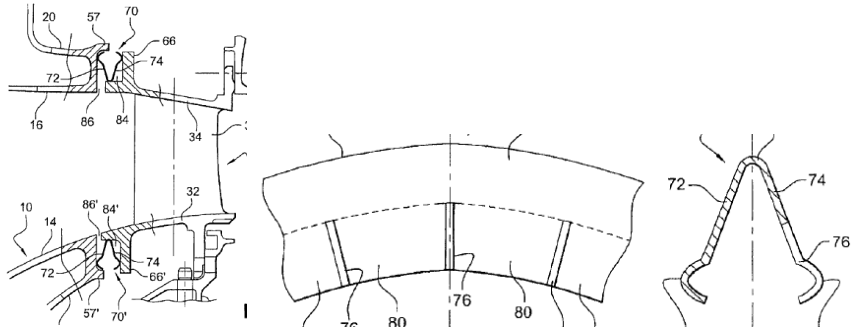

Figure 8-49, SNECMA seal patent

In Figure 8-48 the cross-sectional view of combustor and first stage nozzle is represented for a SNECMA engine: liners are mechanical sustained from the aft part, drastically reduce the relative axial displacement between the two components to be sealed.

As shown in Figure 8-49 the sealing element is similar to the standard commercial types of sealing (Figure 8-44), emphasizing the elastic capability of withstand relative axial displacements. The sealing improvement lies more in the liners constraints architecture than in the content of innovation of the sealing element itself.

By opposite, the solution proposed by Matsuda Y. K et al. [Ref. 118], contains an interesting study of the sealing element assembly, composed by many sub-components allowing both axial and radial significant sliding of the two components to be sealed, in a limited room.

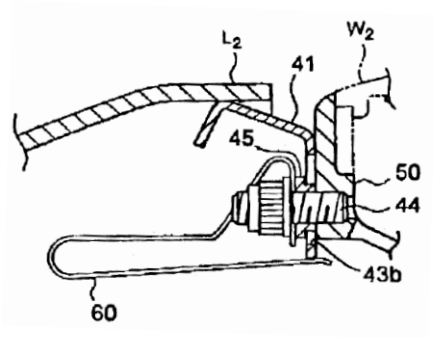

Figure 8-50, Kawasaki seal patent concept

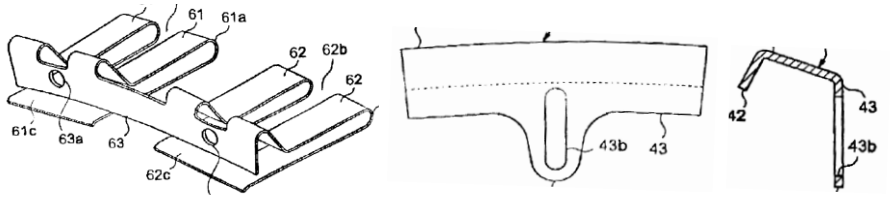

Figure 8-51, Kawasaki seal patent sub-components

A possible limitation to this sophisticate proposal can be found in the reliability of the whole sealing system, since its performance is related to the correct behaviour of many sub components.

A novelty element in this list of double sliding solutions can be found in the patent of Spooner M. P. [Ref. 123], where is presented, for a significant sliding architecture in Figure 8-52 both in axial and radial directions, the adoption of a third element, composed by many sub-parts, to be used for providing separately sealing by liners side with admitted axial sliding and by first nozzle sectors side with admitted radial sliding, see Figure 8-53.

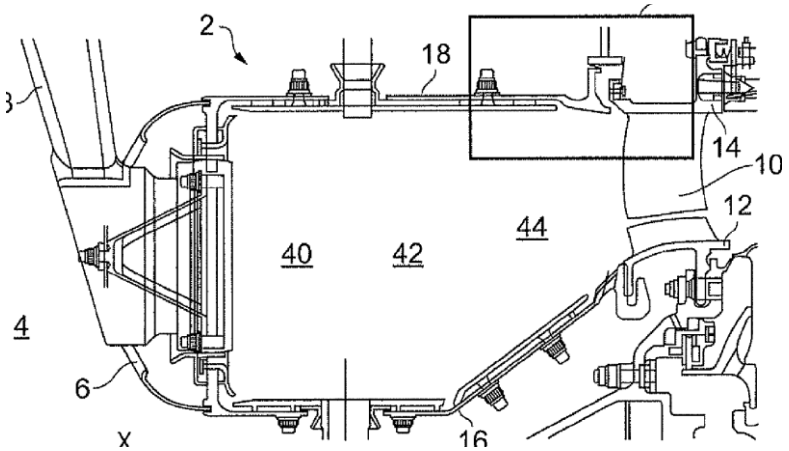

Figure 8-52, Rolls-Royce combustor architecture – liners forward constrained

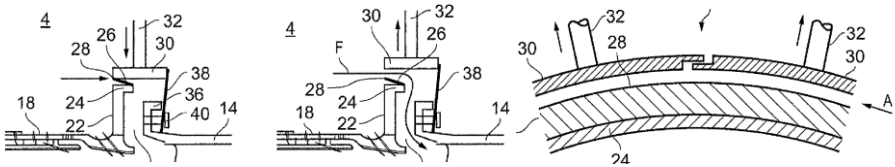

Figure 8-53, Rolls-Royce seal patent

A similar approach is suggested also in the Honeywell patent of Woodcock G. 0.et al. [Ref. 124]: more complex is the geometry of the third element added to provide separately sealing by liners side with admitted axial sliding and by first nozzle sectors side with admitted radial sliding. It must be noticed also that the suggested geometry of the liner aft-end is quite complex to be obtained, suggesting the adoption of welded connection within the liners sub-components.

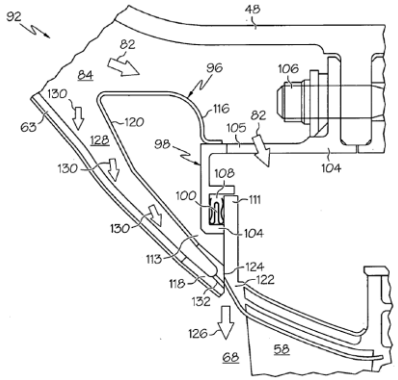

Figure 8-54, Honeywell seal patent application publication

For the last group of solutions, called hinge seal, for the presence of a rotating sealing part respect to one of the two parts to be sealed, the best example to shown is the leaf seal solution, in details analyzed in chapter 8.1.

The GE patent presented by Drerup V. M. et al. since the 1992 [Ref. 112] was reporting different kinds of the elastic organ preloading the leaf seals, as shown in Figure 8-55.

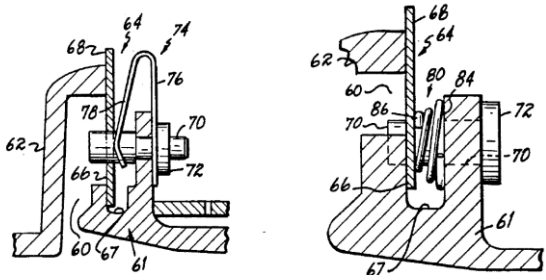

Figure 8-55, General Electric patent - leaf seal – annular combustor

An interesting attempt to use this sealing system also on the combustor cans architecture is proposed by Flanagan J. S. et al. [Ref. 121] as shown in Figure 8-56.

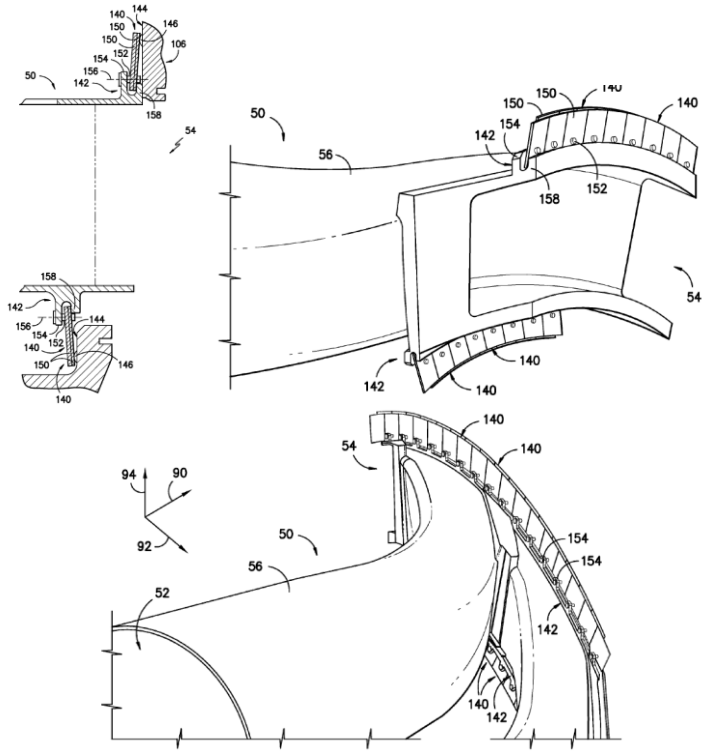

Figure 8-56, General Electric patent - leaf seal – cans combustor

Finally, an interesting solution of high excursion ring seal has been patented by Lampes E. H. [Ref. 116]: the seals have different cross-sectional configurations for specifically sealing different components. For example, the seals may have a W-shaped cross-section, or an E-shape, or simply circular cross-sections depending upon the specific application requiring sealing. Some seal are full rings, or they may be circumferentially split at one location to eliminate undesirable hoop stress therein. Another type of seal is in the form of a flat, straight leaf seal disposed in complementary slots between adjoining components.

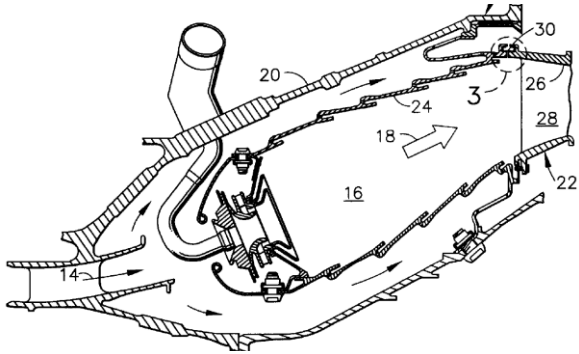

Figure 8-57, General Electric patent – high excursion ring seal

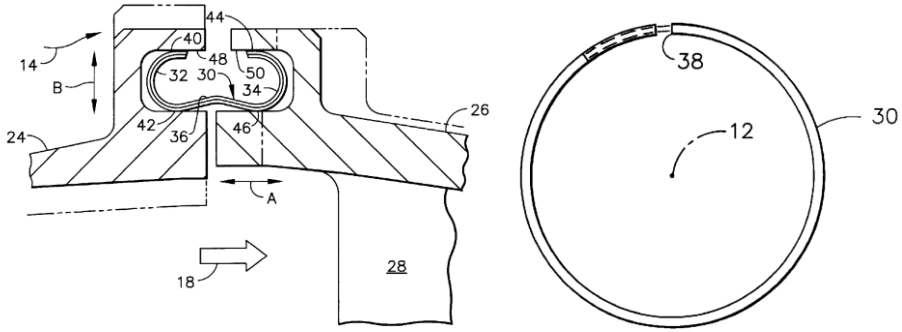

Figure 8-58, General Electric patent – high excursion ring seal detail

9 Conclusions

The baffle design process and optimization for the liner cooling architecture of the BHGE NovaLT class of industrial gas turbine has been presented. One critical aspect of this architecture is that the evaluation of overall cooling effectiveness should consider the thermal expansion of the solid parts, which affect the actual cooling passage area. This strong coupling between cooling process and thermally deformed geometry of the system, suggests the adoption of a full conjugate aero-thermal-strain design approach.

An in house one-dimensional code (GA code), developed for conjugate aero-thermal-strain analysis has been presented: it allows a quick analysis of forced convection liners cooling system for industrial annular combustors.

A validation has been performed comparing the temperature and thermal strain estimated by the GA code with the results obtained by a detailed FEM thermo-structural analysis. Correlations adopted in the GA code have been calibrated using experimental measurements of pressures and temperatures acquired in a full annular combustor rig of BHGE NovaLT16 industrial gas turbine.

The validated code has been adopted in the NovaLT12 gas turbine project, since the conceptual phase, to accommodate the combustor baffles design.

The code has been provided with two additional optimization routines, developed to automatically improve the baffle design for an enhancement of the liners durability, without penalizing engine performance. Maintaining the same coolant pressure losses and minimizing the axial gradients of metal temperature by means of a variable gap baffle geometry, a significant reduction of thermal induced stresses has been achieved, leading to an increase of the number of cycles before crack nucleation by a factor of about 2 and 3 respectively for inner and outer liner in the region of forced convection.

Next steps of the presented design optimization will be the validation of the manufacturing tolerances of baffles and liners assumed during the design phase, which can disclose additional scenarios of optimization. Similarly, the comparison with the experimental metal temperatures and pressures, which will be acquired during the test campaign in the full annular rig under construction, can lead to a finer tuning of the

proposed optimal solution, allowing the reduction of uncertainty margins assumed in the design phase.

The adoption of a one-dimensional conjugate tool for the quick design, since the early phases of combustor development, represents an element of novelty, moving a step forward the technology in the field of baffles design. A similar concept can be conveniently adopted also in other components of the hot gas path which can experience significant thermal induced deformations and it can represent an additional area of future development.

Reliability of the liner cooling system depends also by the reliability of the leakage prediction across the interface between liners and turbine first stage nozzles. In parallel to the baffle design optimization, a detailed methodology of durability analysis for the leaf seal sealing system has been developed. The proposed analysis and design process represents an improvement of the commonly adopted try and error design methodology, impacting significantly on the development time and costs for this kind of seals.

A research on publications and patents on the sealing systems between liners and turbine first stage nozzle has been presented, being an interesting reference for selection and design of the most suitable sealing system. Finally, a new alternative sealing design for the NovaLT gas turbine class has been performed: in the frame of this thesis, there is not reported any detail about, since such new seal design is currently under a duty of confidentiality, as trade secret.

10 Bibliography

Ref. 1 – Mettas, A., 2010, "Design for Reliability: Overview of the Process and Applicable Techniques", International Journal of Performability Engineering Vol. 6, No. 6, pp. 577-586

Ref. 2 – Krohn, S., 2009, "The Economics of Wind Energy (A Report by the European Wind Energy Association)", Paperback

Ref. 3 - Lefebvre, A. H., 1999, "Gas Turbine Combustion", Taylor&Francis, United State of America

Ref. 4 – Zeldovich Y. B., Sadovnikov P. Y. and Frank-Kamenetskii D. A., 1947, "Oxidation of nitrogen in combustion", Academy of Science, U.S.S.R. Moscow Leningrad

Ref. 5 – Correa S., 1992, "A review of NOx formation under gas turbine combustion conditions", Journal of Combustion and Technology, 87: 329–362

Ref. 6 – Correa S. M., 1992, "Carbon monoxide emissions in lean premixed combustion", Journal of Propulsion and Power, 8(6): 1144–1151

Ref. 7 – Lieuwen T.,1999, "Investigation of combustion instability mechanisms in premixed gas turbines", PhD thesis, Georgia Institute of Technology

Ref. 8 – Dowling A.P., 1995, "The calculation of thermoacoustic oscillations", Journal of Sound and Vibration, 180(4): 557–581

Ref. 9 – Simonetti F., 2010, "Numerical and Experimental Investigation on the Acoustic Behaviour of Multi-Perforated Liners in Aero-Engines", PhD thesis, University of Florence

Ref. 10 – Dupere I. D. J., 2003, Dowling A. P., "The use of Helmholtz resonators in a practical combustor. Proceedings of ASME Turbo Expo, GT2003-38429

Ref. 11 – Camporeale S. M., Fortunato B. and Mastrovito M., 2008, "Prediction of thermoacoustic instability in combustion chamber equipped with passive dampers", Proceedings of ASME Turbo Expo, GT2008-51387

Ref. 12 – Zhao D., Morgans A. S., 2009, "Tuned passive control of combustion instabilities using multiple Helmholtz resonators", Journal of Sound and Vibration, 320:744–757

Ref. 13 – Huang S. H., 2013, "Additive manufacturing and its societal impact: a literature review", The International Journal of Advanced Manufacturing Technology, Volume 67, Issue 5–8, pp 1191–1203

Ref. 14 – Frazier W. E., 2014, "Metal Additive Manufacturing: A Review", Journal of Materials Engineering and Performance, Vol. 23, Is. 6, pp 1917–1928

Ref. 15 – Atzeni E. and Salmi A., 2012, "Economics of additive manufacturing for end-usable metal parts", The International Journal of Advanced Manufacturing Technology, Vol. 62, Is. 9-12, pp 1147–1155

Ref. 16 – Holweg M., 2015, "The Limits of 3D Printing", Harvard Business Review

Ref. 17 – Clark D., Bache M. R. and Whittaker M. T., 2007, “Shaped metal deposition of a nickel alloy for aero engine applications”, Journal of Materials Processing Technology, Vol. 203, Is. 1–3, pp 439-448

Ref. 18 – Gou N., and Leu M. C., 2013, “Additive manufacturing: technology, applications and research needs”, Frontiers of Mechanical Engineering, Vol. 8, Is. 3, pp 215-243

Ref. 19 – Gasser A., Backes G., Kelbassa I., Weisheit A. and Wissenbach K., 2010, “Laser Metal Deposition (LMD) and Selective Laser Melting (SLM) in Turbo-Engine Applications”, Laser Technik Journal, Vol. 7, Is. 2, pp.58-63

Ref. 20 – Zitun, Y., 2015, "The 3D printer revolution comes to the IAF", Ynet News

Ref. 21 – Zelinski, P., 2017, "GE team secretly printed a helicopter engine, replacing 900 parts with 16", Modern Machine Shop

Ref. 22 – Asti A., Gamberi F., Del Vescovo G., Carta R., Giannini N., Ignesti M., Orazi C. and Pieroni N., 2018, “Heavy Duty Gas Turbine Performance and Endurance Testing: the NovaLT™16 experience”, Proceedings of ASME Turbo Expo, GT2018-76350

Ref. 23 – Chiellini R., 2014, “GE’s New Two-Shaft Gas Turbine”, Compressor TECH2

Ref. 24 – Hasset S. and Del Sala B., 2014, “GE Launches New Flagship NovaLT16 Gas Turbine and Signs MOU with TransCanada for Further Development”, GE Oil & Gas Press Release

Ref. 25 – 2014, “Gas-Pumping Unit GPU-16 Ladoga", Rep Holding Press Release

Ref. 26 – Han, 2000, “Gas Turbine Heat Transfer And Cooling Technology”

Ref. 27 – Bunker R. S., 2017, “Evolution of Turbine Cooling”, Proceedings of ASME Turbo Expo, (GT2017-63205)

Ref. 28 – LeGrives, 1986, “Cooling Techniques for Modern Gas Turbines”, Concepts ETI, Inc.

Ref. 29 – Lakshminarayana B., 1996, “Fluid Dynamics and Heat Transfer of Turbimachinery”

Ref. 30 – Modi R. and Ceccherini G., 2013, “Gas Turbine Combustion Deepening Course”

Ref. 31 – Surace M., 2001, “Investigation of Impingement systems for Gas Turbine Combustor Cooling”, PhD thesis, University of Florence

Ref. 32 – Ebeling, C. E., 1997, “An Introduction to Reliability and Maintainability Engineering”, Boston, McGraw-Hill Companies Inc.

Ref. 33 – Han J. C., Dutta S. and Ekkad S., 2000, “Gas Turbine Heat Transfer and Cooling Technology”, Second, Taylor & Francis

Ref. 34 –Florschuetz L., Truman C. and Metzger D., 1981, “Streamwise flow and heat transfer distributions for jet array impingement with crossflow,” Journal of Heat Transfer, vol. 103, pp. 337–342

Ref. 35 – Facchini B., Surace M. and Tarchi L., 2005, “Impingement cooling for modern combustors: experimental analysis and preliminary design,” ASME Conference Proceedings, no. GT2005-68361

Ref. 36 – Andrews G. E., Bazdidi-Tehrani F., Hussain C. I. and Pearson J. P., 1991, "Small Diameter Film Cooling Hole Heat Transfer: The Influence of Hole Length," ASME Paper, no. 91-GT-344

Ref. 37 – Andrews G. E., Khalifa I. M., Asere A. A. and Bazdidi-Tehrani F., 1995, "Full Coverage Effusion Film Cooling with Inclined Holes," ASME Paper, no. 95-GT-274

Ref. 38 – Gustafsson K. M. B., 2001, "Experimental Studies of Effusion Cooling," Chalmers University of technology, Department of Thermo and Fluid Dynamics

Ref. 39 – Gerendas M., Höschler K. and Schilling T., 2001, "Development and Modeling of Angles Effusion Cooling for the BR715 Low Emission Staged Combustor Core Demonstrator," in RTO AVT Symposium on Advanced Flow Management: Part B - Heat Transfer and Cooling in Propulsion and Power Systems

Ref. 40 – Kasagi N., Hirata M. and Kumada M., 1981, "Studies of full-coverage film cooling - 1. cooling effectiveness of thermally conductive wall", American Society of Mechanical Engineers, no. 81-GT-37

Ref. 41 – Andrews G. E., Asere A. A., Gupta M. L. and Mkpadi M. C., 1990, "Effusion cooling: the influence of number of hole", Journal of Power and Energy, vol. 204

Ref. 42 – Andrews G. E., Khalifa I. M., Asere A. A. and Bazdidi-Tehrani F., 1995, "Full Coverage Effusion Film Cooling with Inclined Holes," ASME Conference Proceedings, no. 95-GT-274

Ref. 43 – Martiny M., Schulz A. and Witting S., 1995, "Mathematical Model Describing the Coupled Heat Transfer in Effusion Cooled Combustor Walls", ASME Paper, no. 97-GT-329

Ref. 44 – Harrington M. K., McWaters M. A., Bogard D. G., Lemmon C. A. and Thole K. A., 2001, "Full-Coverage Film Cooling with Short Normal Injection Holes," Journal of Turbomachinery, vol. 123, pp. 798–805

Ref. 45 – Martin A. and Thorpe S. J., 2012, "Experiments on Combustor Effusion Cooling Under Conditions of Very High Free-Stream Turbulence", ASME Conference Proceedings, no. GT2012-68863

Ref. 46 – Scrittore J. J., Thole K. A. and Burd S. W., 2005, "Experimental Characterization of Film-Cooling Effectiveness Near Combustor Dilution Holes", ASME Conference Proceedings, no. GT2005-68704

Ref. 47 – Ligrani P., Goodro M., Fox M. and Moon H.-K., 2012, "Full-Coverage Film Cooling: Film Effectiveness and Heat Transfer Coefficients for Dense and Sparse Hole Arrays at Different Blowing Ratios," Journal of Turbomachinery, vol. 134, no. 6, p. 061039

Ref. 48 – Foster N. W. and Lampard D., 1980, "The Flow and Film Cooling Effectiveness Following Injection through a Row of Holes," Journal of Engineering for Power, vol. 102, no. 3, p. 584

Ref. 49 – Hale C. A., Plesniak M. W. and Ramadhyani S., 2000, "Film Cooling Effectiveness for Short Film Cooling Holes Fed by a Narrow Plenum," Journal of Turbomachinery, vol. 122, no. 3, p. 553

Ref. 50 – Baldauf S., Schulz A. and Wittig S., 2001, “High-Resolution Measurements of Local Effectiveness from Discrete Hole Film Cooling”, Journal of Turbomachinery, vol. 123, no. 4, p. 758

Ref. 51 – Martinez-Botas R. F. and Yuen C. H. N., 2000, “Measurement of local heat transfer coefficient and film cooling effectiveness through discrete holes,” ASME Conference Proceedings, no. 2000-GT-243

Ref. 52 – Behrendt T., Lengyel T., Hassa C. and Gerendis M., 2008, “Characterization of Advanced Combustor Cooling Concepts Under Realistic Operating Conditions,” Proc. ASME, no. GT2008-51191

Ref. 53 – Andreini A., Facchini B., Picchi A., Tarchi L. and Turrini F., 2014, “Experimental and theoretical investigation of thermal effectiveness in multiperforated plates for combustor liner effusion cooling,” Journal of Turbomachinery, vol. 136, no. 9

Ref. 54 – Ceccherini A., Facchini B., Tarchi L., Toni L. and Coutandin D., 2009, “Combined Effect of Slot Injection, Effusion Array and Dilution Hole on the Cooling Performance of a Real Combustor Liner”, ASME Conference Proceedings, no. GT2009-48845

Ref. 55 – Wurm B., Schulz A., Bauer H. J. and Gerendásv, 2012, “Impact of Swirl Flow on the Cooling Performance of an Effusion Cooled Combustor Liner”, Journal of Engineering Gas Turbines Power., vol. 134, no. 12, pp. 121503–121503

Ref. 56 – Andreini A., Becchi R., Facchini B., Picchi A. and Turrini F., 2015, “Effect of Slot Injection and Effusion Array on the Liner Heat Transfer Coefficient of a Scaled Lean-Burn Combustor with Representative Swirling Flow”, Journal of Engineering Gas Turbines Power., vol. 138, no. 4, pp. 041501–041501

Ref. 57 – Andreini A., Becchi R., Facchini B., Mazzei L., Picchi A. and Turrini F., 2015, “Adiabatic Effectiveness and Flow Field Measurements in a Realistic Effusion Cooled Lean Burn Combustor”, Journal of Engineering Gas Turbines Power., vol. 138, no. 3, pp. 031506–031506

Ref. 58 – Andreini A., Da Soghe R., Facchini B., Mazzei L., Colantuoni S. and Turrini F., 2014, “Local Source Based CFD Modeling of Effusion Cooling Holes: Validation and Application to an Actual Combustor Test Case,” ASME Journal of Engineering Gas Turbine Power, vol. 136, no. 1, pp. 011506-011506-11

Ref. 59 – Rida S., Reynolds R., Chakracorty S. and Gupta K., 2012, “Imprinted effusion modeling and dynamic C_D calculation in gas turbine combustors,” Proceedings of ASME Turbo Expo, vol. GT2012-68804

Ref. 60 – Mazzei L., Andreini A., Facchini B. and Bellocci L., 2016, “A 3D Coupled Approach for the Thermal Design of Aero-Engine Combustor Liners,” ASME paper GT2016-56605, no. 49798, p. V05BT17A009

Ref. 61 – Gicquel L. Y. M., Staffelbach G. and Poinsot T., 2012, “Large Eddy Simulations of gaseous flames in gas turbine combustion chambers,” Progress in Energy and Combustion Science, vol. 38, pp. 782–817

Ref. 62 – Boudier G., Gicquel L. Y. M., Poinsot T., Bissières D. and Bérat C., 2007, "Comparison of LES, RANS and experiments in an aeronautical gas turbine combustion chamber," Proceedings of the Combustion Institute, vol. 31, no. 2, pp. 3075–3082

Ref. 63 – Stow S. R., Zedda M., Triantafyllidis A., Garmory A., Mastorakos E. and Mosbach T., 2011, "Conditional Moment Closure LES Modelling of an Aero-Engine Combustor at Relight Conditions," ASME Paper GT2011-45100

Ref. 64 – Sen B. A., Guo Y., McKinney R. G., Montanari F. and Bedford F. C., 2012, "Pratt and Whitney Gas Turbine Combustor Design Using ANSYS Fluent and User Defined Functions," ASME Paper GT2012-70145

Ref. 65 – Mahapatra D., Basani J. and Rida S., 2015, "Assessment of Scale Adaptive Simulation Model for Honeywell Combustor," in ASME Paper GT2015-43573

Ref. 66 – Rida S., Chakravorty S., Basani J., Orsino S. and Ansari N., 2015, "An Assessment of Flamelet Generated Manifold Combustion Model for Predicting Combustor Performance," ASME Paper GT2015-42340

Ref. 67 – Wolf P., Balakrishnan R., Staffelbach G., Gicquel L. Y. and Poinsot T., 2012, "Using LES to study reacting flows and instabilities in annular combustion chambers," Flow, turbulence and combustion, vol. 88, no. 1, pp. 191–206

Ref. 68 – Boileau M., Staffelbach G., Cuenot B., Poinsot T. and Bérat C., 2008, "LES of an ignition sequence in a gas turbine engine," Combustion and Flame, vol. 154, no. 1–2, pp. 2–22

Ref. 69 – Fedina E., Fureby C., Borzov S., Gusev V. and Stepanova T., 2011, "Combustion LES of CESAR Multi-Burner Annular Combustor," in 49th AIAA

Ref. 70 – 2013, FP7-JTI 620143, DREAMCODE - Development of Reliable Emission and Atomization Models for Combustor Design

Ref. 71 – 2014, FP7-JTI 620180, DYNAMO - Design methods for durabilitY aNd operAbility of low eMissions cOmbustors

Ref. 72 – Gimenez G., Errera M., Baillis D., Smith Y. and Pardo F., 2016, "A coupling numerical methodology for weakly transient conjugate heat transfer problems," International Journal of Heat and Mass Transfer, vol. 97, pp. 975–989

Ref. 73 – Schmidt M. and Starke C., 2015, "Coupled heat-transfer simulations of turbines in consideration of unsteady flows," International Journal of Thermal Sciences, vol. 96, pp. 305–318

Ref. 74 – He L. and Oldfield M., 2011, "Unsteady conjugate heat transfer modeling," Journal of turbomachinery, vol. 133, no. 3, p. 031022

Ref. 75 – Jaure S., Duchaine F., Staffelbach G. and Gicquel L. Y. M., 2013, "Massively parallel conjugate heat transfer methods relying on large eddy simulation applied to an aeronautical combustor," Computational Science & Discovery, vol. 6, no. 1, p. 015008

Ref. 76 – Duchaine F., Mendez S., Nicoud F., Corpron A., Moureau V. and Poinsot T., 2009, "Conjugate heat transfer with Large Eddy Simulation for gas turbine components," Comptes Rendus Mécanique, vol. 337, no. 6, pp. 550–561

Ref. 77 – Duchaine F. et al., 2015, "Analysis of high performance conjugate heat transfer with the OpenPALM coupler," Computational Science & Discovery, vol. 8, no. 1, p. 015003

Ref. 78 – Cottin G., Savary N., Laroche E. and Millan P., 2011, "Modeling of the heat flux for multi-hole cooling applications," in Proceedings of ASME Turbo Expo, vol. GT2011-46330

Ref. 79 – Bailey J. C., Intile J., Fric T. F., Tolpadi A. K., Nirmalan N. V. and Bunker R. S., 2002, "Experimental and numerical study of heat transfer in a gas turbine combustor liner", Proceedings of the ASME Turbo Expo 2002, no. GT2002-30183

Ref. 80 – Kiewel H., Aktaa J. and Munz D., 2002, "Advances in the Inelastic Failure Analysis of Combustor Structures", in: High Intensity Combustors - Steady Isobaric Combustion. Final Report of the Collaborative Research Centre, 167, Wittig S. and Vohringer O., eds., Wiley-VCH, Weinheim

Ref. 81 – Kim K. M., Yun N., Yun H. J., Lee D. H., Cho H. H. and Kang S., 2010, "Conjugated heat transfer and temperature distributions in a gas turbine combustion liner under base-load operation", Journal of Mechanical Science and Technology, 24 (9), 1939-1946

Ref. 82 – Matarazzo S., Laget H., 2011, "Modelling of the Heat Transfer in a Gas Turbine Liner Combustor", Proceedings of Seventh Mediterranean Combustion Symposium

Ref. 83 – Shahi M., Kok J. B. W. and Alemela P. R., 2012, "Simulation of 2-way fluid structure interaction in a 3d model combustor", Proceedings of the ASME Turbo Expo 2012, no. GT2012-69681

Ref. 84 – Tinga T., Van Kampen, J. F., De Jager, B. and Kok, J. B. W., 2005, "Gas Turbine Combustor Liner Life Assessment Using a Fluid / Structural Approach", NLR-TP-2005-627

Ref. 85 – Tinga T., Van Kampen, J. F., De Jager, B. and Kok, J. B. W., 2007, "Gas Turbine Combustor Liner Life Assessment Using a Combined Fluid/Structural Approach", Journal of Engineering for Gas Turbines and Power, Vol. 129

Ref. 86 – Kane M. and Yavuzkurt S., 2009, "Calculation of gas turbine blade temperatures using an iterative conjugate heat transfer approach", International Symposium on Heat Transfer in Gas Turbine Systems

Ref. 87 – Siw S., Chyu M. K., Slaughter W., Karaivanov V. and Alvin M.A., 2009, "Influence of internal cooling configuration on metal temperature distributions of future coal-fuel based turbine airfoils", Proceedings of the ASME Turbo Expo 2009, no. GT2009-59829.

Ref. 88 – Berger S., Richard S., Staffelbach D., Duchaine F., and Gicquel L., 2015, "Aerothermal Prediction of an Aeronautical Combustion Chamber Based on the Coupling of Large Eddy Simulation, Solid Conduction and Radiation Solvers", Proceedings of ASME Turbo Expo 2015, no. GT2015-42457

Ref. 89 – Mazzei L., Andreini A., Facchini B. and Bellocci L., 2016, "A 3D coupled Approach for the Thermal Design of Aero-Engine Combustor Liners", Proceedings of ASME Turbo Expo 2016, no. GT2016-56605

Ref. 90 – Andreini A., Ceccherini A., Facchini B., Turrini F. and Vitale I., 2009, "Assessment of a Set of Numerical Tools for The Design of Aero-Engines Combustors: Study of a Tubular Test Rig", Proceedings of ASME Turbo Expo 2009, no. GT2009-59539

Ref. 91 – Gosselin P., De Champlain A. and Kretschmer D., 1999, "Prediction of wall heat transfer for a gas turbine combustor", Proceedings of the Institution of Mechanical Engineers, Part A: Journal of Power and Energy, A05998

Ref. 92 – Kretschmer D. and Odgers J., 1978, "A simple method for the prediction of wall temperatures in a gas turbine combustor", ASME paper 78-GT-90

Ref. 93 – Andreini A., Carcasci C., Ceccherini A., Facchini B., Surace M., Coutandin D., Gori S. And Peschiulli A., 2007, "Combustor liner temperature prediction: a preliminary tool development and its application on effusion cooling systems", CEAS2007 European Air and Space Conference Century Perspectives, paper 026

Ref. 94 – Bonini A., Andreini A., Carcasci C., Facchini B., Ciani A. and Innocenti L., 2012, "Conjugate Heat Transfer Calculations on GT Rotor Blade for Industrial Applications. Part I: Equivalent Internal Fluid Network Setup and Procedure Description", Proceedings of the ASME Turbo Expo 2012, no. GT2012-69846

Ref. 95 – Vacca A. and Cerutti M., 2007, "Analysis and Optimization of a Two-Way Valve using Response Surface Methodology", International Journal of Fluid Power 8, no. 3, pp. 43-57

Ref. 96 – Cerutti M., Bozzi L., Bonzani F. and Carcasci C., 2010, "An Efficient Procedure for the Analysis of Heavy Duty Gas Turbine Secondary Flows in Different Operating Conditions", Proceedings of the ASME Turbo Expo 2010, no. GT2010-22938

Ref. 97 – Pucci E., Cerutti M., Peano G., Facchini B. and Andreini A., 2016, "Optimization process of liners cooling system of industrial annular combustors", Proceedings of the PGI

Ref. 98 – Pucci E., Cerutti M., Peano G., Facchini B. and Andreini A., 2017, "Cooling system optimization of combustor liners", Proceedings of the ASME Turbo Expo 2010, no. GT2017-64758

Ref. 99 – Han J. C., 1988, "Heat Transfer and Friction Characteristics in Rectangular Channels with Rib Turbulators", Journal of Heat Transfer, 110, 321-328

Ref. 100 – Han J. C., Ou S., Park J. S. and Lei C. K., 1989, "Augmented Heat Tranfer in Rectangular Channels of Narrow Aspect Ratios with Rib Turbulators", International Journal of Heat Mass Transfer, 32, 1619-1630

Ref. 101 – Han J. C. and Park J. S., 1988, "Developing Heat Transfer in Rectangular Channels with Rib Turbulators", International Journal of Heat Mass Transfer, 31, 183-195

Ref. 102 – Han J. C., Park J. C. and Lei C. K., 1985, "Heat Transfer Enhancement in Channels with Turbulence Promoters", Journal of Engineering for Gas Turbines and Power, 107, 628-635

Ref. 103 – Han J. C., 1984, "Heat Transfer and Friction in Channels with Two Opposite Rib-Roughened Walls", Journal of Heat Transfer, 106, 774-781

Ref. 104 – Brandt D. E. and Wesorick R. R., 1994, "GE gas turbine design philosophy", GER3434D

Ref. 105 – Boyce M. P., 2001, "Gas Turbine Engineering Handbook", 2nd ed., Gulf Professional Publising

Ref. 106 – 1995, "Effects of compressible annular seals", Proceeding of the 24th Turbomachinery Symposium, Texas A&M University, p. 175

Ref. 107 – Mayeux T., Paul F. Jr. and Paul L., 2014, "Design improvements enhance dry gas seal's ability to handle reverse pressurization", Proceeding of the 25th Turbomachinery Symposium, Texas A&M University, 8.726 6.2.

Ref. 108 – Hash D. O. inventor, 1986, General Electric Company assignee, "High Excursion Seal with Flexible Membrane to Prevent Gas Leakage Through Hinge", United States Patent, no. 4,575,099

Ref. 109 – Bagepalli B. S., Dinc O. S. and Barnes J. inventors, 1993, General Electric Company assignee, "Self-Accommodating Brush Seal for Gas Turbine Combustor", United States Patent, no. 5,265,412

Ref. 110 – Aksit M. F., Benoit J. A., Aslam S., Bland R. J. L. and Bagepalli S. inventors, 1992, General Electric Company assignee, "Flexible cloth seal for turbine combustors", European Patent Specification, EP 1 239 118 B1

Ref. 111 – Aksit M. F., Benoit J. A., Aslam S., Bland R. J. L. and Bagepalli S. inventors, 2002, General Electric Company assignee, "Low leakage flexible cloth seal for turbine combustors", United States Patent Application Publication, no. 0211744 A1

Ref. 112 – Drerup V. M., Hess J. R. and Plemmons L. W. inventors, 1992, General Electric Company assignee, "Leaf seals", United States Patent, no. 5,118,120

Ref. 113 – Bagepalli B. S., Taura J. C., Aksit M. F., Demiroglu M. and Predmore D. R. inventors, 1999, General Electric Company assignee, "Flexible Cloth Seal Assembly", United States Patent, no. 5,915,697

Ref. 114 – Ono M. inventor, 1999, Mitsubishi Jukogyo Kabushiki Kaisha assignee, "Spring Seal Device for Combustor", United States Patent, no. 5,987,879

Ref. 115 – Eignor J. G., Poccia N. P. and Tomlinson l. O. inventors, 2000, General Electric Company assignee, "Flexible seal for gas turbine expansion joints", United States Patent, no. 6,065,756

Ref. 116 – Lampes E. H. inventor, 2001, General Electric Company assignee, "High Excursion Ring Seal", United States Patent, no. 6,199,871

Ref. 117 – Smallwood M. S. and Rice E. C. inventors, 2002, Allison Advance Development Company assignee, "Combustor liner support and seal assembly", United States Patent, no. 6,347,508

Ref. 118 – Matsuda Y. K., Kobayashi M. K., Yoshimura T. A. and Miyamoto H. A. inventors, 2005, Kawasaki Jukogyo Kabushiki Kaisha assignee, “Sealing structure for combustor liners”, United States Patent, no. 6,854,738

Ref. 119 – Giri S. N. inventor, 2012, General Electric Company assignee, “Formed flexible seal”, United States Patent Application Publication, no. 0306168 A1

Ref. 120 – Buchal T., Frank G., Gruschka U., Krutzfeldt J., Rogos K. U. and Schaberg A. inventors, 2013, Siemens Aktiengesellschaft assignee, “High temperature resistant sealing assembly, especially for gas turbine”, United States Patent, no. 8,365,538

Ref. 121 – Flanagan J. S., Lebegue J. S., McMahan K. W, Dillard D. J. and Pentecost R. R. inventors, 2013, General Electric Company assignee, “Leaf seal for transition duct in turbine system”, United States Patent, no. 8,459,041

Ref. 122 – Pieussergues C. and Sandelis D. J. M. inventors, 2014, SNECMA assignee, “Sealing between a combustion chamber and s turbine nozzle in a turbomachine”, United States Patent, no. 8,661,828

Ref. 123 – Spooner M. P. inventor, 2014, Rolls-Royce PLC assignee, “Combustor for a gas turbine engine.”, United States Patent, no. 8,661,828

Ref. 124 – Woodcock G. 0., Tucker B. R., Smoke J., Kujala S. and Kuhn T. inventors, 2010, Honeywell International Inc. assignee, “Combustor-turbine seal interface for gas turbine engine”, United States Patent Application Publication, no. 0307166 A1